WAVELET TRANSFORM BASED ELECTROCARDIOGRAM COMPRESSION AND COMPARISON WITH DCT/DST METHODS

by

Mustafa NAMDAR

B.S., E.E., Yıldız Technical University, 1997

Submitted to Institute of Biomedical Engineering
in partial fulfillment of the requirements
for the degree of
Master of Science
in
Biomedical Engineering

Boğaziçi University
June 2006

WAVELET TRANSFORM BASED ELECTROCARDIOGRAM COMPRESSION AND COMPARISON WITH DCT/DST METHODS

APPROVED BY:

Assoc. Prof. Dr. Halil Özcan GÜLÇÜR …….
(Thesis Supervisor)

Prof. Dr. Mehmed ÖZKAN …….

Assoc. Prof. Dr. Bülent BİLİR …….

DATE OF APPROVAL:

ACKNOWLEDGMENTS

I would like to express my sincere thanks to my thesis supervisor, Assoc. Prof. Dr. Halil Özcan Gülçür. He provided me with necessary support, advice, facilities and enthusiasm required to successfully complete this thesis. His efforts in helping me in the development of the project, through technical feedbacks are much appreciated. I would like to thank Prof. Dr. Ahmet Ademoğlu, who provided me with valuable leads into the subject of wavelet transforms. I also would like to thank Ertuğrul Burteçin Aksel for his support and assistance throughout the progress of this thesis.

ABSTRACT

WAVELET TRANSFORM BASED ELECTROCARDIOGRAM COMPRESSION AND COMPARISON WITH DCT/DST METHODS

In this thesis we investigate wavelet transform based ECG compression techniques and compare them with conventional approaches. A major issue addressed is how to guarantee a user-specified error limit measured by the percent root mean square difference (PRD) for the reconstructed ECG signal to be controlled at every segment while keeping the compression ratio (CR) as large as possible with reasonable implementation complexity.

Two wavelet transform based compression methods, one based on discrete orthonormal wavelet transform ($DOWT$) and the other based on wavelet packet transforms are studied in detail. Decomposition, uniform quantization, and entropy coding are applied successively to compress the digital ECG signal while entropy decoding, and inverse transformation are applied to reconstruct the original signal. Different types of wavelet families are used to analyze the effect on CR and PRD. More conventional discrete sine / cosine transform based methods are also studied for comparison purposes.

Two numerical metrics PRD and CR are used as the major performance evaluation parameters to quantitatively compare one method to another. The CR is a measure of compression efficiency; the PRD gives information about the performance of the compression scheme and the distortion measured. Using the techniques developed, two different types of ECG signals (normal and an arrhythmic) are compressed analyzed and the results are reported. In each technique, while the PRD increases, the CR also increases. In general, the highest CR values are obtained with the wavelet transform; the lowest PRD values are obtained with the wavelet packet transform.

Keywords: Biomedical Signal Compression, Electrocardiogram, Wavelet Transform, Discrete Sine Transform, Discrete Cosine Transform, Arrhythmia.

ÖZET

ELECTROKARDİOGRAM İŞARETLERİNİN DALGACIK DÖNÜŞÜMÜ YÖNTEMİ İLE SIKIŞTIRILMASI VE DCT/DST METODLARIYLA KARŞILAŞTIRILMASI

Bu tez çalışmasında, elektrokardiogram işaretinin dalgacık dönüşümü temelli sıkıştırılması incelenmiş ve bu yöntem geleneksel sıkıştırma yaklaşımları ile karşılaştırılmıştır. Tez çalışmasında ele alınan en önemli konu, yeniden elde edilen her bir EKG parçasında, denetlenen yanılgıların karelerinin toplamlarının karekökü (PRD) ile, kullanıcı tarafından tanımlanan yanılgı düzeyini güvence altına almak ve sıkıştırma oranını (CR) benimsenilen uygulama karmaşıklığı ile birlikte, olabildiğince yüksek düzeyde tutmaktır.

Birisi ayrık birimdik dalgacık donüşümü ve diğeri ise dalgacık paket dönüşümü temelli iki sıkıştırma yöntemi üzerinde detaylı olarak çalışılmıştır. Sayısal elektrokardiogram işaretini sıkıştırmak için sırasıyla ayrıştırma, düzgün kuantalama ve entropi kodlama uygulanmaktayken, özgün işareti yeniden elde etmek için de, entropi kodçözme ve ters dönüşüm uygulanmaktadır. CR ve PRD parametreleri üzerindeki etkileri çözümleyebilmek için farklı tipte dalgacık aileleri kullanılmıştır. Aynı zamanda, daha geleneksel ayrık sinüs / kosinüs dönüşüm temelli yöntemler üzerinde de karşılaştırma amaçlı olarak çalışılmıştır.

PRD ve CR metrikleri, bir yöntemi diğeri ile sayısal olarak karşılaştırmak amacıyla en önemli başarım değerlendirme ölçütleri olarak kullanılırlar. CR bir sıkıştırma verimliliğinin ölçütüdür; PRD ise sıkıştırma başarımı ve ölçülen işaret bozunumu ile ilgili bilgi verir. İki farklı elektrokardiogram işareti (olağan ve aritmik) geliştirilen yöntemler kullanılarak, sıkıştırılmış, çözümlenmiş ve sonuçlar raporlanmıştır. Her bir yöntemde PRD artarken CR de artmaktadır. Genel olarak, en yüksek CR değerleri dalgacık dönüşümü ile elde edilirken, en düşük PRD değerleri ise dalgacık paket dönüşümü ile elde edilmektedir.

Anahtar Kelimeler: Biomedikal İşaret Sıkıştırma, Elektrokardiogram, Dalgacık Dönüşümü, Ayrık Sinüs Dönüşümü, Ayrık Kosinüs Dönüşümü, Aritmi.

TABLE OF CONTENTS

LIST OF FIGURES

LIST OF TABLES

LIST OF SYMBOLS

a_0	Input discrete signal
a_0'	Reconstructed signal
a_J	Approximation coefficient
d_j	Detail coefficient
ε_i^d	MSE in quantization of d_j
ε_J	MSE in quantization of a_J
γ_0	Reconstruction MSE
σ	Power of the original signal
μ_i	Samples of the original signal
L	Length of ECG segment
ρ_0	Percent Root Mean Square Difference value
J	Decomposition level
Δ	Quantization step size
X_{org}	Samples of original signals
X_{rec}	Samples of reproduced signal
W_i	DCT computation of signal $segment_i$
A	Compressed data size in WP
B	Compressed data size in WPT
e	Actual quantization mean square error

LIST OF ABBREVIATIONS

CR	Compression Ratio
CWT	Continuous Wavelet Transform
DCT	Discrete Cosine Transform
DOWR	Discrete Orthonormal Wavelet Reconstruction
DOWT	Discrete Orthonormal Wavelet Transform
DST	Discrete sine Transform
DWT	Discrete Wavelet Transform
FFT	Fast Fourier Transform
ICWT	Inverse Continuous Wavelet Transform
IDCT	Inverse Discrete Cosine Transform
IDCT	Inverse Discrete Cosine Transform
IDST	Inverse Discrete sine Transform
IDWT	Inverse Discrete Wavelet Transform
LSB	Least Significant Bit
LZW	Lempel-Ziv Welsch
MSE	Mean Square Error
PCM	Pulse Code Modulation
PRD	Percent Root Mean Square Difference
RMSE	Reconstruction Mean Square Error
SNR	Signal to Nosie Ratio
WPT	Wavelet Packet Transform
WT	Wavelet Transform

1. INTRODUCTION

1.1 Background and Motivation

The aim of electrocardiogram (ECG) data compression is to compress the amount of digitized ECG data as much as possible with reasonable implementation complexity while maintaining clinically acceptable signal quality. In order to achieve this goal an electrocardiogram (ECG) data compression method is presented which is based on orthonormal wavelet transform and a uniform quantization strategy with high compression ratio and low implementation complexity [1].

In recent years, many schemes for ECG compression have been proposed, which can be grouped into two categories: Direct methods and transform methods.

In direct methods, the compression is done directly on the ECG samples. Examples include the AZTEC (amplitude zone time epoch coding), TP (turning point), CORTES (coordinate reduction time encoding system), and SAPA (scan-along polygonal approximation), peak-picking, cycle to cycle are the examples of the direct methods [1].

In the transform methods, the original samples are transformed to another domain in the hope of achieving better compression performance. Some examples include Fourier descriptors, Walsh Transform, Karhunen-Loeve Transform, Discrete Cosine Transform, and recently developed Wavelet Transform [2], [3].

In most cases, direct methods are superior to transform methods with respect to system complexity and error control mechanism. However, transform methods usually achieve higher compression ratios and are insensitive to the noise contained in original ECG signals.

For ECG coding systems, the error control problem for a reproduced ECG signal is an important issue because ECG signals are usually non-stationary and if the quality of a reconstructed ECG signal is not guaranteed, the compression process itself will become less useful.

In the case of direct methods, the error limit for a reproduced ECG signal is easily controlled by adjusting a user-specified error threshold. In the case of transform methods, however, the error control is difficult because the distortion of each reconstructed segment of the ECG signal varies with the complex pattern of the segment.

The major issue addressed in this thesis is how to guarantee a user-specified error limit measured by the percent root mean square difference (*PRD*) for the reconstructed ECG signal to be controlled at every segment while keeping the compression ratio as large as possible with reasonable implementation complexity.

In this thesis, first a discrete orthonormal wavelet transform (*DOWT*) based ECG coding system by which a user-specified *PRD* of the reproduced ECG segments are guaranteed with the acceptable signal quality is studied. Discrete Sine / Cosine Transforms are the second method studied in this thesis. The last method that is implemented is the wavelet packet transform method. In this method, different types of wavelet families are used to analyze the effect on *CR* and *PRD* [4].

In the first part, decomposition, uniform quantization, and entropy coding are applied successively to compress the digital ECG signal. In the second part, namely, in the decoder part, entropy decoding, and inverse transformation are applied to reconstruct the original signal.

The performance evaluation parameters, namely *PRD* and *CR* are used to compare one method to another. Two different ECG signals are analyzed, and the results are reported. In all of the four methods, compression of digital ECG signal is realized with the same programming language, MATLAB.

In the early years, direct methods have been used to compress the ECG signals. Due to the higher compression ratios, transform methods are becoming more popular and new transform methods are being investigated for high *CR* and low *PRD* .

1.2 Objectives

The objective of this thesis is to investigate wavelet transform based electrocardiogram (ECG) data compression methods that compress digitized ECG data as much as possible with reasonable implementation complexity while maintaining clinically acceptable signal quality and to compare them with conventional approaches. Different wavelet transform based compression methods, based on both discrete orthonormal wavelet transform (*DOWT*) and on wavelet packet transforms will be studied in detail. The issue of how to guarantee a user-specified error limit measured by the percent root mean square difference (*PRD*) for the reconstructed ECG signal to be controlled at every segment while keeping the compression ratio (*CR*) as large as possible with reasonable implementation complexity will be studied in detail.

1.3 Outline of the Thesis

This chapter introduces the thesis. In Chapter 2, the anatomy and the physiology of the heart, heart's electrical activity and ECG signal components are discussed. The wavelet and the wavelet packet methods are presented in Chapter 3. Basic wavelet functions, continuous and discrete wavelet transforms, one and multi level decomposition and reconstruction issues are presented in the same chapter.

Chapter 4 is related with the other transform methods, namely, Discrete Sine and Cosine Transforms [5].

The digital signal compression issue is handled in the chapter of 5. Compression performance, error criterion, quantization, and LZW coding concepts are defined in the same section.

The 6th chapter is the application and implementation chapter. All the results related with compression methods (*WT* , *WPT* , *DST* , *DCT*) are determined and displayed.

The last section is the result and the conclusion section. The implementation results are submitted in the tables, for every signal, for each wavelet family, and for

different decomposition level. A detailed report is available in the last chapter of this thesis. Suggestion for the future work is also added at the end.

2. THE HEART AND THE ECG SIGNAL

2.1 The Heart

2.1.1 Anatomy and physiology of the heart

The heart whose sole purpose is to circulate blood through the circulatory system consists of four hollow chambers. The anatomy of the heart is displayed in Figure 2.1. The upper two chambers, the right and left atria, are thin-walled; the lower two, the right and left ventricles are thick-walled and muscular. The walls of the ventricles are composed of three layers of tissue: the innermost thin layer is called the endocardium; the middle thick, muscular layer, the myocardium; and the outermost thin layer, the epicardium. The walls of the left ventricle are more muscular and about three times thicker than those of the right ventricle [6].

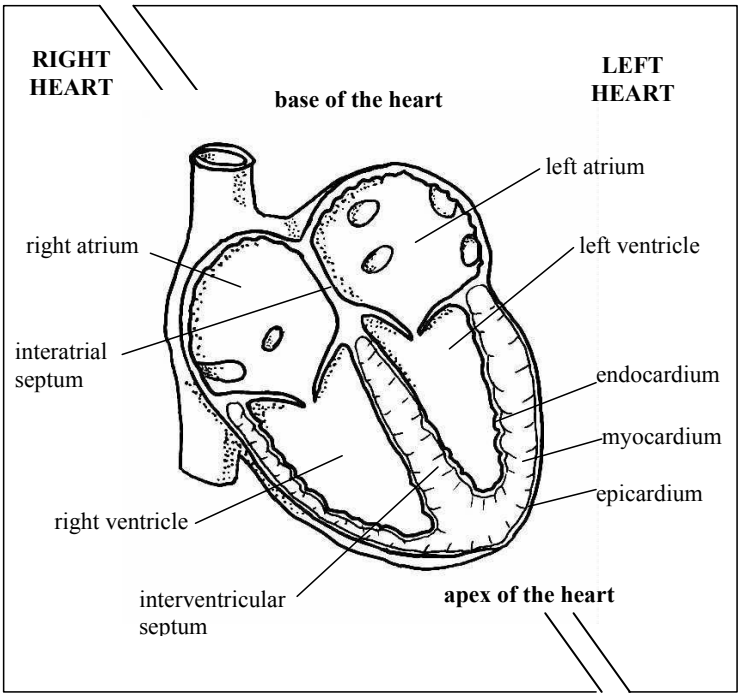

Figure 2.1 Anatomy of the heart.

The atrial walls are also composed of three layers of tissue like those of the ventricles, but the middle muscular layer is much thinner. The two atria form the base of the heart; the ventricles form the apex of the heart.

The interatrial septum (a thin membranous wall) separates the two atria, and a thicker, more muscular wall, the interventricular septum, separates the two ventricles. The two septa, in effect, divide the heart into two pumping systems, the right heart and the left heart, each one consisting of an atrium and a ventricle.

The right heart pumps blood into the pulmonary circulation (the blood vessels within the lungs and those carrying blood to and from the lungs). The left heart pumps blood into the systemic circulation (the blood vessels in the rest of the body and those carrying blood to and from the body).

The right atrium receives unoxygenated blood from the body via two of the body's largest veins (the superior vena cava and inferior vena cava) and from the heart itself by way of the coronary sinus. The blood is delivered to the right ventricle through the tricuspid valve. The right ventricle then pumps the unoxygenated blood through the pulmonic valve and into the lungs via the pulmonary artery. In the lungs, the blood picks up oxygen and releases excess carbon dioxide.

The left atrium receives the newly oxygenated blood from the lungs via the pulmonary veins and delivers it to the left ventricle through the mitral valve. The left ventricle then pumps the oxygenated blood out through the aortic valve and into the aorta, the largest artery in the body. From the aorta, the blood is distributed throughout the body where the blood releases oxygen to the cells and collects carbon dioxide from them.

The heart performs its pumping action over and over in a rhythmic sequence. First, the atria relax (atrial diastole), allowing the blood to pour in from the body and lungs. As the atria fill with blood, the atrial pressure rises above that in the ventricles, forcing the tricuspid and mitral valves to open and allowing the blood to empty rapidly into the relaxed ventricles. Then the atria contract (atrial systole), filling the ventricles to capacity.

Following the contraction of the atria, the pressures in the atria and ventricles equalize, and the tricuspid and mitral valves begin to close. Then, the ventricles contract vigorously, causing the ventricular pressure to rise sharply. The tricuspid and mitral valves close completely, and the aortic and pulmonic valves snap open, allowing the blood to be ejected forcefully into the pulmonary and systemic circulations.

Meanwhile, the atria are again relaxing and filling with blood. As soon as the ventricles empty of blood and begin to relax, the ventricular pressure falls, the aortic and pulmonic valves shut tightly, the tricuspid and mitral valves open, and the rhythmic cardiac sequence begins anew.

The period from the opening of the aortic and pulmonic valves to their closing, during which the ventricles contract and empty of blood, is called ventricular systole. The following period from the closure of the aortic and pulmonic valves to their reopening, during which the ventricles relax and fill with blood, is called ventricular diastole. The sequence of one ventricular systole followed by a ventricular diastole is called the cardiac cycle, commonly defined as the period from the beginning of one heart beat to the beginning of the next.

2.1.2 Electrical conduction system of the heart

The electrical conduction system of the heart which is displayed on Figure 2.2, is composed of the following structures: Sinoatrial (SA) node, Internodal atrial conduction tracts and the interatrial conduction tract (Bachmann's bundle), Atrioventricular (AV) junction consisting of the atrioventricular (AV) node and bundle of His, Right bundle branch, left bundle branch, and left anterior and posterior fascicles, Purkinje network.

The prime function of the electrical conduction system of the heart is to transmit minute electrical impulses from the SA node (where they are normally generated) to the atria and ventricles, causing them to contract.

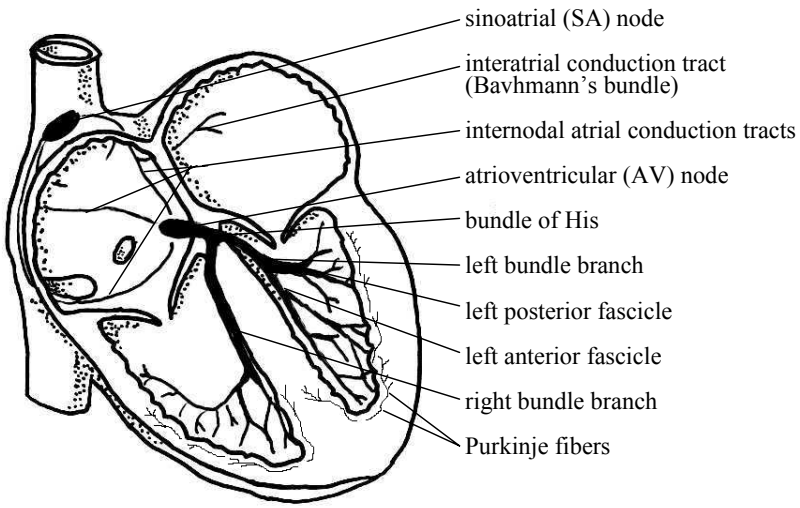

Figure 2.2 Electrical conduction system.

The SA node lies in the wall of the right atrium near the inlet of the superior vena cava. It consists of pacemaker cells that generate electrical impulses automatically and regularly.

The three internodal atrial conduction tracts, running through the walls of the right atrium between the SA node and the AV node, conduct the electrical impulses rapidly from the SA node to the AV node in about 0.03 second. The interatrial conduction tract (Bachmann's bundle), a branch of one of the internodal atrial conduction tracts, extends across the atria, conducting the electrical impulses from the SA node to the left atrium.

The AV node lies partly in the right side of the interatrial septum in front of the opening of the coronary sinus and partly in the upper part of the interventricular septum above the base of the tricuspid valve. The primary function of the AV node is to relay the electrical impulses from the atria into the ventricles in an orderly and timely way. A ring of fibrous tissue insulates the reminder of the atria from the ventricles, preventing electrical impulses from entering the ventricles except through the AV node.

The electrical impulses slow as they travel through the AV node, taking about 0.06 to 0.12 second to reach the bundle of His. The delay is such that the atria can contract and empty, and the ventricles fill before they are stimulated to contract.

The bundle of his lies in the upper part of the interventricular septum connects the AV node with the two bundle branches. Once the electrical impulses enter the bundle of His, they travel more rapidly on their way to the bundle branches, taking 0.03 to 0.05 second.

The right bundle branch and the left common bundle branch arise from the bundle of His, straddle the interventricular septum, and continue down both sides of the septum. The left common bundle branch further divides into two major divisions: the left anterior fascicle and the left posterior fascicle. The bundle branches and their fascicles subdivide into smaller and smaller branches, the smallest ones connecting with the Purkinje network, an intricate web of tiny Purkinje fibers spread widely throughout the ventricles beneath the endocardium. The ends of the Purkinje fibers finally terminate at the myocardial cells. The bundle of His, the right and left bundle branches, and the Purkinje network are also known as the His-Purkinje system of the ventricles.

The electrical impulses travel very rapidly to the Purkinje network through the bundle branches in less than 0.01 second. All in all, it normally takes the electrical impulses less than 0.2 second to travel from the SA node to the Purkinje network in the ventricles.

2.1.3 Electrophysiology of the heart

Cardiac cells are capable of generating and conducting electrical impulses that are responsible for the contraction and relaxation of myocardial cells. These electrical impulses are the result of brief but rapid flow of positively charged ions (primarily sodium and potassium ions and, to a lesser extent, calcium ions) back and forth across the cardiac cell membrane. The difference in the concentration of such ions across the cell membrane at any given instant is called the electrical potential and is measured in millivolts (mV) [6].

When a myocardial cell, for example, is in the resting state, a high concentration of positively charged sodium ions (Na+) (cations) is present outside the cell. At the same time, a high concentration of negatively charged ions (especially organic phosphate ions, organic sulfate ions, and protein ions) (anions) mixed in with a smaller

concentration of positively charged potassium ions (K+) is present inside the cell, making the interior of the cell electrically negative with reference to its positive exterior. Under these conditions, a negative electrical potential exists across the cell membrane. This is made possible by the cell membrane being impermeable to (1) positively charged sodium ions during the resting state and (2) negatively charged phosphate, sulfate, and protein ions at all times. When a cell membrane is impermeable to an ion, it does not permit the free flow of that ion across it.

The resting cardiac cell can be depicted as having a layer of positive ions surrounding the cell membrane and an equal number of negative ions lining the inside of the cell membrane directly opposite each positive ion. When the ions are so aligned, the resting cell is called polarized.

The electrical potential across the membrane of a resting cardiac cell is called the resting membrane potential. The resting membrane potential in atrial and ventricular myocardial cells and the specialized cells of the electrical conduction system (except those of the SA and AV nodes) is normally –90 mV. It is somewhat less in the SA and AV nodal cells, –70 mV.

Upon stimulation by an electrical impulse, the membrane of a polarized myocardial cell, for example, becomes permeable to positively charged sodium ions, allowing sodium to flow into the cell. This causes the interior of the cell to become less negative. When the membrane potential drops to about –60 mV from its resting potential of –90 mV, large pore in the membrane (the fast sodium channels) momentarily opens. These channels facilitate the rapid, free flow of sodium across the cell membrane, resulting in a sudden large influx of positively charged sodium ions into the cell. This causes the exterior of the cell to become rapidly negative with respect to the now positive interior. At the moment when the interior of the cell becomes maximally positive and the exterior maximally negative, the cell is depolarized. The process by which the cell's resting, polarized state is reversed is called depolarization.

The fast sodium channels are typically found in the myocardial cells and the specialized cells of the electrical conduction system other than those of the SA and AV nodes. The cells of the SA and AV nodes have, instead of fast sodium channels slow

calcium-sodium channels the open when the membrane potential drops to about –50 mV. They permit the entry of positively charged calcium and sodium ions into the cells during depolarization at a slow and gradual rate. The result is a slower rate of depolarization as compared to the depolarization of cardiac cells with fast sodium channels.

As soon as a cardiac cell depolarizes, positively charged potassium ions flow out of the cell, initiating a process by which the cell returns to its resting, polarized state. This process, called repolarization, involves a complex exchange of sodium, calcium, and potassium ions across the cell membrane.

Depolarization of one cardiac cell acts as an electrical impulse (or stimulus) to adjacent cells and causes them to depolarize. The propagation of the electrical impulse from cell to cell produces a wave of depolarization which can be measured as an electric current flowing in the direction of depolarization. As the cells repolarize, another electric current is produced, similar to, but opposite in direction to, the first one. The direction of flow and magnitude of the electric currents generated by the depolarization and repolarization of the myocardial cells of the atria and ventricles can be detected by surface electrodes and recorded as the electrocardiogram (ECG). Depolarization of the myocardial cells produces the P wave and QRS complex, and repolarization of the cells results in the T wave in the electrocardiogram. At below, depolarization and repolarization of a muscle fiber is depicted on Figure 2.3 [6].

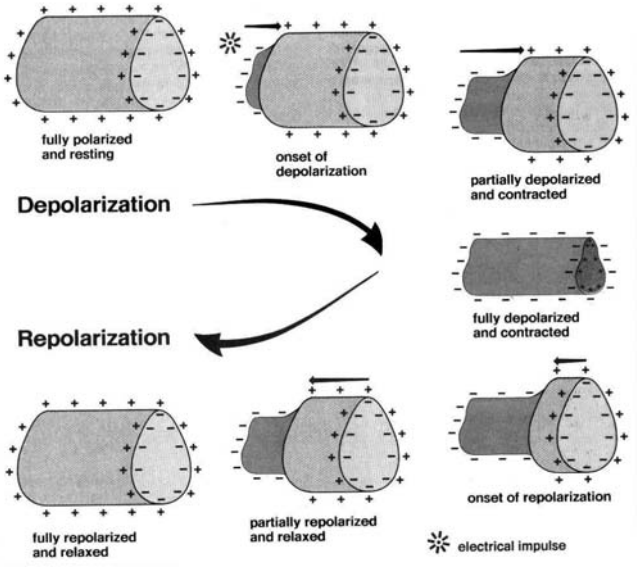

Figure 2.3 Depolarization and repolarization of a muscle fiber.

2.2 The Electrocardiogram

2.2.1 Electrical basis of the electrocardiogram

The electrocardiogram (ECG) is a graphic record of the changes in magnitude and direction of the electrical activity, or, more specifically, the electric current, that is generated by the depolarization and repolarization of the atria and ventricles. The electrical basis of the ECG is displayed on Figure 2.4. This electrical activity is readily detected by electrodes attached to the skin. But neither the electrical activity that results from the generation and transmission of electrical impulses which are too feeble to be detected by skin electrodes nor the mechanical contractions and relaxations of the atria and ventricles (which do not generate electrical activity) appear in the electrocardiogram.

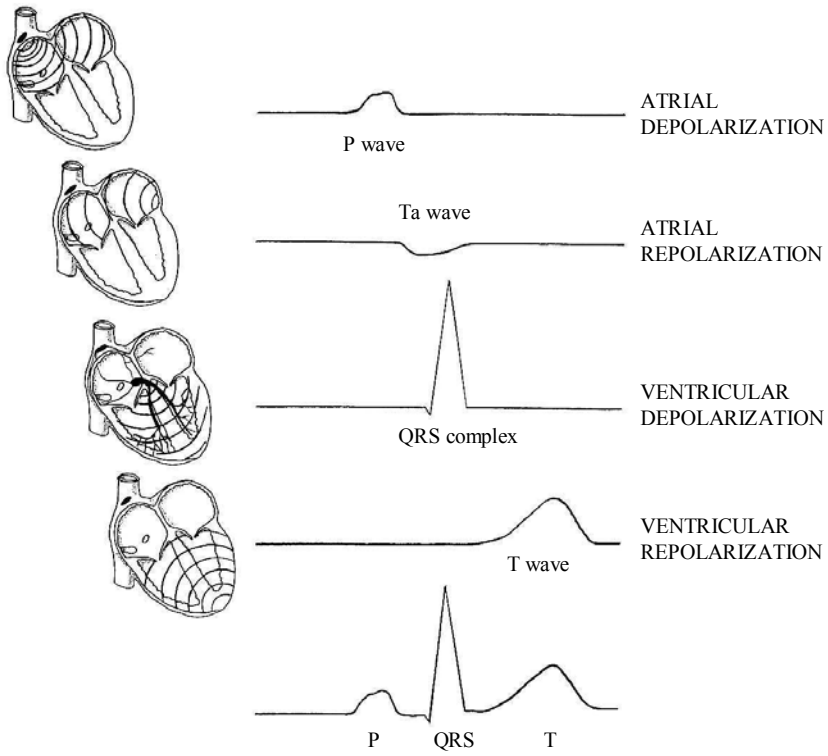

Figure 2.4 Electrical basis of the ECG.

2.2.2 Components of the electrocardiogram

After the electric current generated by depolarization and repolarization of the atria and ventricles is detected by electrodes, it is amplified, displayed on an oscilloscope, recorded on ECG paper, or stored in memory. The electric current generated by atrial depolarization is recorded as the P wave, and that generated by ventricular depolarization is recorded as the Q, R and S waves: the QRS complex. Atrial repolarization is recorded as the atrial T wave (Ta), and ventricular repolarization, as the ventricular T wave, or simply, the T wave. Because atrial repolarization normally occurs during ventricular depolarization, the atrial T wave is buried or hidden in the QRS complex. [6].

In a normal cardiac cycle, the P wave occurs first, followed by the QRS complex and the T wave, shown in Figure 2.5.

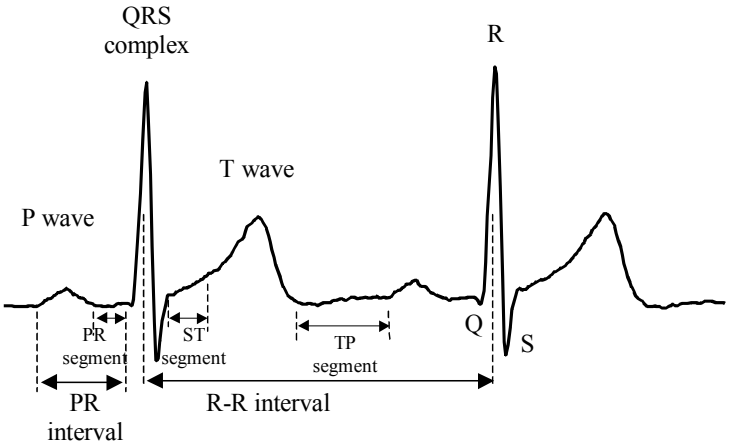

Figure 2.5 Components of the ECG.

The sections of the ECG between the waves and complexes are called segments and intervals: the PR segment, the ST segment, the TP segment, the PR interval, the QT interval, and the R-R interval. Intervals include waves and complexes, whereas segments do not [6].

When electrical activity of the heart is not being detected, the ECG is a straight, flat line the isoelectric line or baseline.

2.2.3 ECG leads

An ECG lead is a record (spatial sampling) of the electrical activity generated by the heart that is sensed by either one of two ways: (1) two discrete electrodes of opposite polarity or (2) one discrete positive electrode and an indifferent, zero reference point. A lead composed of two discrete electrodes of opposite polarity is called a bipolar lead; a lead composed of a single discrete positive electrode and a zero reference point is a unipolar lead.

Depending on the ECG lead being recorded, the positive electrode may be attached to the right or left arm, the left leg, or one of several locations on the anterior chest wall. The negative electrode is usually attached to an opposite arm or leg or to a reference point made by connecting the limb electrodes together.

For a detailed analysis of the heart's electrical activity, usually in the hospital setting, an ECG recorded from 12 separate leads (the 12-lead ECG) is used. The 12-lead ECG is also used in the pre hospital phase of emergency care in certain advanced life support services to diagnose acute myocardial infraction and to help in the identification of certain arrhythmias. A 12-lead ECG consists of three standard (bipolar) limb leads (leads I, II, and III), three augmented (unipolar) leads (leads aVR, aVL, and aVF) and six precordial (unipolar) leads (V1, V2, V3, V4, V5, and V6).

When monitoring the heart solely for arrhythmias, a single ECG lead, such as the standard limb lead II, is commonly used, especially in the prehospital phase of emergency care. The combinations of the leads are displayed on the Figures 2.6, 2.7, and 2.8 succesively [6].

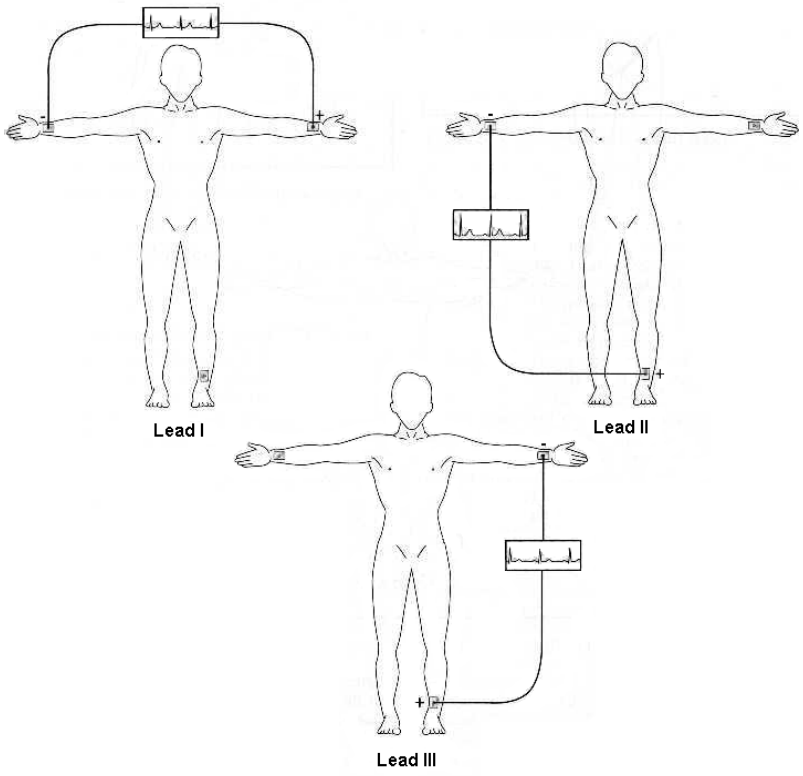

Figure 2.6 The standard (bipolar) limb leads I, II, and III.

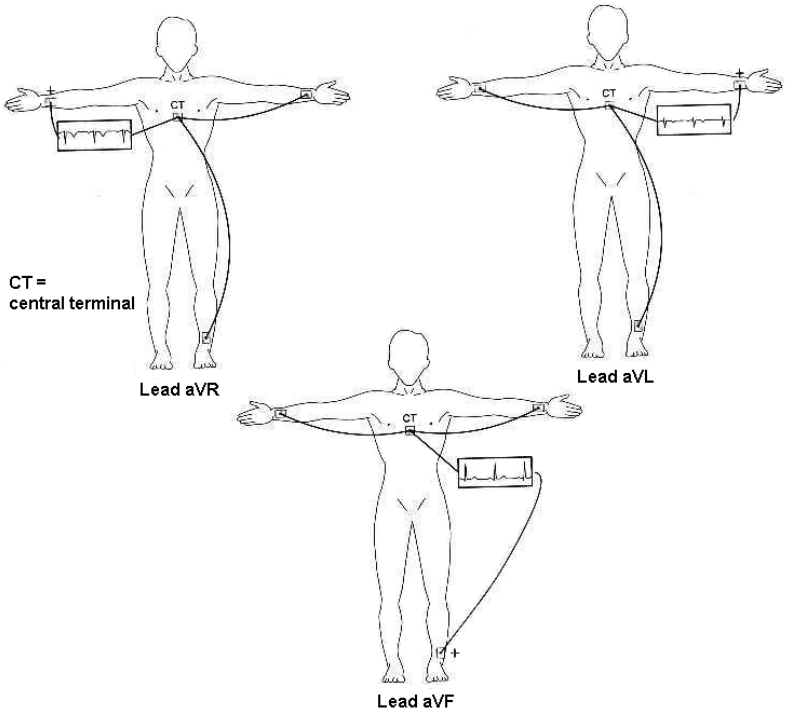

Figure 2.7 The augmented (unipolar) leads aVR, aVL, and aVF.

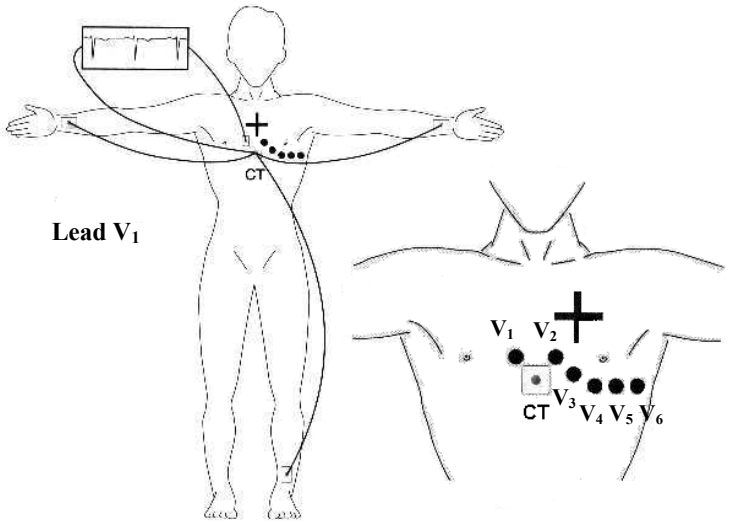

Figure 2.8 Precordial (unipolar) leads.

2.3 MIT-BIH Database

The database used in this work is a collection of files from the MIT-BIH Database CD-ROM. This database is accessible via the internet portal: http://ecg.mit.edu. Here, the digital data is stored in three formats: Header (.hea) file, attribute (.atr) file, and the data (.dat) file.

The ECG recordings in the MIT-BIH database are taken as a reference data by the researchers who are studying on compression, storing, classification of digital ECG signals. At this work, standard digital ECG signal (.dat file) is taken as a reference and used in the implementation phase [7].

3. WAVELETS AND WAVELET PACKETS

3.1 Introduction

This section presents some background information on wavelets and wavelet transforms, including their implementation using filters. This theory is necessary for understanding the material that follows in the literature review and certain other sections of the thesis.

3.2 Fourier Transform

This part develops the need and motivation for studying the wavelet transform. Historically Fourier Transform (FT) has been the most widely used tool for signal processing. As signal processing began spreading Fourier Transform was found to be unable to satisfy the growing need for processing a bulk of signals. Hence, this section begins with a review of Fourier Methods. The shortcoming of Fourier methods is determined. Next, wavelet transform is concerned and expounded how the drawbacks of FT are eliminated [1].

For a continuous time signal $x(t)$ the Fourier Transform equations are as follows.

$$X(f) = \int_{-\infty}^{+\infty} x(t).e^{-j2\pi ft} dt \tag{3.1}$$

$$x(t) = \int_{-\infty}^{+\infty} X(f).e^{j2\pi ft} df \tag{3.2}$$

Equation 3.1 is the analysis equation and Equation 3.2 is the synthesis equation. The sinusoid with different frequencies is displayed on Figure 3.1.

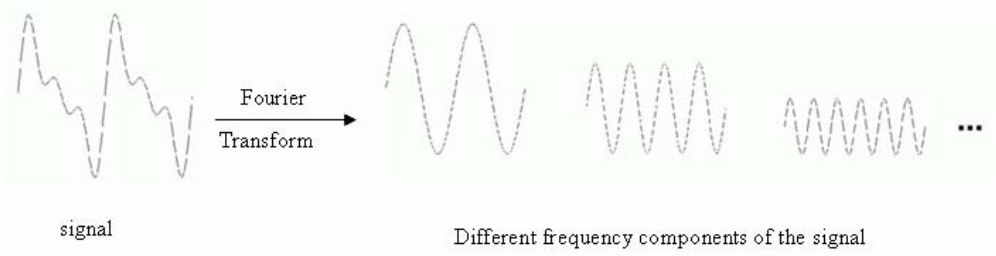

Figure 3.1 Constituent sinusoids of different frequencies.

The synthesis equation suggests that the FT expresses the signal in terms of linear combination of complex exponential signal. For a real signal, it can be shown that the FT synthesis equation expresses the signal in terms of linear combination of sine and cosine terms [8]. A diagrammatic representation of this is depicted on Figure 3.2:

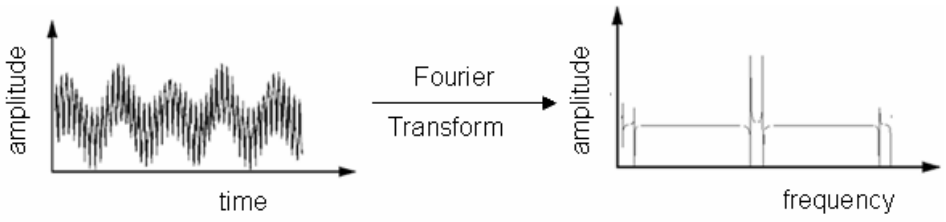

Figure 3.2 Frequency domain transition.

The analysis equation represents the given signal in a different form; as a function of frequency. The original signal is a function of time, whereas the after the transformation, the same signal is represented as a function of frequency. It gives the frequency components in the signal.

Thus the FT is a very useful tool as it gives the frequency content of the input signal it however suffers from a serious drawback. It shows that the FT is unable to distinguish between two different signals. The two signals have same frequency components, but at different times. Thus, the FT is incapable of giving time information of signals. In general, FT is not suitable for the analysis of a class of signals called non-stationary signals [1].

This led to the search of new tools for analysis of signals. One such tool that was proposed was the Short Time Fourier Transform (STFT). STFT has a drawback and was supplanted by Wavelet Transform.

3.3 The Continuous Wavelet Transform

Consider a real or complex-valued continuous-time function $\psi(t)$ with the following properties.

The function integrates to zero

$$\int_{-\infty}^{+\infty} \psi(t)dt = 0 \tag{3.3}$$

It is square integrable or, equivalently, has finite energy:

$$\int_{-\infty}^{+\infty} |\psi(t)|^2 dt < \infty \tag{3.4}$$

A function is called mother wavelet if it satisfies these two properties. The simplest of them is the Haar wavelet. Some other wavelets are Mexican hat, Morlet. Apart from this, there are various families of wavelets. Some of the families are daubechies family, symlet family, coiflet family etc. In this thesis, the main stress is given on the Daubechies family, which has db1 to db10 wavelets [8]. They are shown in the following figures, namely Figures 3.3 and 3.4.

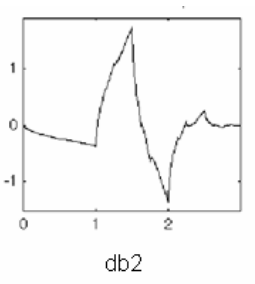

Figure 3.3 Db2 wavelet.

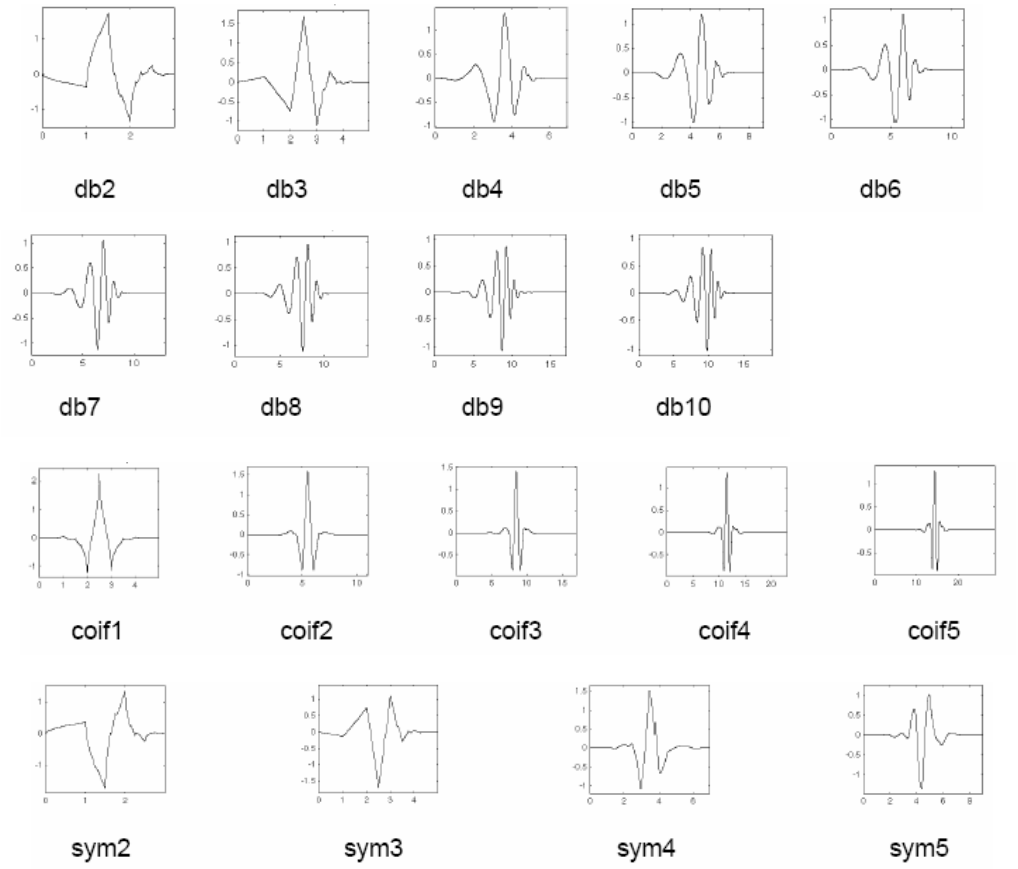

Figure 3.4 Samples of wavelet functions.

As has already been pointed out, wavelet is a waveform of effectively limited duration that has an average value of zero. Compare wavelets with sine waves, which are the basis of Fourier analysis. Sinusoids do not have limited duration, they extend

from minus to plus infinity and where sinusoids are smooth and predictable, wavelets tend to be irregular and asymmetric [8].

Fourier analysis consists of breaking up a signal into sine waves of various Frequencies. Similarly, wavelet analysis is the breaking up of a signal into shifted and scaled versions of the original (or mother) wavelet shown in Figure 3.5.

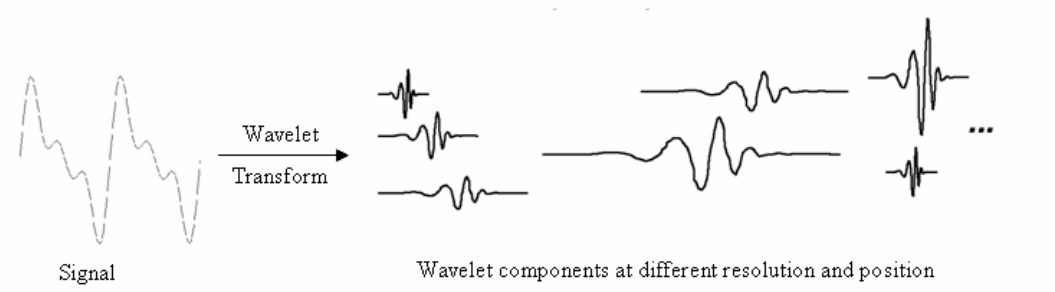

Figure 3.5 Signal decomposition into wavelets.

The above diagram suggests the existence of a synthesis equation to represent the original signal as a linear combination of wavelets which are the basis function for wavelet analysis (recollect that in Fourier analysis, the basis functions are sines and cosines). This is indeed the case. The wavelets in the synthesis equation are multiplied by scalars. To obtain these scalars, an analysis equation is required, just as in the Fourier case.

There are two equations, the analysis and the synthesis equation. They are stated as follows [8]:

Analysis equation or CWT equation:

$$C(a,b) = \int_{-\infty}^{+\infty} f(t) \frac{1}{\sqrt{|a|}} \psi^* \left\{ \frac{t-b}{a} \right\} dt \tag{3.5}$$

Synthesis equation or ICWT:

$$f(t) = \frac{1}{K} \int_{a=-\infty}^{+\infty} \int_{b=-\infty}^{+\infty} \frac{1}{|a|^2} C(a,b) \frac{1}{\sqrt{|a|}} \psi \left\{ \frac{t-b}{a} \right\} d(a) d(b) \tag{3.6}$$

K is a constant; it depends on the wavelet

The basis functions in both Fourier and wavelet analysis are localized in frequency making mathematical tools such as power spectra (power in a frequency interval) useful at picking out frequencies and calculating power distributions.

The most important difference between these two kinds of transforms is that individual wavelet functions are localized in space. In contrast Fourier sine and cosine functions are non-local and are active for all time t.

This localization feature, along with wavelets localization of frequency, makes many functions and operators using wavelets sparse, when transformed into the wavelet domain. This sparseness, in turn results in a number of useful applications such as data compression, detecting features in images and denoising signals.

The quantities a and b appearing in the above equations represent the scale and shift of mother wavelet, respectively.

The wavelet transform of a signal $f(t)$ is the family $C(a,b)$ given by the analysis equation. It depends on two indices a and b. From an intuitive point of view, the wavelet decomposition consists of calculating a "resemblance index" between the signal and the wavelet located at position b and of scale a. If the index is large, the resemblance is strong, otherwise it is slight. The indexes $C(a,b)$ are called coefficients. The dependence of these coefficients on both a and b is responsible for the wavelet transform K is a constant; it depends on the wavelet preserving time and frequency information. These quantities are explained in the following sections [8].

3.3.1 Scaling

Simply put scaling a wavelet means stretching (or compressing) it. To go beyond colloquial descriptions such as stretching, the scale factor often denoted by the letter a. If sinusoids are thought, for example, the effect of the scale factor is very easy to see:

$$f(t) = \begin{Bmatrix} \sin(t), & \text{a} = 1 \\ \sin(2t), & \text{a} = 1/2 \\ \sin(4t), & \text{a} = 1/4 \end{Bmatrix} \tag{3.7}$$

The scale factor works exactly the same with wavelets. The smaller the scale factor, the more compressed the wavelet and vice versa.

It is clear from the diagrams that, for a sinusoid, $Sin(wt)$ the scale factor is related (inversely) to the radian frequency w. Similarly, with wavelet analysis, the scale is related to the frequency of the signal. Thus the higher scales correspond to the most stretched wavelets. The more stretched the wavelet, the longer the portion of the signal with which it is being compared, and thus the coarser the signal features being measured by the wavelet coefficients [8]. The effect of scaling factor is displayed on Figure 3.6.

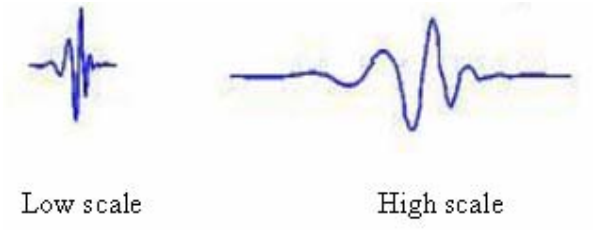

Figure 3.6 The effect of scaling factor.

Thus, there is a correspondence between wavelet scales and frequency as revealed by wavelet analysis:

$$\text{low scale (a)} \rightarrow \text{compressed wavelet} \rightarrow \text{rapidly changing} \rightarrow \text{high frequncy (w)}$$

$$\text{high scale (a)} \rightarrow \text{stretched wavelet} \rightarrow \text{slowly changing} \rightarrow \text{low frequency (w)}$$

3.3.2 Shifting

Shifting a wavelet simply means delaying its onset. Mathematically, delaying a function $f(t)$ by b is represented by $f(t-b)$ and shown in Figure 3.7.

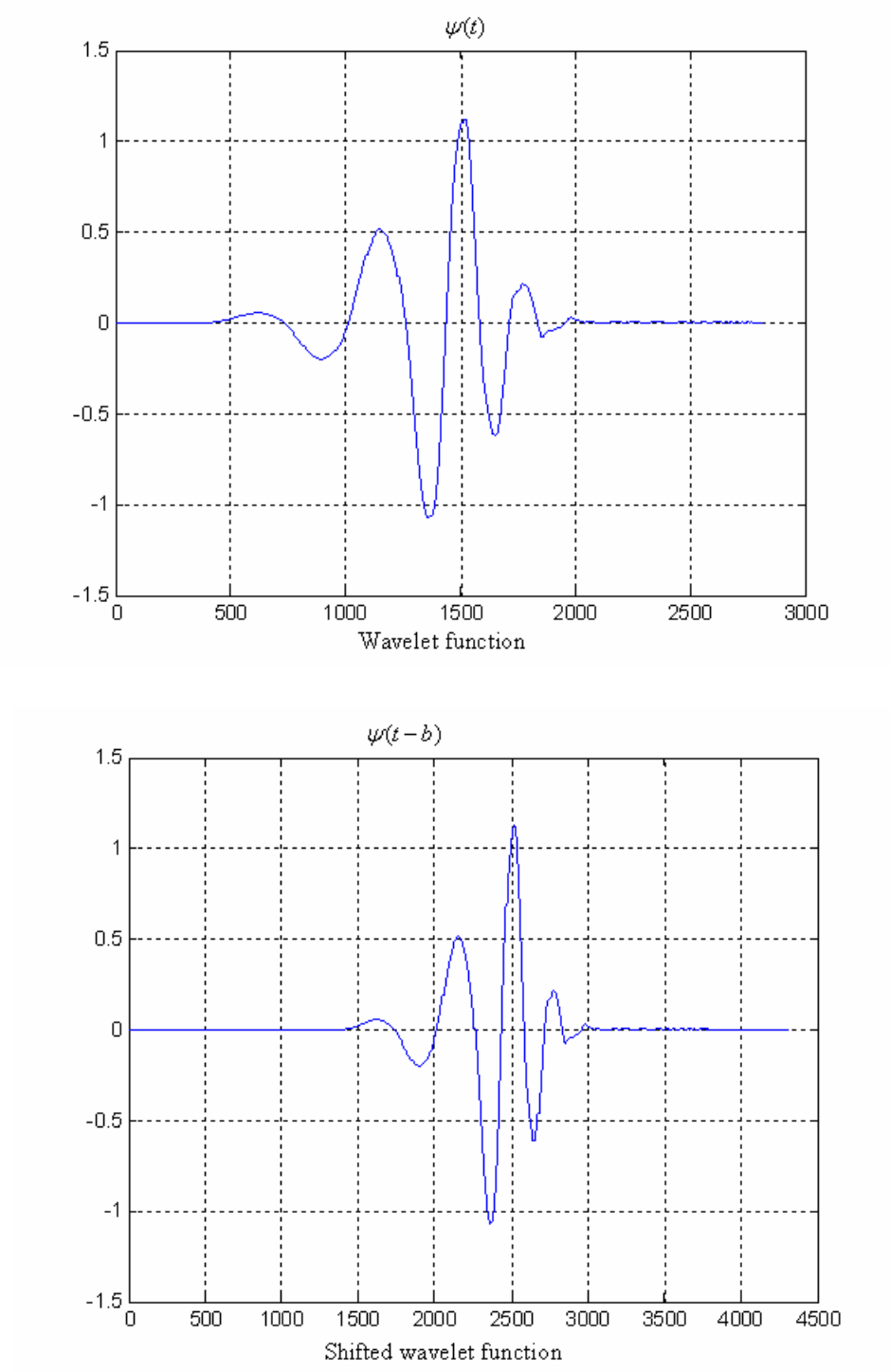

Figure 3.7 Wavelet shifting.

Most important feature of the wavelet transform is the orthogonality. If the wavelet transform of $\psi(t)$ is orthogonal to its scaled and shifted versions, this orthogonal wavelet is known as mother wavelet [9]. The required features of the orthogonal wavelets are defined in the following lines [8].

$$\int_{-\infty}^{+\infty} \phi(t-n)\phi(t-m)dt = \delta(n-m) \tag{3.8}$$

$\phi(t)$ is the scaling function $\delta(n-m)$ delta function

$$\int_{-\infty}^{+\infty} \phi(t-m)\psi(t-n)dt = 0 \tag{3.9}$$

Scaling function is orthogonal to its wavelet

$$\int_{-\infty}^{+\infty} \psi_{jk}(t)\psi_{JK}(t)dt = \delta(j-J)\delta(k-K) \tag{3.10}$$

Reproduced wavelets (child wavelet) are orthogonal to one another. Orthogonality equation is defined as $\sum_{n=0}^{2N-1} c(n)c(n-k) = \delta(k)$, $k = 0,1,2,...,2N-1$ [8].

3.4 Discrete Wavelet Transform

3.4.1 Wavelet decomposition

The Discrete Wavelet Transform (DWT) involves choosing scales and positions based on powers of two the so called dyadic scales and positions. The mother wavelet is rescaled or dilated by powers of two and translated by integers. Specifically, a function $f(t) \in L^2(R)$ can be represented as

$$f(t) = \sum_{j=1}^{L} \sum_{k=-\infty}^{+\infty} d(j,k)\psi(2^{-j}t-k) + \sum_{k=-\infty}^{+\infty} a(L,k)\phi(2^{-L}t-k) \tag{3.11}$$

The function $\psi(t)$ is known as the mother wavelet, while $\phi(t)$ is known as the scaling function. The set of functions

$\left\{\sqrt{2^{-L}}\phi(2^{-L}t-k), \sqrt{2^{-j}}\psi(2^{-j}t-k); j \le L; j, K, L \in Z\right\}$, where Z is the set of integers. It is an orthonormal basis for $L^2(R)$ [8].

The numbers $a(L,k)$ are known as the approximation coefficients at scale L, while $d(j,k)$ are known as the detail coefficients at scale j [8]. These approximation and detail coefficients can be expressed as

$$a(L,k) = \frac{1}{\sqrt{2^L}} \int_{-\infty}^{+\infty} f(t)\phi(2^{-L}t-k)dt \tag{3.12}$$

$$d(j,k) = \frac{1}{\sqrt{2^j}} \int_{-\infty}^{+\infty} f(t)\psi(2^{-j}t-k)dt \tag{3.13}$$

The above 2 equations give a mathematical relationship to compute the approximation and detail coefficients.

This procedure is seldom adopted. A more practical approach is to use Mallat's Fast Wavelet Transform algorithm. The Mallat algorithm for discrete wavelet transform (*DWT*) is, in fact, a classical scheme in the signal processing community, known as a two channel sub band coder using conjugate quadrature filters or quadrature mirror filters (QMF). It is developed in the following sections.

For many signals, the low-frequency content is the most important the signal its identity. The high frequency content imparts nuance. Consider the human voice. If you remove the high-voice sounds different, but you can still tell what's being enough of the low-frequency components, you hear gibberish.

In wavelet analysis, approximations and details are so important. The approximations are the high-scale, low-frequency components of the signal. The details are the low-scale, high-frequency components [8].

The filtering process, at its most basic level, looks like this: The original signal, S, passes through two complementary filters and emerges as two signals.

Unfortunately, if this operation is performed on a real digital signal, it is obtained with twice as much data as it is started with. Suppose, for instance, that the original signal S consists of 1000 samples of data. Then the resulting signals will each have 1000 samples, for a total of 2000. At below, one stage filtering is depicted on Figure 3.8.

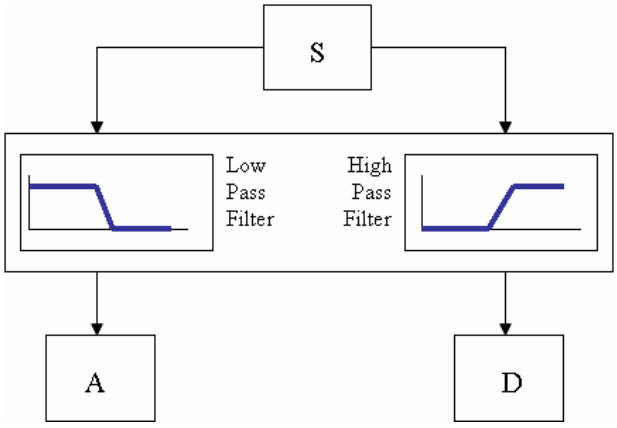

Figure 3.8 One-stage filtering.

These signals A and D are interesting, but 2000 values it is obtained instead of the 1000. There exists a more subtle way to perform the decomposition using wavelets. By looking carefully at the computation, it is required to keep only one point out of two in each of the two 2000-length samples to get the complete information. This is the notion of down sampling. Two sequences are produced called *CA* and *CD*, displayed on Figure 3.9.

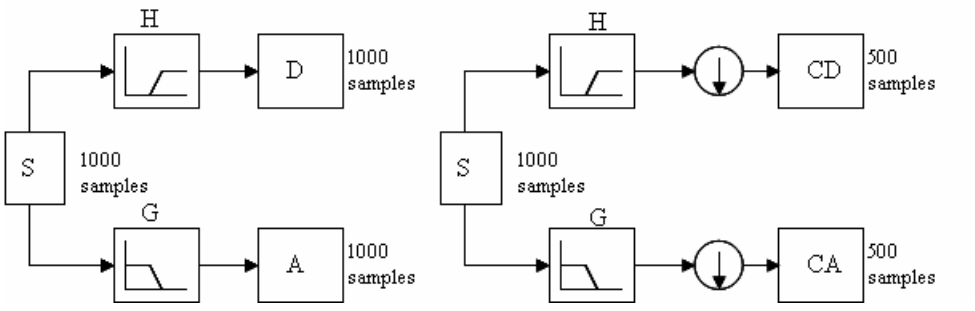

Figure 3.9 Approximation and detail coefficients generation at one-stage.

The process on the right, which includes down sampling, produces *DWT* coefficients. It may be observed that the actual lengths of the detail and approximation coefficient vectors are slightly more than half the length of the original signal. This has to do with the filtering process, which is implemented by convolving the signal with a filter. The convolution "smears" the signal, introducing several extra samples into the result.

In this section, it is considered only one-stage decomposition of the signal into *CA* and *CD* coefficient. This process can be repeated to get multiple-level decomposition, discussed next.

The decomposition process can be iterated, with successive approximations being decomposed in turn, so that one signal is broken down into many lower resolution components. This is called the wavelet decomposition tree and shown in Figure 3.10 [8].

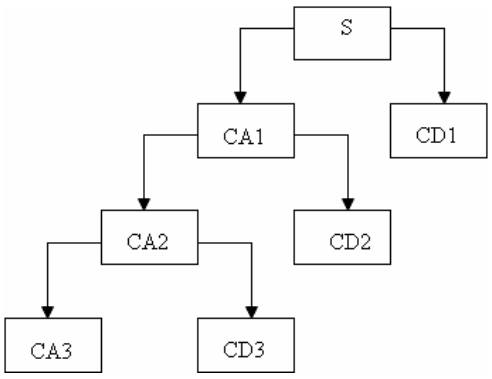

Figure 3.10 Multiple-level decomposition.

Since the analysis process is iterative, in theory it can be continued indefinitely. In reality, the decomposition can proceed only until the individual details consist of a single sample or pixel. In practice, you'll select a suitable number of levels based on the nature of the signal, or on a suitable criterion such as entropy. Thus the fast wavelet transform algorithm can be stated as:

Given a signal s of length N, the DWT consists of $\log_2 N$ stages at most. Starting from S, the first step produces two sets of coefficients: approximation coefficient CA_1 and detail coefficient CD_1. These vectors are obtained by convolving s with the low-pass filter Lo_D for approximation, and with the high-pass filter Hi_D for detail, followed by dyadic decimation [8].

The next step splits the approximation coefficients CA_1 in two parts using the same scheme, replacing s by CA_1 and producing CA_2 and CD_2 and so on.

Now that it is seen the decomposition of a signal into wavelet (approximation and detail) coefficient s, it is natural to ask whether the reverse is possible, i.e., is it possible to generate the original signal back from the coefficients, and if yes, how to achieve this. Fortunately, there does exist a method to do it, and it is very similar to the one used for decomposition. The next few sections demonstrate this.

The first level approximation and detail components of the original signal that is shown in Figure 3.11, is displayed in Figure 3.12.

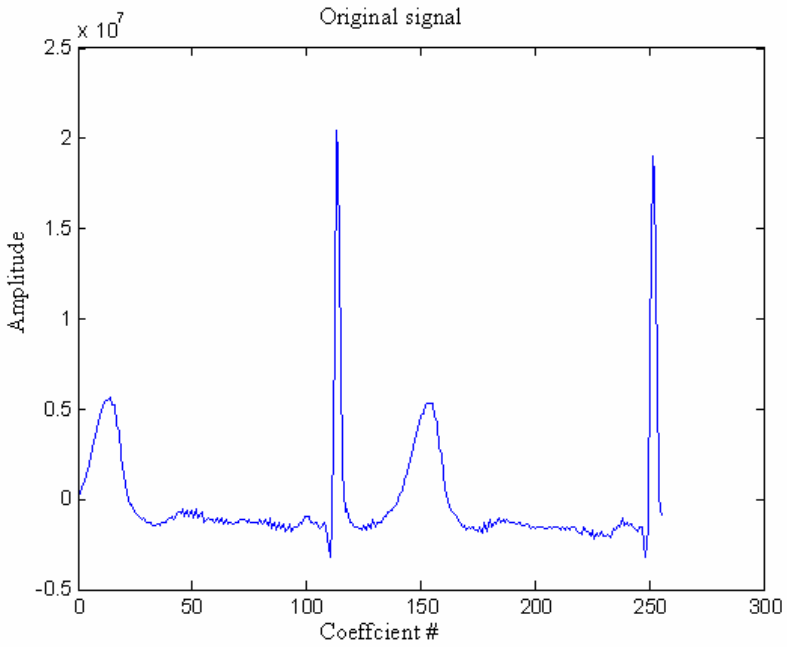

Figure 3.11 original signals [0-256].

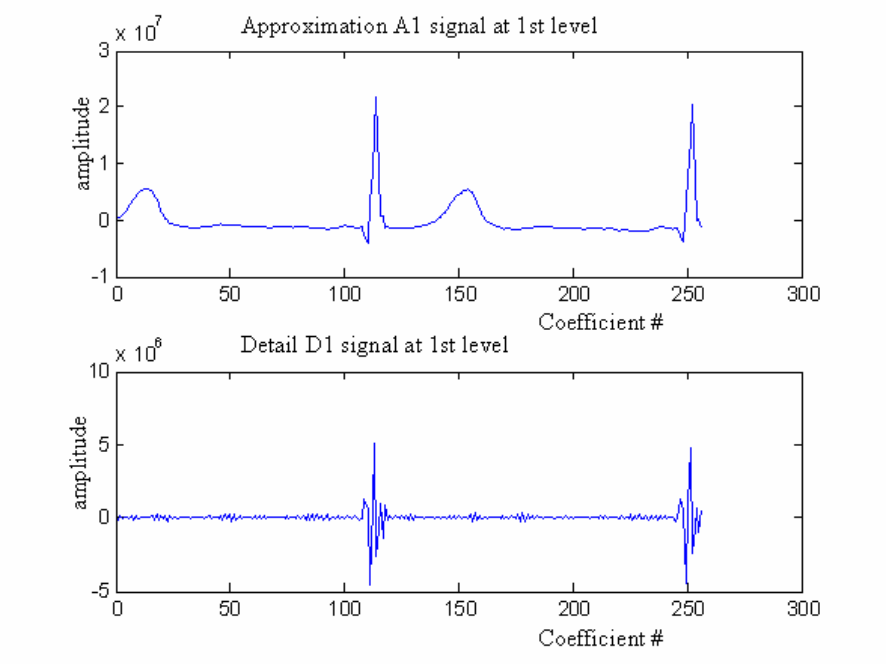

Figure 3.12 Approximation and detail signal components [0-256].

3.4.2 Wavelet reconstruction

It has been investigated how the discrete wavelet transform can be used to analyze, or decompose, signals and images. This process is called decomposition or analysis. The other half of the story is how those components can be assembled back into the original signal without loss of information. This process is called reconstruction, or synthesis. The mathematical manipulation that affects synthesis is called the inverse discrete wavelet transform (*IDWT*). To synthesize a signal, it is reconstructed from the wavelet coefficients [8].

Where wavelet analysis involves filtering and down sampling, the wavelet reconstruction process consists of up sampling and filtering. Up sampling is the process of lengthening a signal component by inserting zeros between samples, is depicted on Figure 3.13 and Figure 3.14, as follows.

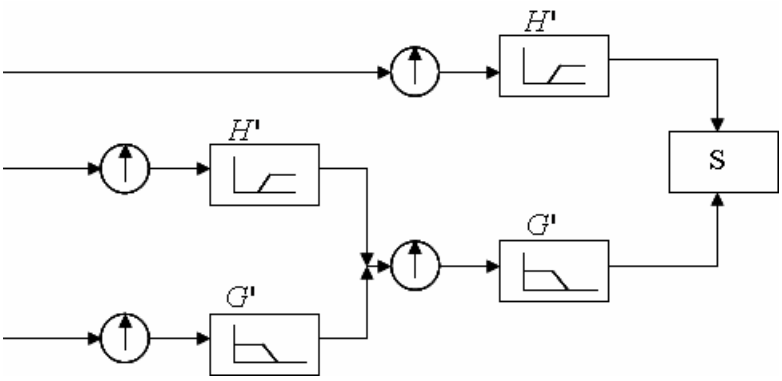

Figure 3.13 Reconstructing the original signal from the wavelet coefficients.

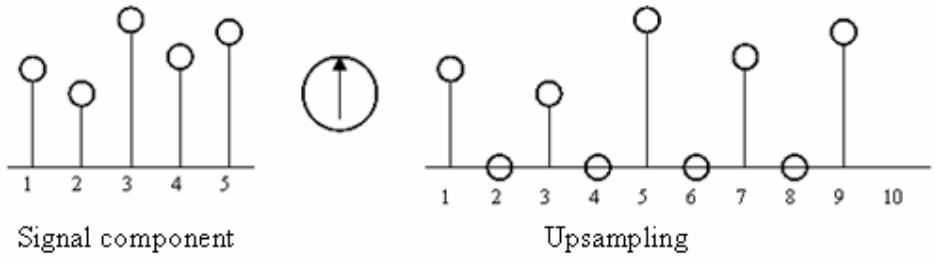

Figure 3.14 Up sampling process.

The filtering part of the reconstruction process also bears some discussion, because it is the choice of filters that is crucial in achieving perfect reconstruction of the original signal. The down sampling of the signal components performed during the decomposition phase introduces a distortion called aliasing. It turns out that by carefully choosing filters for the decomposition and reconstruction phases that are closely related (but not identical); it can be cancelled out the effects of aliasing. The low-and high pass decomposition filters (L and H), together with their associated reconstruction filters (L'and H') form a system of what is called quadrature mirror filters. The decomposition and reconstruction process is shown in Figure 3.15

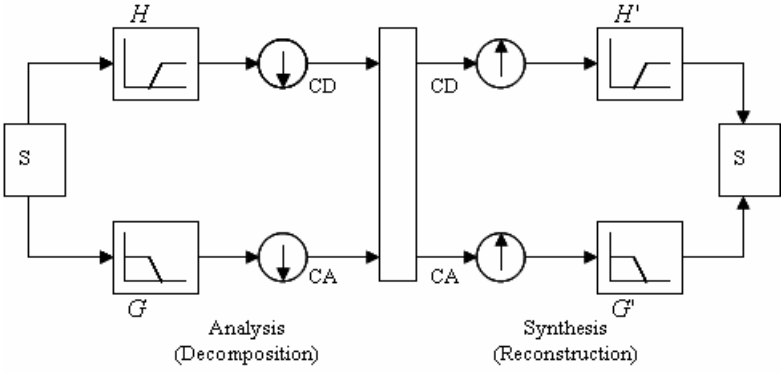

Figure 3.15 Decomposition and reconstruction process.

As an example, let's consider how it would be reconstructed the first-level approximation $A1$ from the coefficient vector CA_1. The coefficient vector CA_1 is passed through the same process that is used to reconstruct the original signal. However, instead of combining it with the level-one detail CD_1 a vector of zeros is provided in place of the detail coefficients vector is displayed on Figure 3.16:

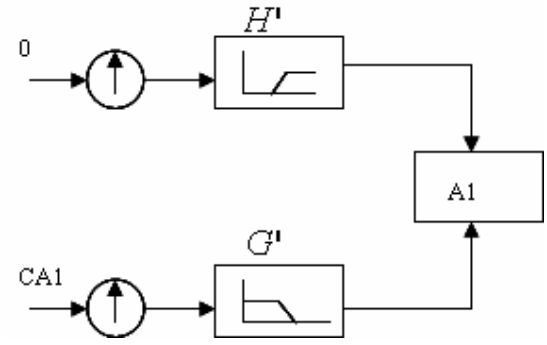

Figure 3.16 Reconstruction of approximation A1

The process yields a reconstructed approximation A_1, which has the same length as the original signal S and which is a real approximation of it. Similarly, it can be reconstructed the first-level detail D_1, using the analogous process, depicted on Figure 3.17.

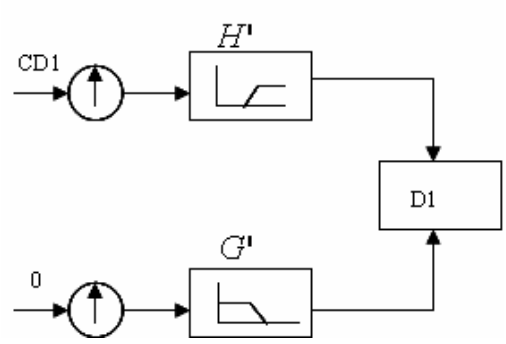

Figure 3.17 Reconstruction of detail D1.

The reconstructed details and approximations are true constituents of the original signal. In fact, they can be combined as:

$$A_1 + D_1 = S \tag{3.14}$$

Note that the coefficient vectors CA_1 and CD_1 because they were produced by down sampling and are only half the length of the original signal cannot directly be combined to reproduce the signal. It is necessary to reconstruct the approximations and details before combining them. Extending this technique to the components of a multilevel analysis, it is found that similar relationships hold for all the reconstructed signal constituents. That is, there are several ways to reassemble the original signal. This process is displayed on Figure 3.18.

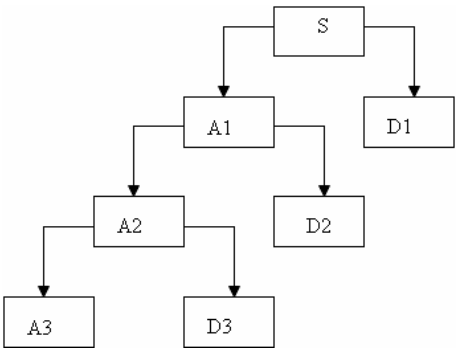

Figure 3.18 Reassembling the original signal.

$$S = A_1 + D_1 \tag{3.15}$$

$$S = A_2 + D_2 + D_1 \tag{3.16}$$

$$S = A_3 + D_3 + D_2 + D_1 \tag{3.17}$$

A multistep analysis-synthesis process is represented in Figure 3.19.

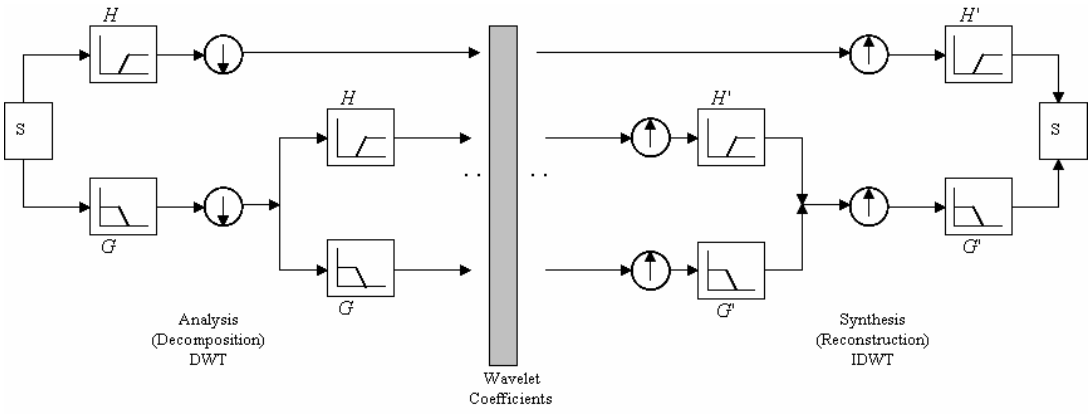

Figure 3.19 Multistep decomposition and reconstruction.

This process involves two aspects: breaking up a signal to its high and the low frequency components, to obtain the wavelet coefficients, and assembling the signal from the coefficients to obtain the original one

In the previous figures, it is shown that the approximations and detail components of the signal is obtained by decomposition at the first level. This process is displayed on Figure 3.20. Besides, the reconstructed signal is displayed on the following figure, namely Figure 3.21.

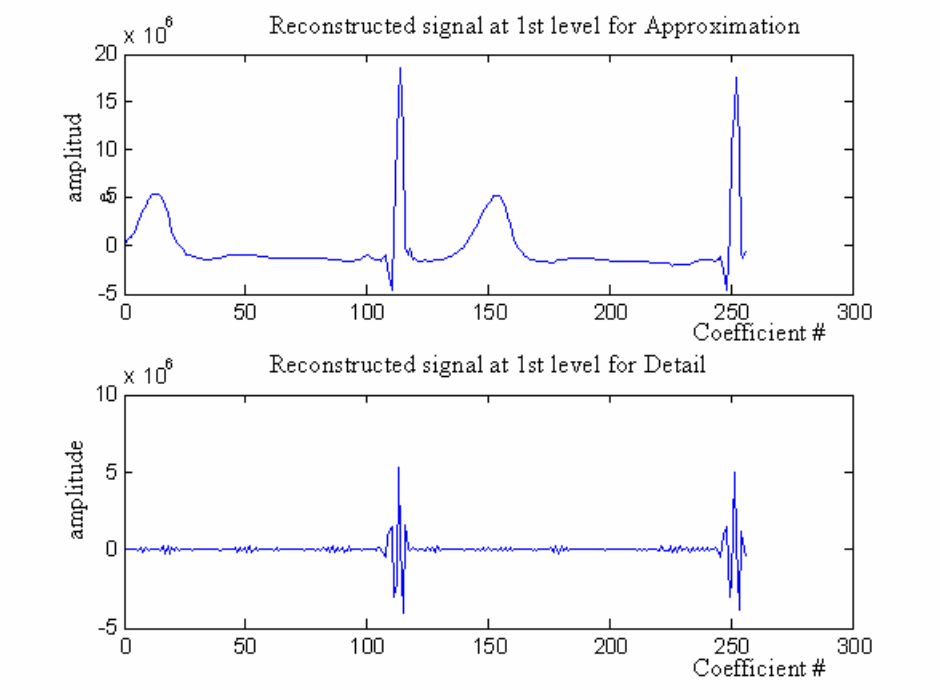

Figure 3.20 Reconstruction of the signal component at 1st level

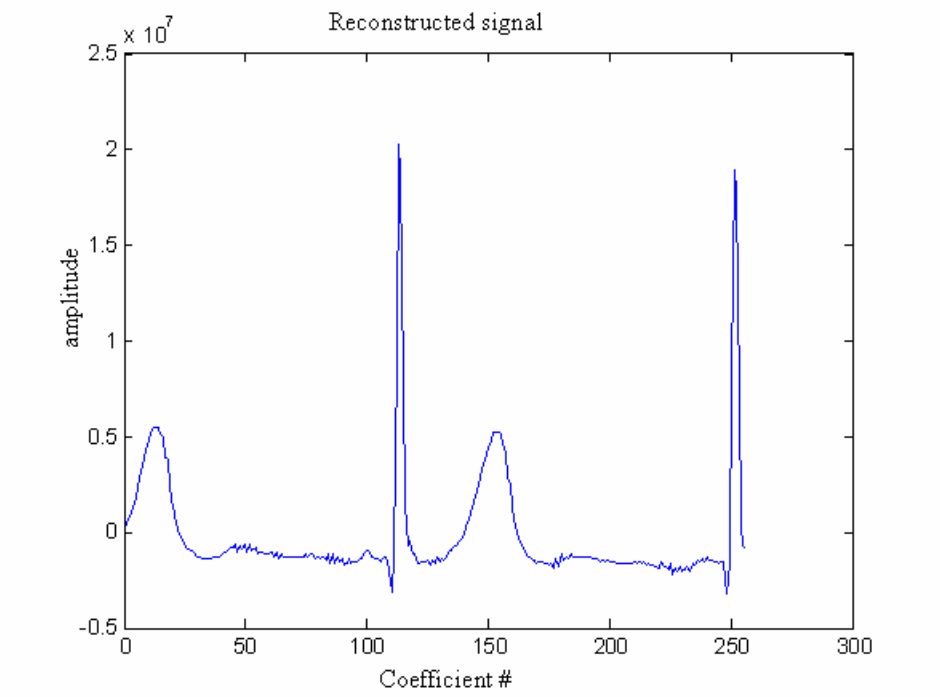

Figure 3.21 Reconstructed signal

3.5 Wavelet Packet Transform Method

The wavelet packet method is a generalization of wavelet decomposition that offers a richer range and a detailed investigation of possibilities for signal analysis. In wavelet analysis, a signal is split into an approximation and a detail. The approximation is then itself split into a second-level approximation and detail, and the process is repeated. For n level decomposition, there are $n+1$ possible ways to decompose or encode the signal. In wavelet packet analysis, the details as well as the approximations can be split. This yields more than $2^{2^{n-1}}$ different ways to encode the signal. This is the wavelet packet decomposition tree, is depicted on Figure 3.22 [8].

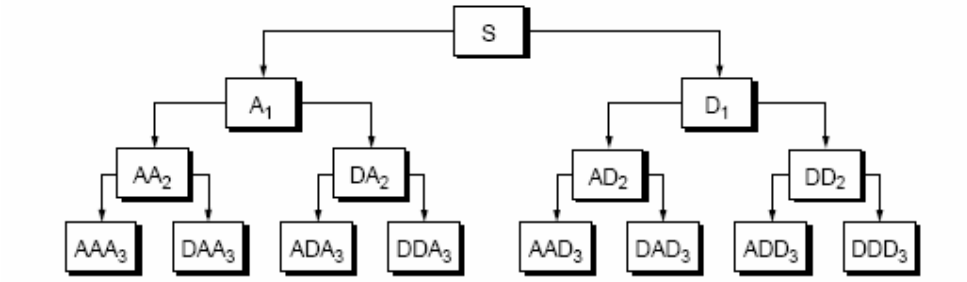

Figure 3.22 Wavelet packet decomposition tree

For instance, wavelet packet analysis allows the signal S to be represented as $A1 + AAD3 + DAD3 + DD2$. This is an example of a representation that is not possible with ordinary wavelet analysis.

3.5.1 Wavelet packet decomposition

In the orthogonal wavelet decomposition procedure, the generic step splits the approximation coefficients into two parts. After splitting it is obtained a vector of approximation coefficients and a vector of detail coefficients, both at a coarser scale. The information lost between two successive approximations is captured in the detail coefficients. Then the next step consists of splitting the new approximation coefficient vector; successive details are never re-analyzed.

In the corresponding wavelet packet situation, each detail coefficient vector is also decomposed into two parts using the same approach as in approximation vector splitting. This offers the richest analysis: the complete binary tree is produced as shown in Figure 3.23 [8].

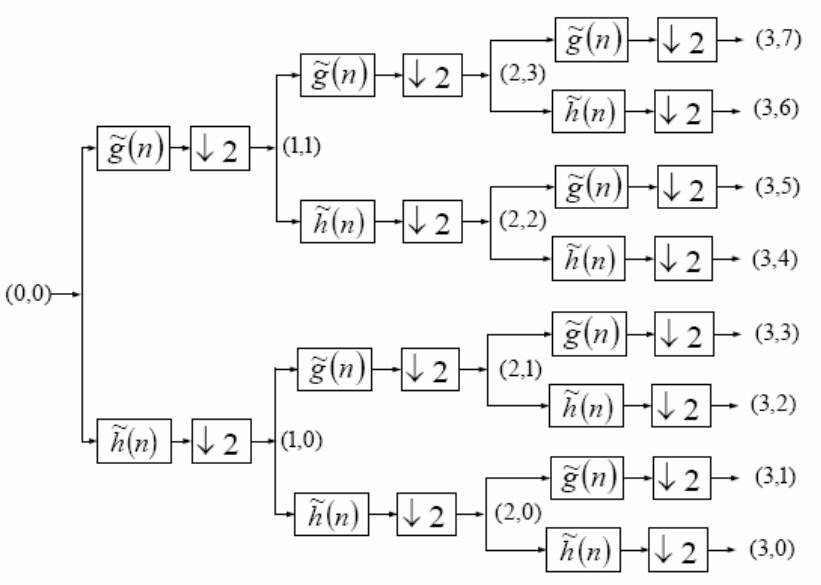

Figure 3.23 Wavelet packet decomposition diagram for three layers

It is started with the two filters of length $2N$, where $h(n)$ and $g(n)$, corresponding to the wavelet. Now by induction let us define the following sequence of functions $W_n(x), n = 0,1,2,...$ by

$$W_{2n}(x) = \sqrt{2}\sum_{k=0}^{2N-1} h(k) W_n(2x-k) \tag{3.18}$$

$$W_{2n+1}(x) = \sqrt{2}\sum_{k=0}^{2N-1} g(k) W_n(2x-k) \qquad \text{where} \tag{3.19}$$

$W_0(x) = \phi(x)$ is the scaling function and $W_1(x) = \psi(x)$ is the wavelet function.

For example for the Haar wavelet:

$$N = 1, h(0) = h(1) = \frac{1}{\sqrt{2}} \tag{3.20}$$

and

$$g(0) = -g(1) = \frac{1}{\sqrt{2}} \tag{3.21}$$

The equations become:

$$W_{2n}(x) = W_n(2x) + W_n(2x-1) \tag{3.22}$$

$$W_{2n+1}(x) = W_n(2x) - W_n(2x-1) \tag{3.23}$$

$W_0(x) = \phi(x)$ is the Haar scaling function and $W_1(x) = \psi(x)$ is the Haar wavelet, both supported in $W_0(x) = \phi(x)$, $W_1(x) = \psi(x)$.

For $n = 0...7$, the W functions shown in Figure 3.24.

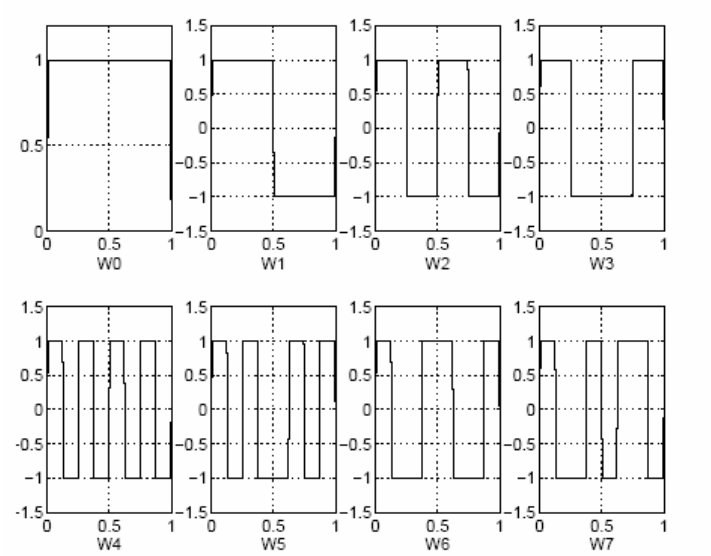

Figure 3.24 Haar wavelet packets.

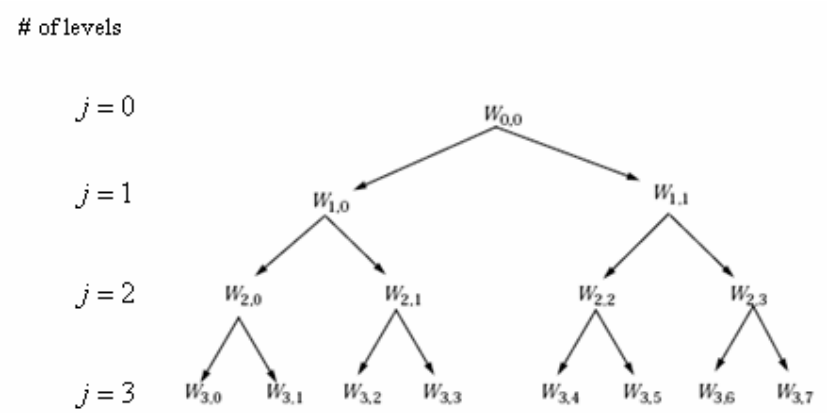

Figure 3.25 Wavelet packet tree.

The set of functions $W_{j,n}(x) = (W_{j,n,k}(x), k \in Z)$ is the wavelet packet shown in the previous figure, namely Figure 3.25. For positive values of integers, j and n wavelet packets are organized in trees. The tree in Figure 3.25 is created to give a maximum level decomposition equal to 3.

The notation $W_{j,n}(x)$, where j denotes scale parameter and n is the frequency parameter defines the position depth in wavelet packet tree.

This last property gives a precise interpretation of splitting in the wavelet packet organization tree, because all the developed nodes are of the form shown in the figure below, Figure 3.26.

$W_{j,n} = (W_{j,n,k}(x), k \in Z)$

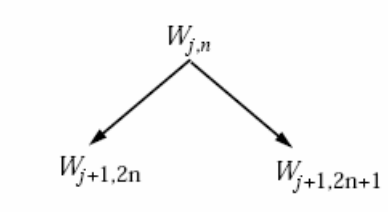

Figure 3.26 Wavelet packet organization.

3.5.2 Wavelet packet reconstruction

The process of the wavelet packet reconstruction is achieved by up sampling and the appropriate filtering. In Figure 3.27, diagram is shown for the reproduced signal using the way mentioned.

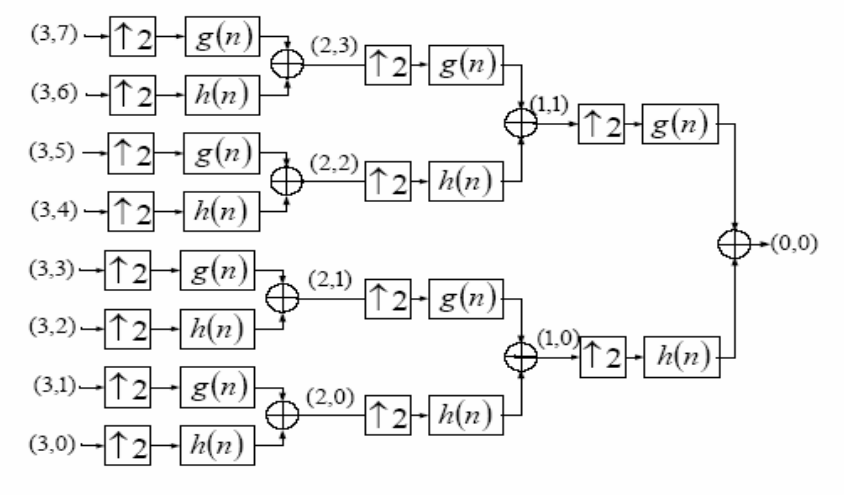

Figure 3.27 Wavelet packet reconstruction diagram for three layers.

As it is available on the discrete wavelet transform $\tilde{h}(n)$ and $h(n)$ low pass filters, $\tilde{g}(n)$ and $g(n)$ are the high pass filters.

Wavelet packet transform is defined by the function of $W_n(2^v t-k)$, $v,k \in Z$ $n \in N$ and provided by the linear combination of wavelets

$$W_0(t) = \phi(t) \tag{3.24}$$

$$W_1(t) = \psi(t) \tag{3.25}$$

$$W_{2n}(t) = \sum_k h_k W_n(2t-k) \tag{3.26}$$

$$W_{2n+1}(t) = \sum_k g_k W_n(2t-k) \tag{3.27}$$

$\phi(t)$ and $\psi(t)$ are the functions generated by $g(n)$ and $h(n)$ filters [8]. The wavelet packet analysis and the synthesis procedure are realized with the filters shown in Figure 3.28.

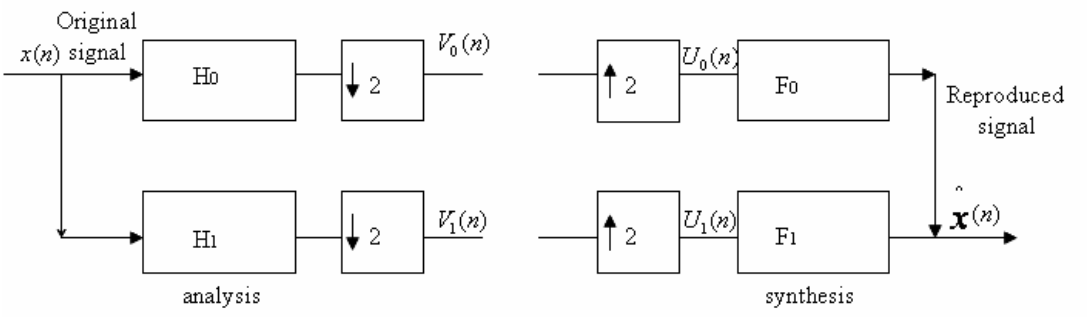

Figure 3.28 Wavelet packet decomposition and reconstruction.

4. DISCRETE COSINE AND DISCRETE SINE TRANSFORM

4.1 Discrete Cosine Transform

A discrete cosine transform (DCT) is defined to compute it using the fast Fourier transform. It is shown that discrete Cosine transform can be used in the area of digital signal processing. Its performance is compared with that of a class of orthogonal transforms and is found to compare closely to that of the Karhunen-Loeve transform, which is known to be optimal. The performances of Karhunen-Loeve and discrete Cosine transforms are also found to compare closely with respect to the rate-distortion criteria.

In recent years, there has been an increasing interest with respect to using a class of orthogonal transforms in the general area of the digital signal processing [3].

The DCT of a data sequence of $x(m)$, $m = 0,1,2,3,...,(M-1)$, is defined as in Equations 4.1 and 4.2.

$$G_x(0) = \frac{\sqrt{2}}{M}\sum_{m=0}^{M-1} x(m), \tag{4.1}$$

$$G_x(k) = \frac{2}{M}\sum_{m=0}^{M-1} x(m).\cos\frac{(2m+1)k\pi}{2M}, k = 1,2,3,...,(M-1) \tag{4.2}$$

The last equation shows that, the basis vectors are sampled cosines which have phase shifts that are not given by an alternating 0 and pattern as in (the sines and cosines) DFT. The DCT basis vectors are displayed as follows [3].

$$b_k = \left\{\sqrt{\frac{2}{N}}\alpha(k)\cos\frac{(2n+1)k\pi}{2N}\right\}_{n=0,1,...,N-1} for, k = 0,1,...,N-1 \tag{4.3}$$

$$\alpha(0) = \frac{1}{\sqrt{2}}, \alpha(k) = 1, k \neq 0$$

Where $G_x(k)$ is the k^{th} DCT coefficient. The set of basis vectors is given in Equation 4.3 which is a class of discrete Chebyshev polynomials. This can be seen by recalling that Chebyshev polynomials can be defined as in following Equations from 4.4 to 4.8, inclusive [3].

$$\hat{T}_0(\varepsilon_p) = \frac{1}{\sqrt{2}} \tag{4.4}$$

$$\hat{T}_k(\varepsilon_p) = \cos(k\cos^{-1}\varepsilon_p), k, p = 1,2,3,...,M \tag{4.5}$$

In (4.5) $\hat{T}_k(\varepsilon_p)$ represents the k^{th} Chebyshev polynomial. ε_p is chosen to be the p^{th} zero of $\hat{T}_M(\varepsilon_p)$ which is given by

$$\varepsilon_p = \cos\frac{(2p-1)\pi}{2M}, p = 1,2,3,...,M \tag{4.6}$$

Substituting ε_p in, $\hat{T}_k(\varepsilon_p)$ Equation 4.5, the set of Chebyshev polynomials can be obtained as follows [3].

$$\hat{T}_0(p) = \frac{1}{\sqrt{2}},\ \hat{T}_k(p) = \cos\frac{(2p-1)k\pi}{2M}, k, p = 1,2,3,...,M \tag{4.7}$$

$$T_0(m) = \frac{1}{\sqrt{2}}, T_k(m) = \cos\frac{(2m+1)k\pi}{2M}, k = 1,2,...,(M-1), m = 0,1,2,...,(M-1) \tag{4.8}$$

To sum up, $\cos\frac{(2m+1)k\pi}{2M}$ is the k^{th} Chebyshev polynomial.

Inverse Discrete Cosine Transform (*IDCT*), is defined by $x(m)$ and calculated in Equation 4.9.

$$x(m) = \frac{1}{\sqrt{2}}G_x(0) + \sum_{k=1}^{M-1} G_x(k)\cos\frac{(2m+1)k\pi}{2M}, m = 0,1,2,...,(M-1) \tag{4.9}$$

The DCT is an orthonormal transform, defined in Equations 4.10 and 4.11

$$\theta = CX, X = C^{-1}\theta \tag{4.10}$$

$$\sum_{m=0}^{M-1} T_k(m)T_l(m) = \begin{Bmatrix} M/2, k = l = 0 \\ M/2, k = l \neq 0 \\ 0, k \neq l \end{Bmatrix} \tag{4.11}$$

The attractiveness of the DCT is two-fold: The first one, it is nearly optimal with high positive values of adjacent sample correlation and the second one it can be computed via the DFT using an FFT algorithm.

The fast computation procedure mentioned in second one, above, consists of extending the input block of N samples to a $2N$ block with even symmetry, taking a $2N$ point DFT, and saving N terms in it. The DFT of a real and symmetric sequence contains only real coefficients corresponding to the cosine terms of the series.

4.2 Discrete Sine Transform

In mathematics, the discrete sine transform (DST) is a Fourier related transform similar to the Discrete Fourier Transform (DFT), but using only real numbers. It is equivalent to the imaginary parts of a DFT of roughly twice the length, operating on real data with odd symmetry (since the Fourier transform of a real and odd function is imaginary and odd), where in some variants the input and/or output data are shifted by half a sample [7].

A related transform is the discrete cosine transform (DCT) mentioned above, which is equivalent to a DFT of real and even functions.

DST s are widely employed in solving partial differential equations by spectral methods, where the different variants of the DST correspond to slightly different odd/even boundary conditions at the two ends of the array.

Formally, the discrete sine transform is a linear, invertible function $F : RN \rightarrow RN$ (where R defines the set of real numbers), or equivalently an NxN square matrix. There are several variants of the DST with slightly modified definitions. The N real numbers

$x_0, x_1, ..., x_{N-1}$ are transformed into the N real numbers $X_0, X_1, ..., X_{N-1}$ according to the formula given in Equation 4.12 [10].

$$X_k = \sum_{n=0}^{N-1} x_n \sin[\frac{\pi}{N+1}(n+1)(k+1)] \tag{4.12}$$

5. DIGITAL SIGNAL COMPRESSION

5.1 Introduction

A typical computerized medical signal processing system acquires a large amount of data that is difficult to store and transmit. It is very desirable to find a method of reducing the quantity of data without loss of important information.

All data compression algorithms seek to minimize data storage by eliminating redundancy where possible. The compression ratio is defined as the ratio of the number of bits of the original signal to the number stored in the compressed signal. A high compression ratio is wanted, typically, but using this alone to compare data compression algorithms is not acceptable. Generally, precision of the original and the reproduced data much affect the compression ratio [7].

A data compression algorithm must also represent the data with acceptable signal quality. In biomedical data compression, the clinical acceptability of the reconstructed signal has to be determined through visual inspection. The reconstructed signal and the original signal compatibility may also be measured by a numerical measure. The compression ratio value is calculated by the Equation of 5.1 [7].

$$CR = \frac{b_{org}}{b_{comp}} \tag{5.1}$$

5.2 Signal Compression and Distortion Measures

The criterion for testing performance of compression algorithms includes three components: compression measure, reconstruction error and computational complexity. The compression measure and the reconstruction error are usually dependent on each other and are used to create the rate-distortion function of the algorithm. The computational complexity component is part of the practical implementation consideration but it is not part of any theoretical measure.

5.3 Error Criterion

One of the most difficult problems in ECG compression applications and reconstruction is defining the error criterion. The purpose of the compression system is to remove redundancy, the irrelevant information (which does not contain diagnostic information). Consequently the error criterion has to be defined such that it will measure the ability of the reconstructed signal to preserve the relevant information. Such a criterion has been defined as *diagnostability*. A similar problem exists in synthesized speech signals, in which the criterion intelligibility is defined.

As yet, there is no such mathematical structure to this criterion, and all accepted error measures are still variations of the Mean Square Error, which are easy to compute mathematically [7].

In most ECG compression algorithms, the Percent Root Mean Square Difference (PRD) measure is employed where $x(n)$ is the original signal, $\tilde{x}(n)$ is the reconstructed signal, and N is the length of the window over which the PRD is calculated. In some of the articles a fixed version of PRD definition is used in Equation 5.2 [4].

$$PRD = \sqrt{\frac{\sum_{n=1}^{N}(x(n)-\tilde{x}(n))^2}{\sum_{n=1}^{N}x^2(n)}}x100 \tag{5.2}$$

In the literature, there are some other error measures for comparing original and reconstructed ECG signals, such as the Root Mean Square Error ($RMSE$) defined in Equation 5.3 [4].

$$RMS = \sqrt{\frac{\sum_{n=1}^{N}(x(n)-\tilde{x}(n))^2}{N}} \tag{5.3}$$

Another distortion measure is the Signal to Noise Ratio, which is expressed as in Equation 5.4 [4].

$$SNR = 10\log\left(\frac{\sum_{n=1}^{N}(x(n)-\bar{x})^2}{\sum_{n=1}^{N}(x(n)-\tilde{x}(n))^2}\right) \tag{5.4}$$

In the above equation $\bar{x}$ is the average value of the original signal. The relation between the SNR and the PRD is

$$SNR = -20\log PRD \tag{5.5}$$

Digital coding is the process, or sequence of processes, that leads to digital representations (sequences of binary digits) of the source signal. The benefits of digital representation are well known, low sensitivity to transmission noise, effective storage, ability to multiplex, error protection and more.

One of the main goals in digital coding of waveforms is reduction of the bit rate, which is required to transmit a certain amount of information. The process of bit rate reduction is performed by the removal of the signal's redundancy, and sometimes causes loss of information. A basic problem in waveform coding is to achieve the minimum possible distortion for a given encoding rate or, equivalently, to achieve a given acceptable level of distortion with the least possible encoding rate.

The first stage of the analog signal coding process is sampling and quantization. The sampling is performed mostly according to the Nyquist criterion after low pass filtering the signal with an anti aliasing filter. After sampling, the signal is time-discrete and amplitude-continuous. In order to represent the sampled signal digitally, one has to perform quantization, mapping the sampled signal's amplitudes from the continuous plane to the discrete plane. The quantization in this stage is usually fine quantization (many quantization levels) so one can treat the sampled signal as almost amplitude-continuous.

At the second stage of the coding process, the redundancy of the signal is removed using appropriate coding techniques, such as, orthogonal transforms, entropy encoding, $ADPCM$, etc.

5.4 Sampling and Uniform Quantization

The PCM is the earliest, the simplest, and the most popular coder in digital coding systems of signals. A PCM coder is nothing more than a waveform sampler followed by an amplitude quantizer.

Let $x(t)$ denote a sample function emitted by a source and let x_n denote the samples taken at a sampling rate $f_s \geq 2w$, where w is the highest frequency in the spectrum of $x(t)$. In PCM, each sample of the signal is quantized to one of 2^R amplitude levels, where R is the number of binary digits used to represent each sample. Thus the rate from the source is Rf_s bits [11].

The quantization process may be modeled mathematically as in the Equation (5.6)

$$\tilde{x}_n = x_n + q_n \tag{5.6}$$

Where $\tilde{x}_n$ represents the quantized value of x_n and q_n represents the quantization error, which it is treated as an additive noise. Assuming that a uniform quantizer is used, having the input-output characteristic illustrated in Figure 5.1, the quantization noise is well characterized statistically by the uniform pdf that is defined in Equation 5.7 [11], [12].

$$p_q(q) = \left\{ \begin{matrix} \frac{1}{\Delta}, |q| \leq \Delta/2 \\ 0, otherwise \end{matrix} \right\}, \; -\Delta/2 \leq q \leq \Delta/2 \tag{5.7}$$

The mean square value of the quantization error is

$$\sigma_x^{\,2} = \frac{\Delta^2}{12} \tag{5.8}$$

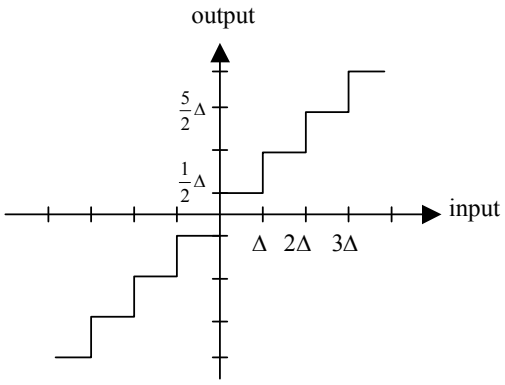

Figure 5.1 Input - Output characteristic for a uniform quantizer.

Many signals such as speech waveforms have the characteristic that small signal amplitudes occur more frequently than large one. However, a uniform quantizer provides the same spacing between successive levels throughout the entire dynamic range of the signal. The block diagram of the sampling, quantization and binary coding in PCM is shown in Figure 5.2 [11], [12].

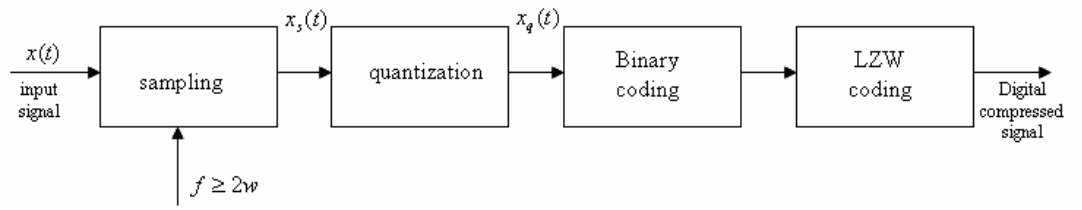

Figure 5.2 Transmitter block diagram in PCM.

5.4.1 Quantization error

Let X be a zero-mean random variable at the quantizer input, with variance σ_x^2 and pdf $p_q(q)$.

$$Y = Q(X) = y_k \tag{5.9}$$

The quantization error $Q = X - Y$ is also a random variable with pdf $p_q(q)$ [13].

$$\sigma_x^2 = E\left[Q^2\right] = \int_{-\infty}^{+\infty} q^2 p_q(q) dq \tag{5.10}$$

Alternatively as $Q = X - Q(X)$ is a function of X

$$\sigma_q^2 = E\left[Q^2\right] = \int_{-\infty}^{+\infty} \left[x - Q(x)\right]^2 p_x(x) dx \tag{5.11}$$

Quantization error variance is the most important quantity for comparing the performances of quantizers, and Equation 5.11 is often used to calculate this variance. Its calculation via Equation 5.10 is possible only if the pdf $p_q(q)$ is known which is typically not the case. However $p_q(q)$ may be approximated by a constant over a finite range in the case of uniform quantization

Consider the example of an input x with amplitudes in the range $x \in (-x_{\max}, x_{\max})$, in this case, quantization step size is defined in the Equation 5.12 [13].

$$\Delta = 2x_{\max} / 2^R \tag{5.12}$$

Quantization errors will have values in the range

$$-\frac{\Delta}{2} \le q \le \frac{\Delta}{2} \tag{5.13}$$

Equation 5.11 goes to the result as in the following line.

$$\sigma_q^2 = \frac{\Delta^2}{12}, \sigma_q{}^2 = \frac{1}{3} x^2{}_{\max} 2^{-2R} \tag{5.14}$$

$$p_e(e) = \begin{Bmatrix} \frac{1}{\Delta}, -\frac{\Delta}{2} \le e \le \frac{\Delta}{2} \\ 0, otherwise \end{Bmatrix} \tag{5.15}$$

The changes of $p(e)$ is displayed in Figure 5.3

$$< e^2 >= E\left[e^2\right] \tag{5.16}$$

$$< e^2 >= \int_{-a/2}^{a/2} e^2 p(e) de = \frac{\Delta^2}{12} \tag{5.17}$$

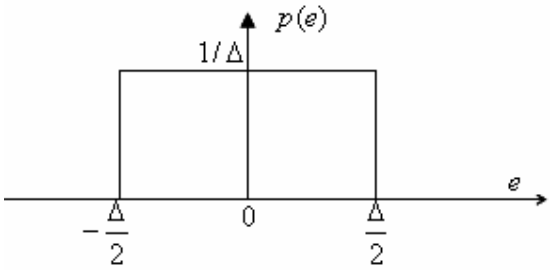

Figure 5.3 PDF of a quantization error.

n-bits quantizer $A_{\max}$ amplitude is applied to the signal with the amplitude of A, in that case the ratio of signal to noise is (S/N) calculated in Equation 5.18 and 5.19 [13].

$$(\frac{S}{N}) = \frac{< x^2(t) >}{< e^2(n) >} = \frac{A^2}{2}\frac{12}{\Delta^2} \tag{5.18}$$

$$(\frac{S}{N}) = \frac{A^2}{2}\frac{12}{(\frac{2A_{\max}}{2^n})^2} = \frac{3}{2}2^{2n}(\frac{A}{A_{\max}})^2 \tag{5.19}$$

Besides, in the form of dB $(\frac{S}{N})$ can be calculated, shown in the Equations 5.20 and 5.21.

$$(\frac{S}{N})_{dB} = 10\log_{10}(\frac{S}{N}) \tag{5.20}$$

$$(\frac{S}{N})_{dB} = 1{,}76 + 6{,}02n + 20\log_{10}(\frac{A}{A_{\max}}) \tag{5.21}$$

5.5 LZW Coding

5.5.1 LZW encoder

LZW source coding algorithm belongs to the class of universal source coding algorithms. It is a variable to fixed length algorithm, where the encoding is performed as described below.

In LZW algorithm, the sequence of the output of the discrete source is parsed into variable length blocks, which are called phrases. A new phrase is introduced every time a block of letters from the source differs from some previous phrase in the last letter. The phrases are listed in a dictionary, which stores the location of the existing phrases. In encoding a new phrase, it is simply specified the location of the existing phrase in the dictionary and append the new letter [12].

In block coding, first the partition process of the data vector into blocks of equal length is done. In Lempel-Ziv coding, it is first started by partitioning the data vector into variable-length blocks instead. The procedure via which this partitioning takes place is called Lempel-Ziv parsing. The $1st$ variable-length block arising from the Lempel-Ziv parsing of the data vector $X = (X_1, X_2, ..., X_n)$ is the single sample X_1. The second block in the parsing is the shortest prefix of $(X_2, ..., X_n)$ which is not equal to X_1. Suppose this second block is $(X_2, ..., X_j)$. Then, the third block in Lempel-Ziv parsing will be the shortest prefix of $(X_{j+1}, ..., X_n)$ which is not equal to either X_1 or $(X_2, ..., X_j)$. In general, suppose the Lempel-Ziv parsing procedure has produced the first k variable-length blocks $(B_1, B_2, ..., B_k)$ in the parsing, and $X^{(k)}$ is that part left of X after $(B_1, B_2, ..., B_k)$ have been removed. Then the next block B_{k+1} in the parsing is the shortest prefix of $X^{(k)}$ which is not equal to any of the preceding blocks $(B_1, B_2, ..., B_k)$. (If there is no such block, then $B_{k+1} = X^{(k)}$ and the Lempel-Ziv parsing procedure terminates.) [12].

By construction, the sequence of variable-length blocks $B_1, B_2, ..., B_t$ produced by the Lempel-Ziv parsing of X are distinct, except that the last block B_t could be equal to one of the preceding ones.

Consider the example of an input X and Lempel-Ziv parsing of $X = (1,1,0,1,1,0,0,0,1,1,0,1)$ is $B1 = 1, B2 = 10, B3 = 11, B4 = 0, B5 = 00, B6 = 110, B7 = 1$. This is shown in Figure 5.4. Binary representation of the groups is in the table of 5.1 [12].

X →	1	10	1 1	0	0 0	1 1 0	1

Figure 5.4 X data sequence.

LZW parsing process is displayed on the Table 5.1. Binary representation of groups is displayed on Table 5.2

Table 5.1
Lempel-Ziv parsing for X data sequence.

Bi		index	group
B1	1	1	(0,1)
B2	1 0	2	(1,0)
B3	1 1	3	(1,1)
B4	0	4	(0,0)
B5	0 0	5	(4,0)
B6	1 1 0	6	(3,0)
B7	1	7	(0,1)

Table 5.2
Binary representation of groups.

group	integer form	Ii
(0,1)	$0.(2^1)+1.(2^0)$	1
(1,0)	$1.(2^1)+0.(2^0)$	2
(1,1)	$1.(2^1)+1.(2^0)$	3
(0,0)	$0.(2^1)+0.(2^0)$	0
(4,0)	$4.(2^1)+0.(2^0)$	8
(3,0)	$3.(2^1)+0.(2^0)$	6
(0,1)	$0.(2^1)+1.(2^0)$	1

LZW encoder output is the binary conversion of the Ii. $\log_2(k.j)$ provides the information of bit representation status, shown in Table 5.3 [14].

Table 5.3
LZW encoder output (Zi).

Z_i	I_i	$\log_2(k.j)$	x bit representation
1	1	$\log_2(2.1)$	1 bit representation
10	2	$\log_2(2.2)$	2 bit representation
011	3	$\log_2(2.3)$	3 bit representation
000	0	$\log_2(2.4)$	3 bit representation
1000	8	$\log_2(2.5)$	4 bit representation
0110	6	$\log_2(2.6)$	4 bit representation
0001	1	$\log_2(2.7)$	4 bit representation

As it is shown in the following table, namely Table 5.4, the output of the encoder is the binary data sequence arranged in order.

Table 5.4
Zi arranged in order.

LZW encoder output (Zi)						
1	10	011	000	1000	0110	0001
Z_1	Z_2	Z_3	Z_4	Z_5	Z_6	Z_7

The input of LZW encoder block, is the binary data, shown in Figure 5.5

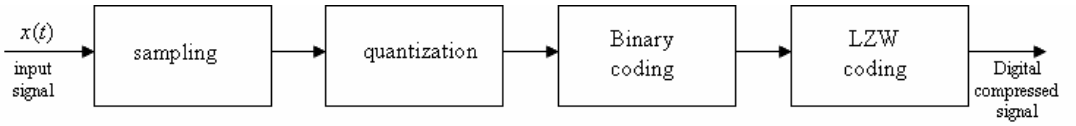

Figure 5.5 LZW encoder block diagram.

5.5.2 LZW decoder

LZW decoding process takes the reference of the data sequence which is the output of encoder. Codebit table is again used for the decoding issue, displayed on Table 5.5

Bit representation is calculated, then partitioning up the encoder output according to the allocations in the above table. Converting these to integer form Ii is obtained, in Table 5.6. Dividing each of these integers by two, the quotient and remainder in each case, the pairs are formed

Table 5.5
LZW codebit table.

Codebit table			
parsing block number	# of codebits		
1	$\log_2(k.j)$	$(k=2,\ j=1)$	1 bit representation
2	$\log_2(k.j)$	$(k=2,\ j=2)$	2 bit representation
3	$\log_2(k.j)$	$(k=2,\ j=3)$	3 bit representation
4	$\log_2(k.j)$	$(k=2,\ j=4)$	3 bit representation
5	$\log_2(k.j)$	$(k=2,\ j=5)$	4 bit representation
6	$\log_2(k.j)$	$(k=2,\ j=6)$	4 bit representation
7	$\log_2(k.j)$	$(k=2,\ j=7)$	4 bit representation

Table 5.6
LZW decoder output.

LZW decoder output							
	1	10	011	000	1000	0110	0001
Ii	1	2	3	0	8	6	1
groups	(0,1)	(1,0)	(1,1)	(0,0)	(4,0)	(3,0)	(0,1)

In Table 5.7, the binary data arrangement process is displayed for decoding process.

Table 5.7
Binary data assignment.

Bi	binary form	index	group
B1	1	1	(0,1)
B2	1 0	2	(1,0)
B3	1 1	3	(1,1)
B4	0	4	(0,0)
B5	0 0	5	(4,0)
B6	1 1 0	6	(3,0)
B7	1	7	(0,1)

As it is depicted on Table 5.8, below, the original data sequence is recovered again.

Table 5.8
X data sequence.

X	1	1 0	1 1	0	0 0	1 1	1
	B1	B2	B3	B4	B5	B6	B7

Decoding process is displayed on Figure 5.6, below.

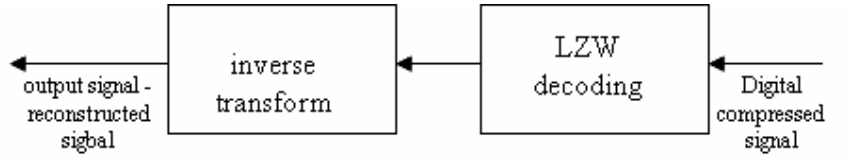

Figure 5.6 LZW decoding block diagram.

6. IMPLEMENTATION METHODS

6.1 Wavelet Transform

The aim of electrocardiogram (ECG) data compression is to reduce the amount of digitized ECG data as much as possible with reasonable implementation complexity while maintaining clinically acceptable signal quality.

In order to achieve our goal a new electrocardiogram (ECG) data compression method is presented which is based on orthonormal wavelet transform and a uniform quantization strategy by which a predetermined percent root mean square difference (*PRD*) can be guaranteed with high compression ratio and low implementation complexity.

6.2 A Generalized DOWT Based Coding System

Since detailed mathematical aspects of wavelet theory can be found elsewhere, here, it is described merely the structure of a *DOWT* -based coding system shown in Figure 6.1

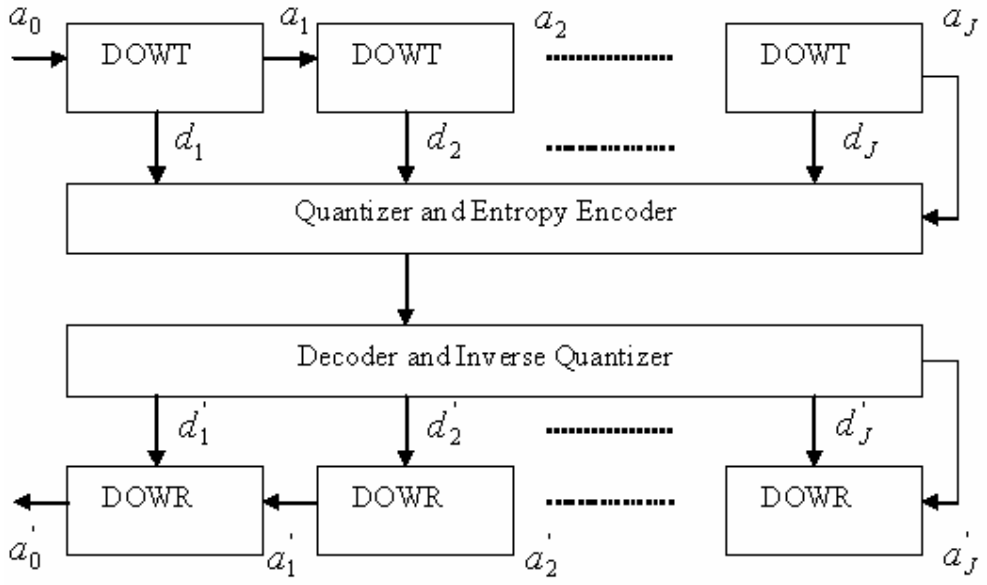

Figure 6.1 A generalized DOWT based coding system.

The input discrete signal of a_0 is successively decomposed into a set of subsignals $\{a_J,(d_j)\},1\le j\le J$ of by the $DOWT$ units, where a_J is a smoothed version of a_0 and $d_j,1\le j\le J$ are the differential subsignals between the original signal and its smoothed versions at different resolutions. The decomposed subsignals are then quantized and entropy-encoded in order to be transmitted to a receiver [16]. If the transmission is error free, the quantized subsignals of a'_J and d'_j, $1\le j\le J$ are used to progressively reconstruct the original signal by the discrete orthonormal wavelet reconstruction transform (DOWR). When the decomposed subsignals of $\{a_J,(d_j)\}$, $1\le j\le J$ are quantized, the reconstruction error between the original signal a_0 and the reconstructed signal a'_0 occurs [7]. Let ε_j^d and ε_J denote the mean square error (MSE) occured in the quantization of d_j and a_J, respectively, then the reconstruction MSE ($RMSE$) γ_0 between the original signal a_0 and its reconstructed signal a'_0 is given by

$$\gamma=\varepsilon_J+\sum_{j=1}^{J}\varepsilon_j^d \tag{6.1}$$

Above equation indicates an important feature of the $DOWT$ -based coding system that the $RMSE$ (γ_0) between the original signal and its reproduced version can be exactly calculated from the quantization MSE of the decomposed subsignals (a_J and d_j) [7].

ε_j^d : mean square error (MSE) occured in the quantization of d_j

ε_J : mean square error (MSE) occured in the quantization of a_J,

γ_0 : reconstruction MSE ($RMSE$) between the original signal a_0 and its reconstructed signal a'_0.

6.2.1 Definition of coding

A widely used quantitative distortion measure for ECG coding is the *PRD* defined by Equation 6.2 where γ is the *RMSE* between the original signal and the reconstructed signal, σ is the power of the original signal, calculated in Equation 6.5. For a user-specifed *PRD* of ρ_0, the corresponding *RMSE* can be calculated from Equation 6.2 [7].

$$PRD = \sqrt{\frac{\gamma}{\sigma}} \tag{6.2}$$

$$\gamma_0 = \rho_0^2 . \frac{1}{L} \sum_{i=1}^{L} \mu_i^2 \tag{6.3}$$

$$\gamma_0 = \varepsilon_J + \sum_{j=1}^{L} \varepsilon_j^d = \gamma_0$$

$$PRD \rightarrow \rho_0$$

$PRD = \rho_0 = \sqrt{\frac{\gamma_0}{\sigma}}$ taking the squares of both sides in the equation

$$\rho_0^2 = \frac{\gamma_0}{\sigma} \Rightarrow \gamma_0 = \rho_0^2 . \sigma$$

$$RMSE \Rightarrow \gamma = \rho_0^2 \sigma \tag{6.4}$$

In Equation 6.3, where μ_i are the samples of the original signal and L is the length of an ECG segment being evaluated. Thus the problem of guaranteeing a user specified *PRD* of ρ_0 is equivalent to guaranteeing the corresponding *RMSE* of γ_0 determined by Equation 6.4 [7].

$$\sigma = \frac{1}{L} \sum_{i=1}^{L} \mu_i^2 \tag{6.5}$$

The optimal solution corresponds to the theoretical bound of the rate distortion performance which is only achieved by an ideal quantizer and an ideal entropy encoder. It is difficult to get an exact expression of the quantization MSE for a general information source. However when the quantization step size is small enough, the expected quantization MSE's of ε_j^d and ε_J can be approximated as in the Equation 6.6 [7].

$$\varepsilon_J = \frac{1}{2^J}\gamma_0, \varepsilon_j{}^d = \frac{1}{2^j}\gamma_0 \tag{6.6}$$

Therefore as long as the quantization MSE's are achieved, the desired $RMSE$ γ_0 or the equivalent PRD of ρ_0 is obtained.

6.2.2 Uniform quantization

$Db2$ wavelet model is used providing one stage decomposition $CA1$ and $CD1$. This process is repeated to get the successive approximation and detail coefficients. Based on the decomposition level, $J = 5$, $CA5$ in the 5^{th} level and CDi_s $(i = 1:4)$ are produced. Uniform quantization is applied for the approximation and detail coefficients. So, the quantization step size, Δ, is different from one another. Due to the coefficients decomposed in different decomposition levels, each sample is represented by 8 bits, namely digital signal is sampled with 8 bits resolution. The quantization bin size is defined as in the following Equation, 6.7.

$$\Delta = (2 * A_{\max})/(2^n) \tag{6.7}$$

$n = 8$ bits., $A_{\max}$ is changing for every coefficients at different layers. $A_{\max}$ is valued as $\max(abs(CA5))$, $\max(abs(CD1))$, $\max(abs(CD2)$, $\max(abs(CD3))$, $\max(abs(CD4))$, $\max(abs(CD5))$ successively.

6.3 Implementation

Based on the above analysis, it will be possible to implement the proposed ECG compression system with the following procedures where $\rho_0, L, J, \mu_i, \eta$ denote, a user

specified PRD, the segment length, the number of layers of the wavelet decomposition, the input ECG samples, and the precision of quantization, respectively.

Implementation consists of 2 parts, namely encoder and decoder.

Encoder part:

Initialization, segmenting and buffering L input samples.

Wavelet decomposition.

Uniform quantization [for each (d_j and a_J, $j = 1,2,3,4,...,J$)].

Entropy coding (LZW encoder is used).

Decoder part:

Entropy decoding (LZW decoder used).

Wavelet reconstruction.

In order to make the results quantitatively comparable to other ECG compression methods, here, it will be adapted the most widely-used numerical indexes of PRD, compression ratio (CR) [7]. The compression ratio is used to measure the compression efficiency, which is defined by the ratio of the bits of the original data to those of the compressed data [7].

$$CR = \frac{original \text{ data bit size}}{\text{compressed data bir size}} \tag{6.8}$$

PRD is taken as a reference about the performance of the compression schema used, and formulized in the Equation 6.8. Besides, it also gives the information of the distortion rate of the reconstructed signal waveform and how the reproduced signal is compatible with the original one.

$$PRD = \frac{\sqrt{\sum_{i=1}^{n} (X_{org}(i) - X_{rec}(i))^2}}{\sqrt{\sum_{i=1}^{n} X_{org}(i)^2}} * 100 \qquad (6.9)$$

$X_{org}(i)$: samples of the original signals

$X_{rec}(i)$: samples of the reproduced signal

6.3.1 Segmenting the original signal

The original ECG signal includes 7680 samples, taken from the MIT-BIH Database. The reference signal mentioned above is divided into 8 segments. Except the last one (8^{th}) each ECG segment has 1024 samples itself.

7680 samples = (1024 samples * 7 segments) + 512 samples.

first 7 segments → each includes 1024 samples itself.

the last ECG segment (8^{th}) → contains 512 samples.

The proposed algorithm was implemented on the PC which has Pentium 4, CPU 2.4 GHz, 256 MB RAM configuration. $Db2$ family is used in the wavelet decomposition method and the layer was set to $J = 5$.

In the following figures, from Figure 6.2 to 6.9 totally 7 segments (1 to 7) which has 1024 samples, and the last one (8^{th} *segment*) with 512 samples are displayed.

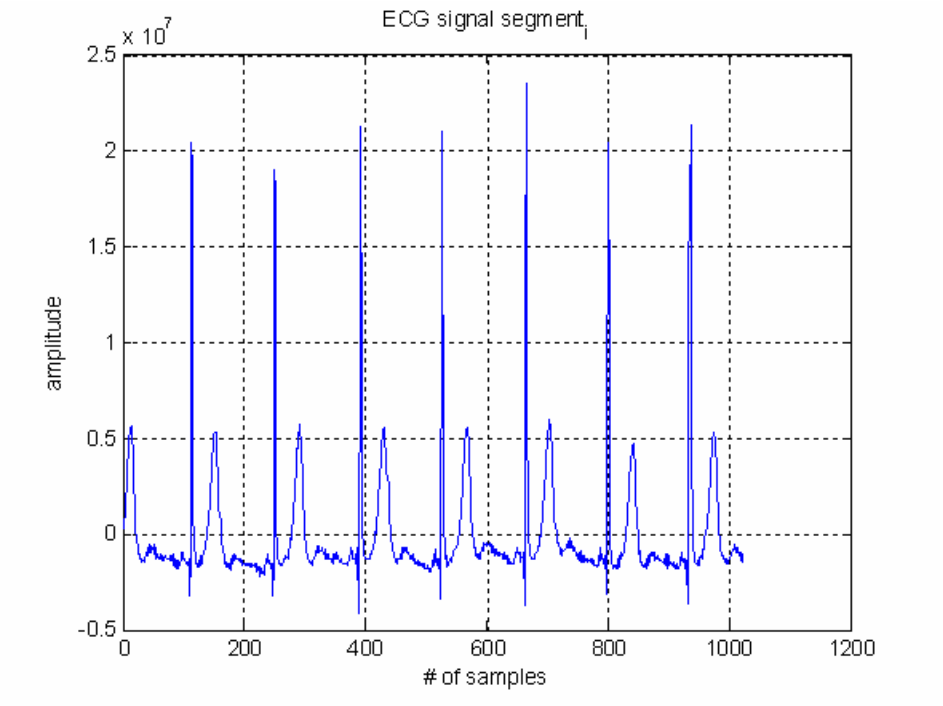

Figure 6.2 1st ECG segment with 1024 samples.

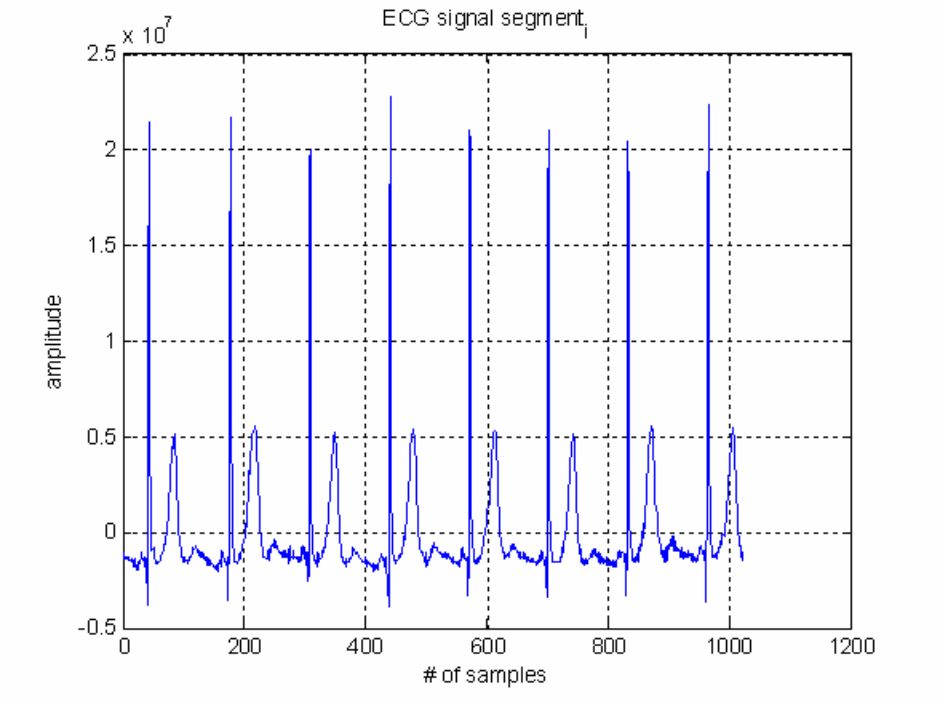

Figure 6.3 2nd ECG segment with 1024 samples.

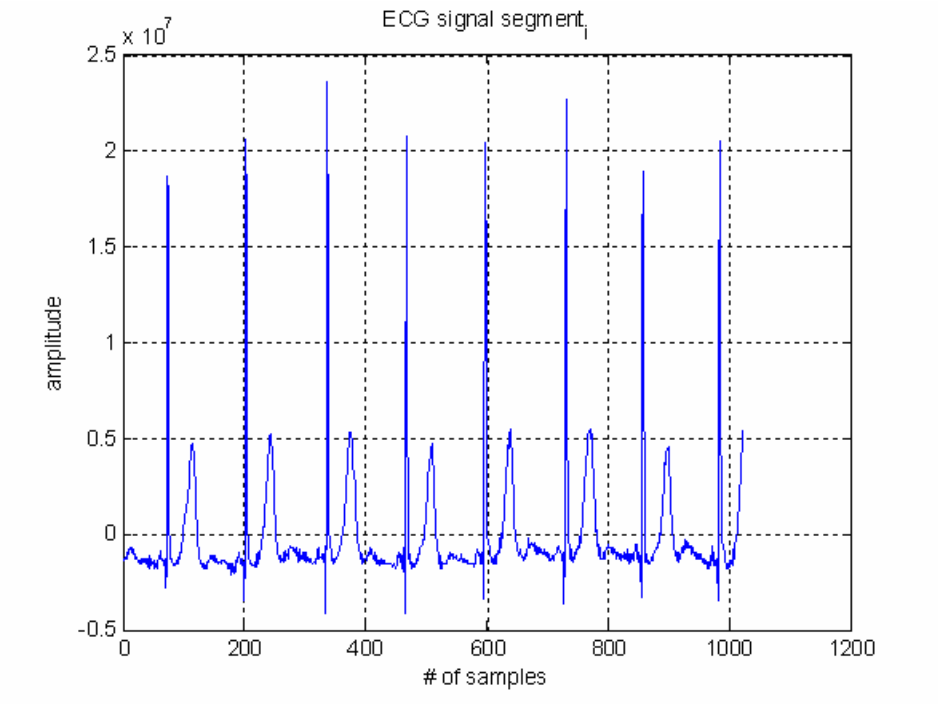

Figure 6.4 3rd ECG segment with 1024 samples.

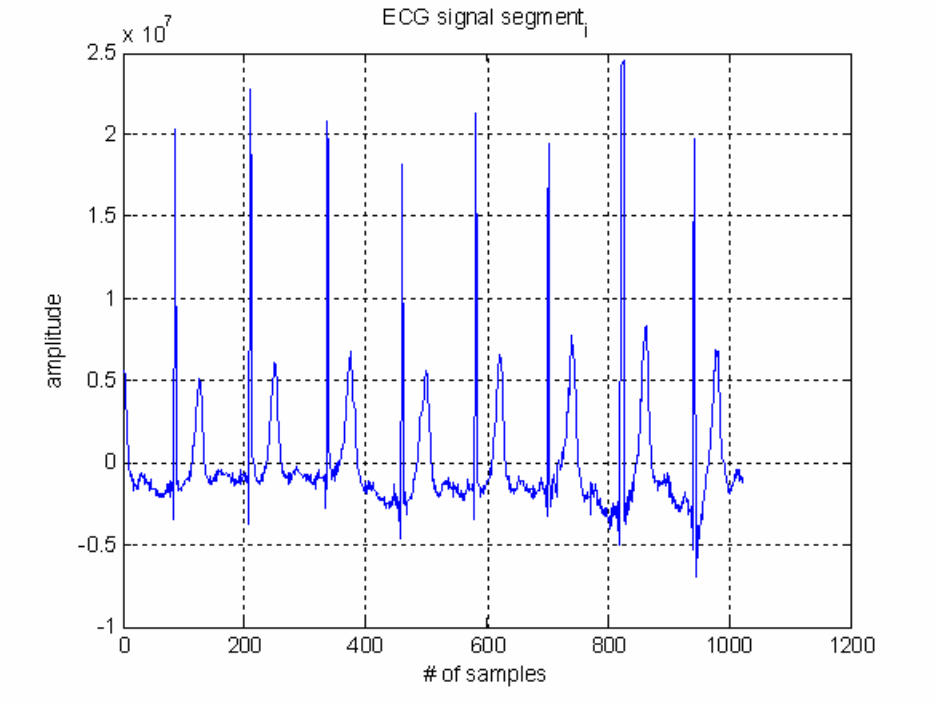

Figure 6.5 4th ECG segment with 1024 samples.

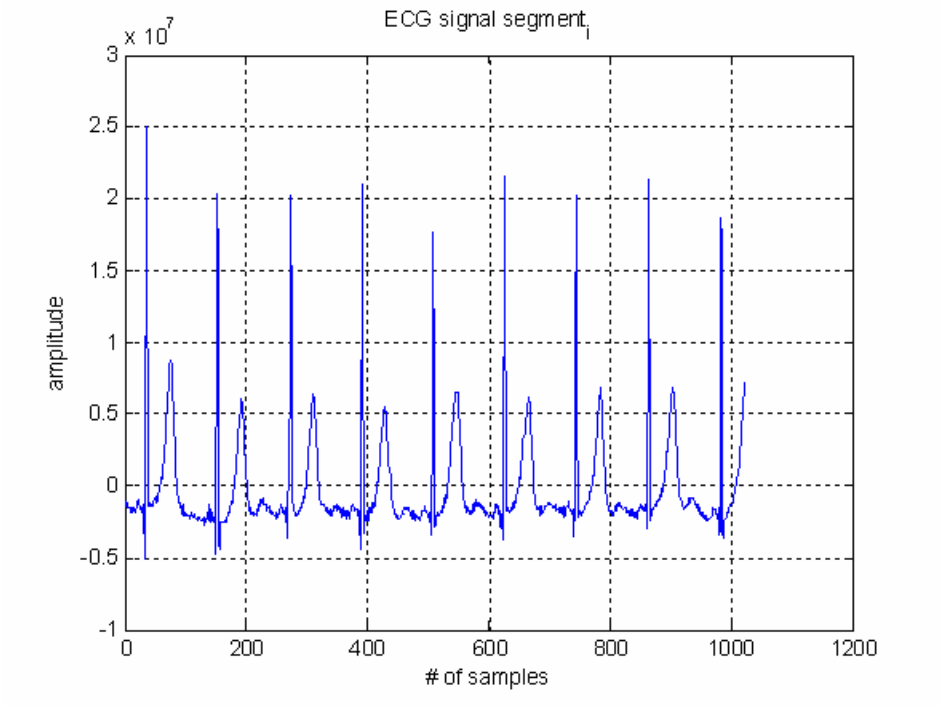

Figure 6.6 5th ECG segment with 1024 samples.

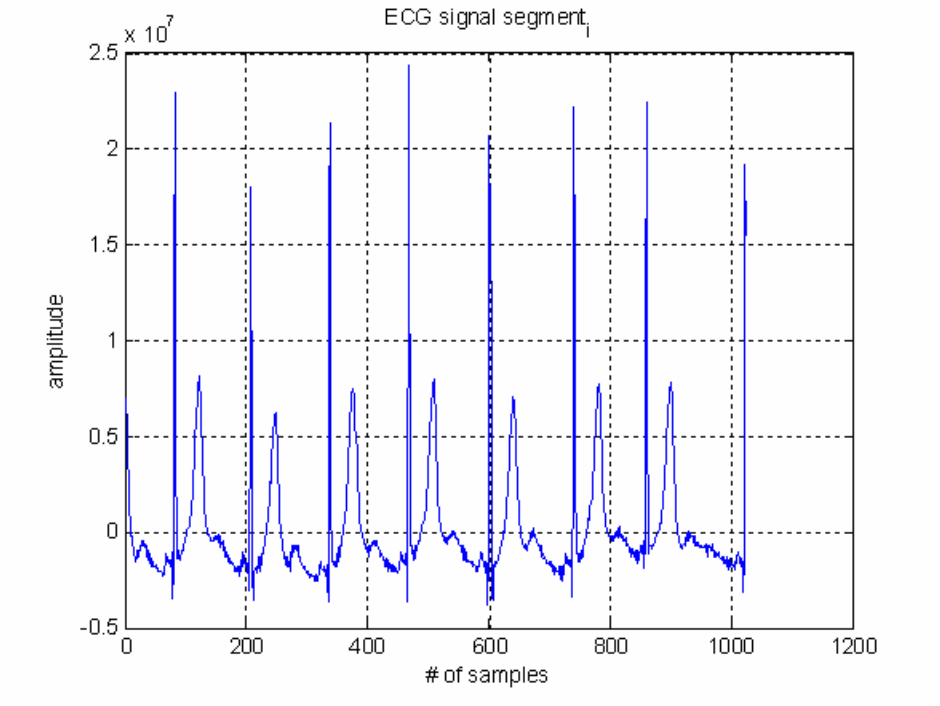

Figure 6.7 6th ECG segment with 1024 samples.

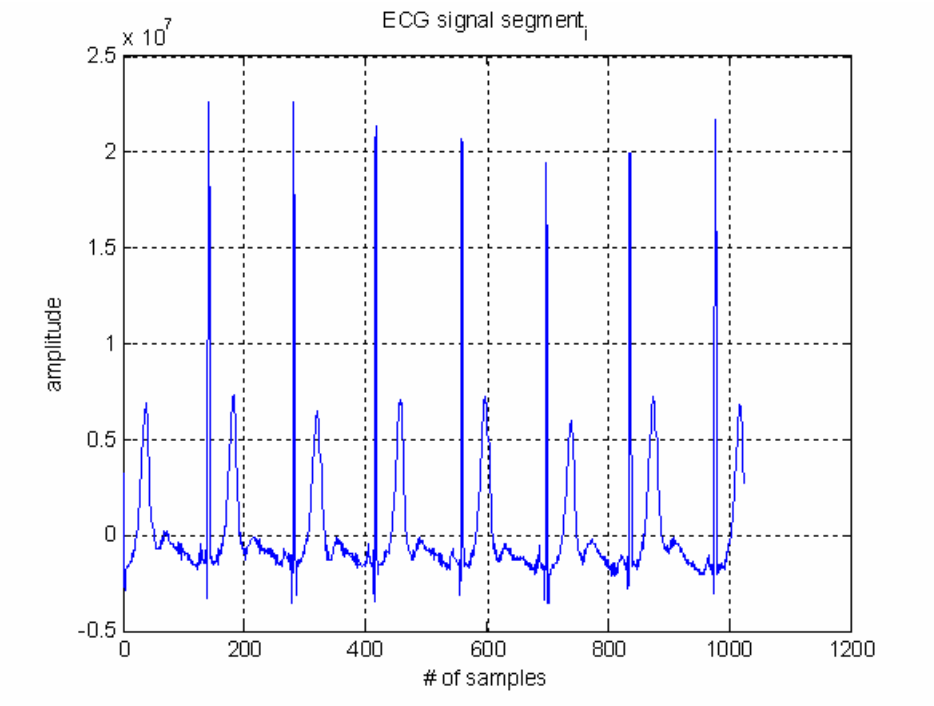

Figure 6.8 7th ECG segment with 1024 samples.

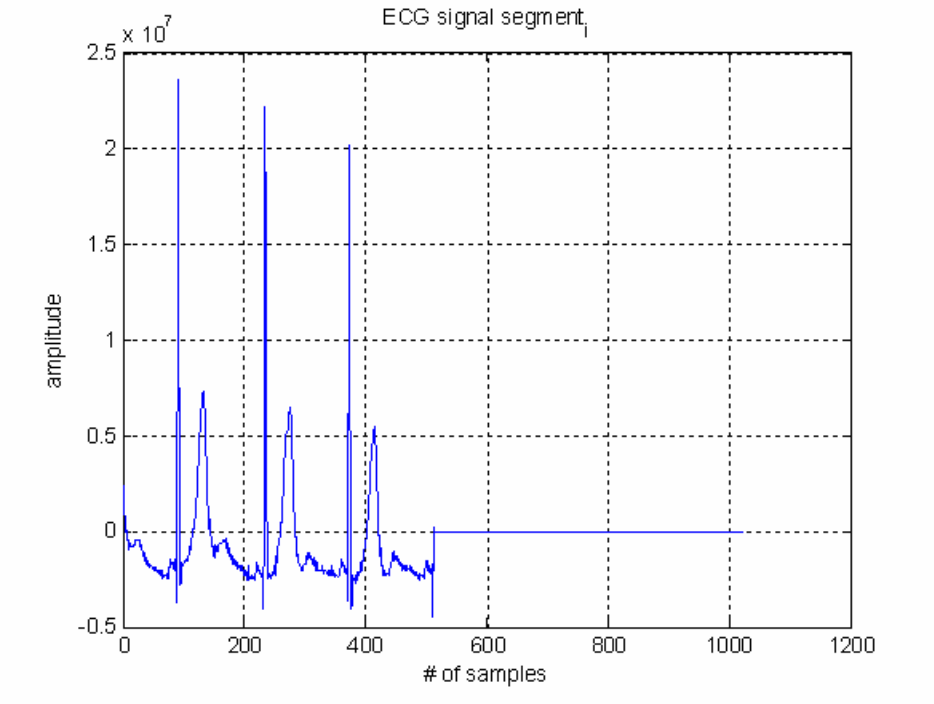

Figure 6.9 8th ECG segment with 512 samples.

6.3.2 Wavelet decomposition

For many signals, the low-frequency content is the most important part. It is what gives the signal its identity. The high-frequency content, on the other hand, imparts flavor or nuance. For instance, consider the human voice. If the high-frequency components are removed, the voice sounds different, but it is still told what's being said. However if the low-frequency components is removed, gibberish is heard.

In wavelet analysis, it is often spoken of approximations and details. The approximations are the high-scale, low-frequency components of the signal. The details are the low-scale, high-frequency components.

The filtering process, at its most basic level, looks like in Figure 6.10. The same procedure includes down sampling and up sampling is seen in the next, in Figure 6.11, in detailed form.

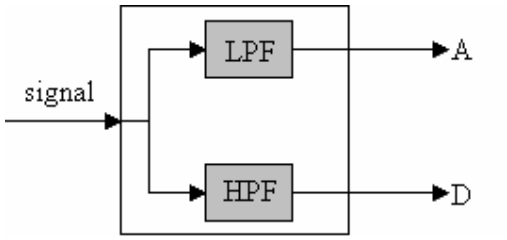

Figure 6.10 The filtering process.

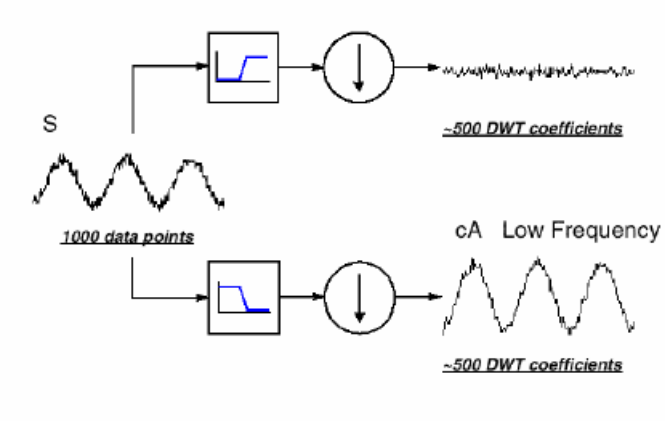

Figure 6.11 Filtering and down sampling.

The decomposition process can be iterated, with successive approximations being decomposed in turn, so that one signal is broken down into many lower resolution components. This is called the wavelet decomposition tree, shown in the Figure 6.12 [8].

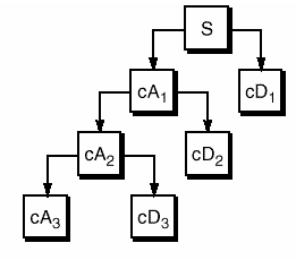

Figure 6.12 Wavelet decomposition tree.

In the implementation process the decomposition tree goes to the level of 5. For example, in the 1^{st} level of analysis, approximation $A1$ and detail $D1$ can be obtained with the use of $CA1$ & $CD1$ coefficients. If the original signal is taken into consideration as a whole segment with 7680 samples, the 1^{st} level signals can be displayed in Figure 6.13, below.

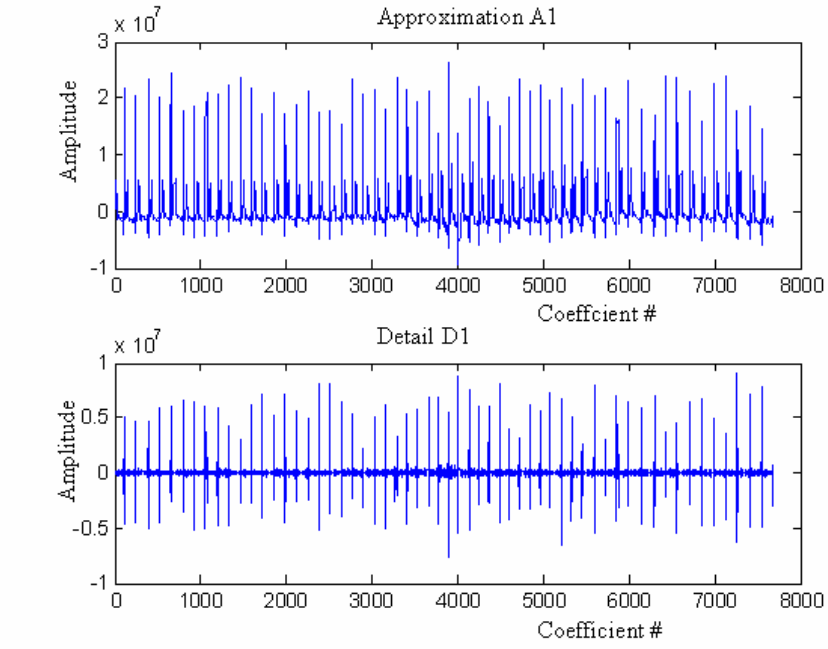

Figure 6.13 1st level decomposition of the original signal

If only the first 256 points of original ECG signal [0...256] is considered, the analyzed coefficients are formed as in Figure 6.14.

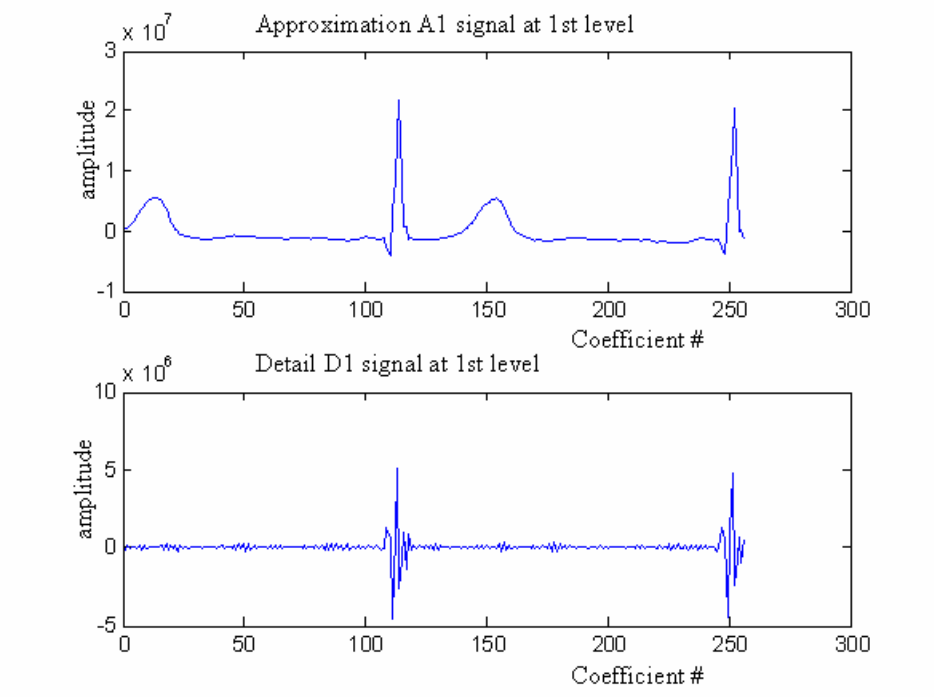

Figure 6.14 1st level decomposition for the interval of 0 to 256.

6.3.3 Wavelet synthesis

In the previous section it was mentioned that, discrete wavelet transform is used to analyze, or decompose the original signal. The other half of the story is how those components can be assembled back into the original signal without loss of information. This process is called reconstruction or synthesis shown in Figure 6.15. The original signal is trying to be reproduced to the original one.

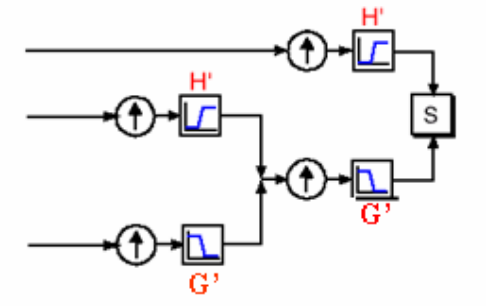

Figure 6.15 Filtering and up sampling.

Where wavelet analysis involves filtering and down sampling, the wavelet reconstruction process consists of up sampling and filtering [8].

A multi-step analysis-synthesis process is shown in Figure 6.16

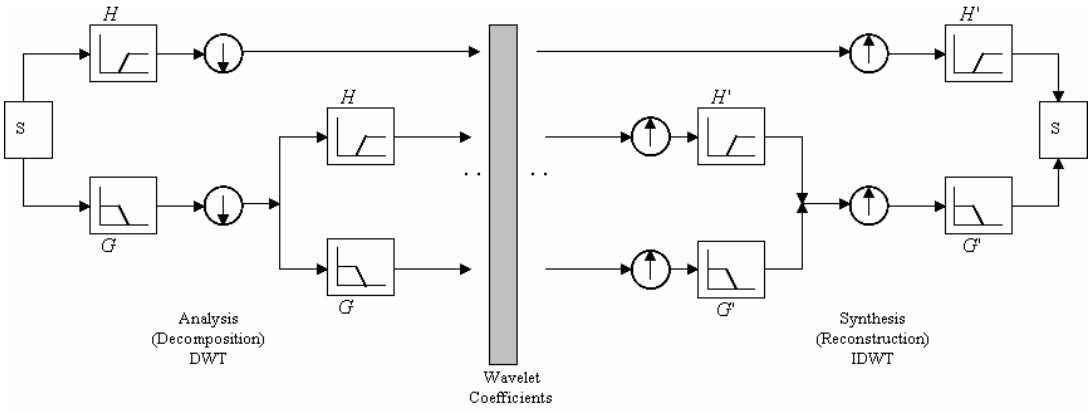

Figure 6.16 Multi-step analysis and reconstruction.

The result of the decomposition process of the original signal with 7680 samples is shown in the Figure 6.18. Besides, the sizes of the signal segments in each level for the multistep decomposition can also be presented in Figure 6.17.

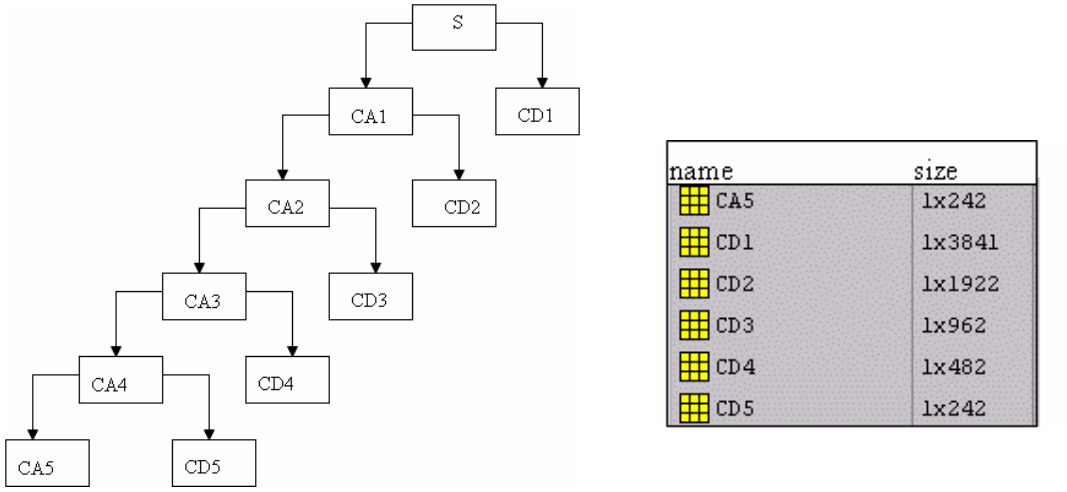

Figure 6.17 Size of the coefficients at different levels.

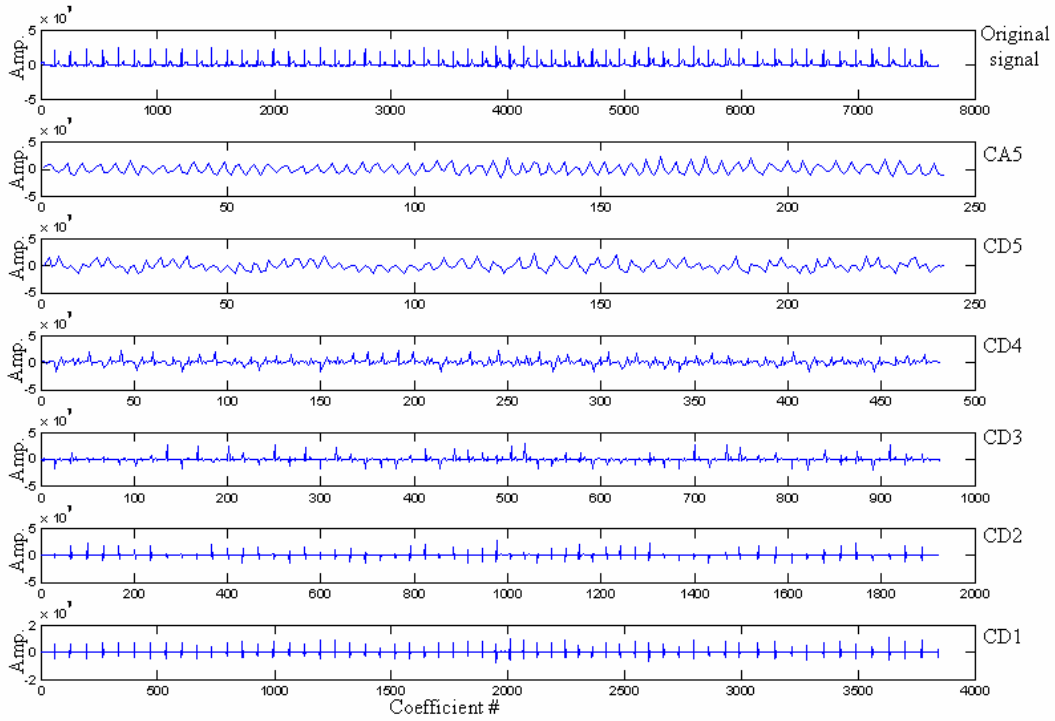

Figure 6.18 5 level decomposition of ECG signal.

6.3.4 Uniform Quantization

For each a_J and $d_j, 1 \le j \le J$, uniform quantization is realized. Quantization bin size of Δ, is different for each a_J and d_j components can be calculated in the Equations 6.10 and 6.11.

$$a_J \rightarrow \Delta = (2\max(abs(CA5)))/(2^n) \tag{6.10}$$

$$d_j \rightarrow \Delta = (2\max(abs(CDi)))/(2^n) \tag{6.11}$$

Quantized signal components are shown in the following figures from 6.20 to 6.25. For the equations seen above, $i = 1:5, n = 8$, Δ_s are calculated. MSE is generated in the quantization of approximation and detail coefficients. Mean square error and quantization step size values for each segment (Δ) are shown in the Table 6.1. MSE corresponds to the ε_j^d and ε_J parameters. In Figure 6.19, the original ECG signal is shown for the limited interval.

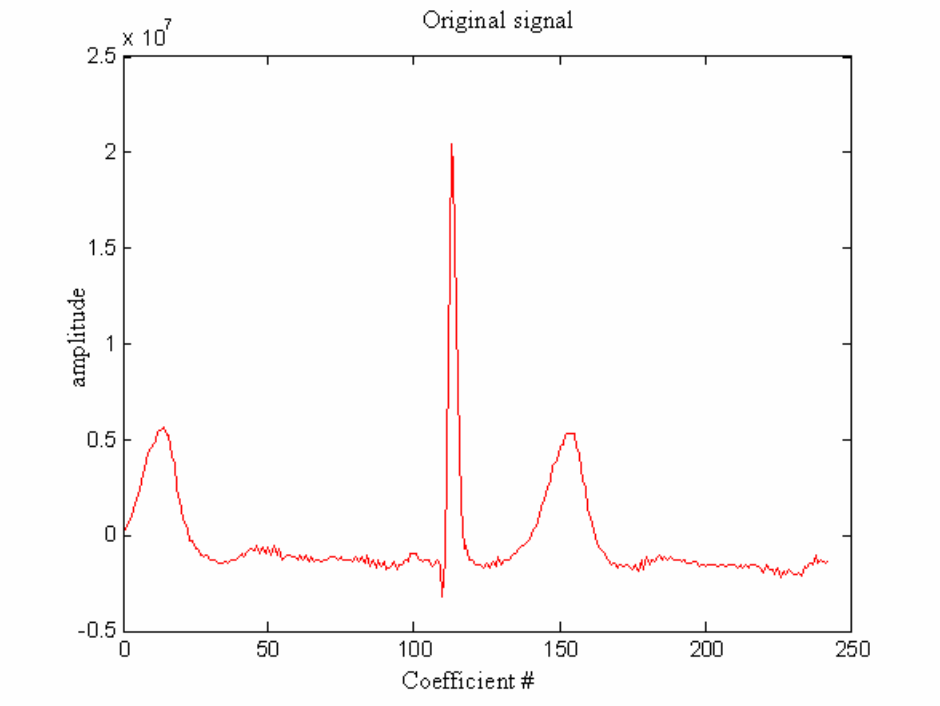

Figure 6.19 Original ECG signal [0-242].

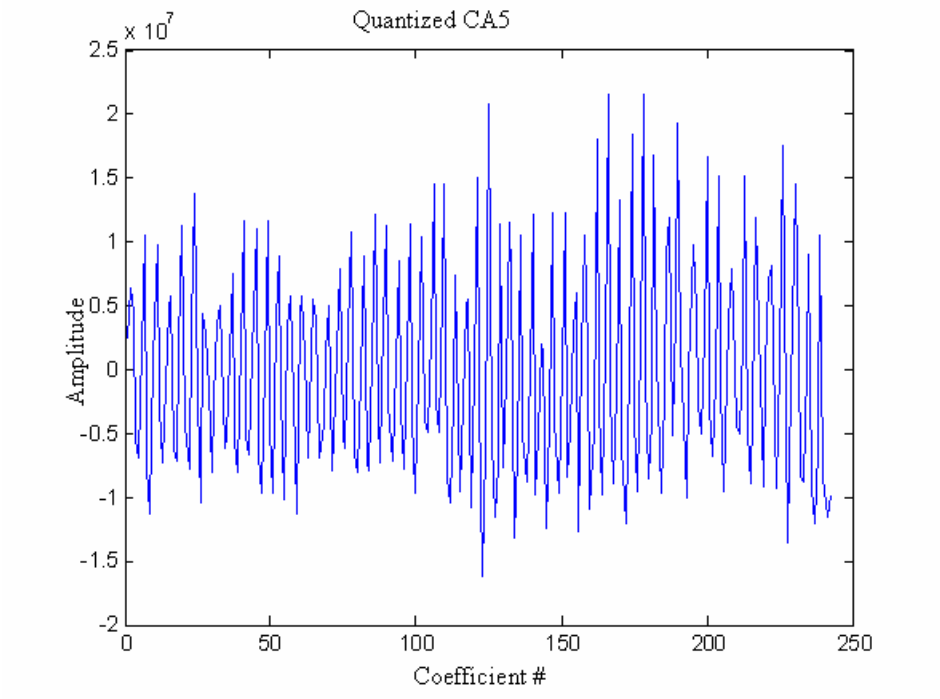

Figure 6.20 Quantized CA5 [0-242].

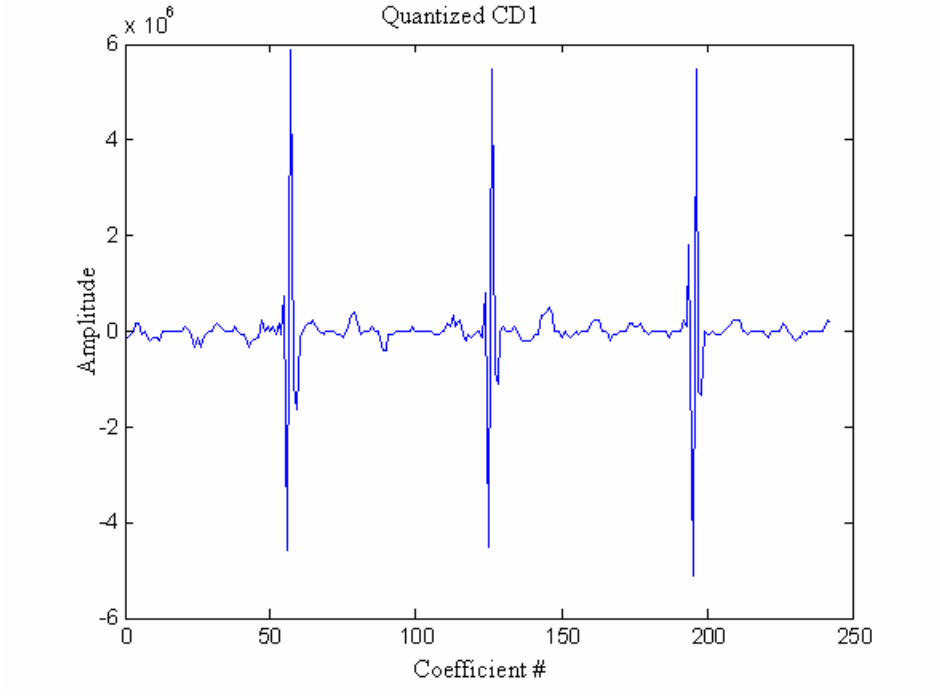

Figure 6.21 Quantized CD1 [0-242].

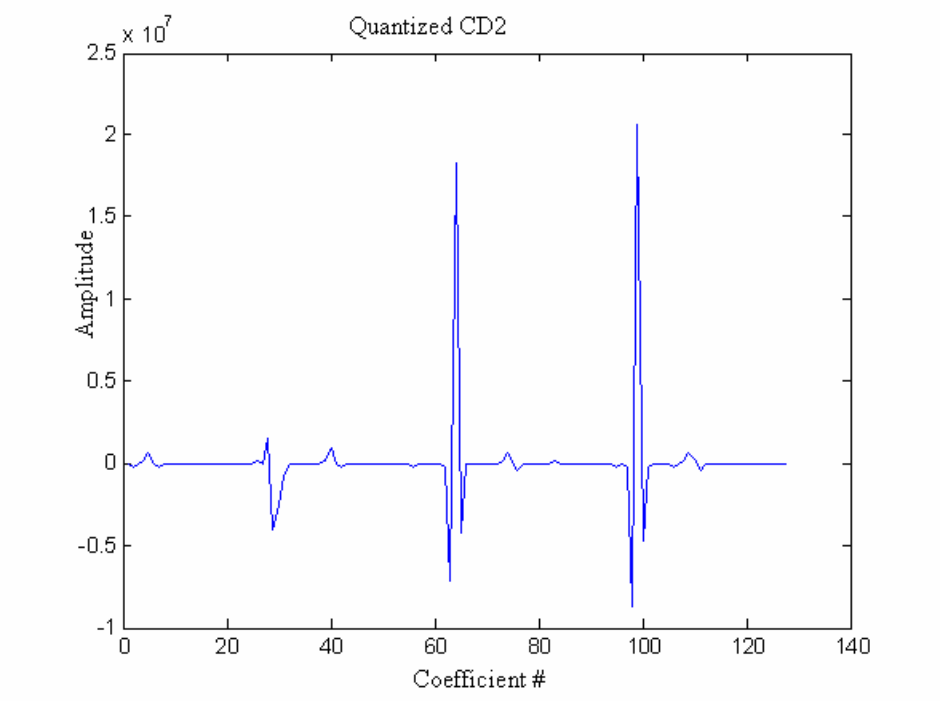

Figure 6.22 Quantized CD2 [0-128].

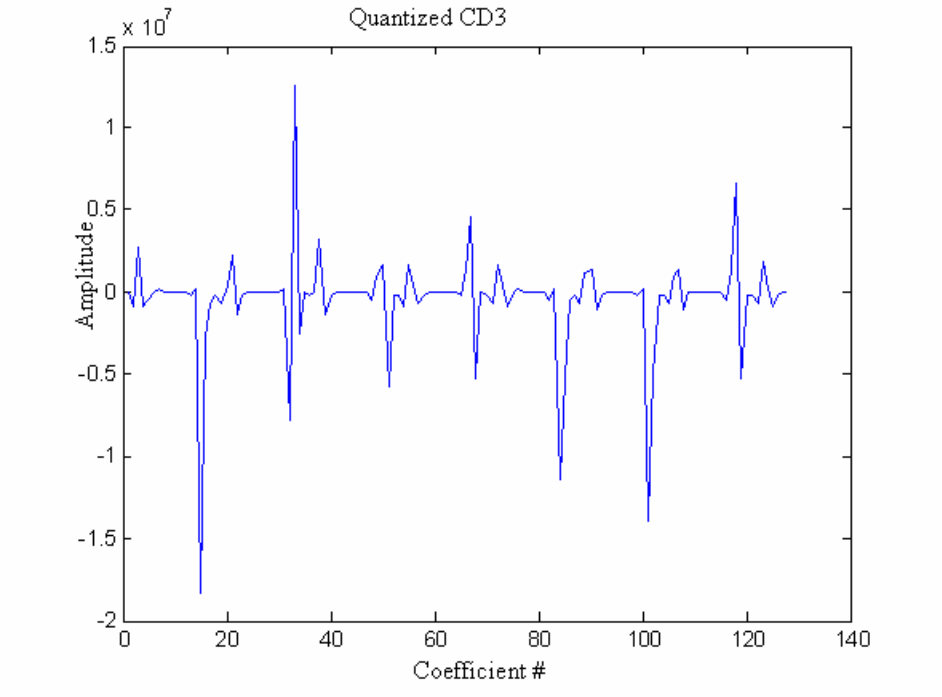

Figure 6.23 Quantized CD3 [0-128].

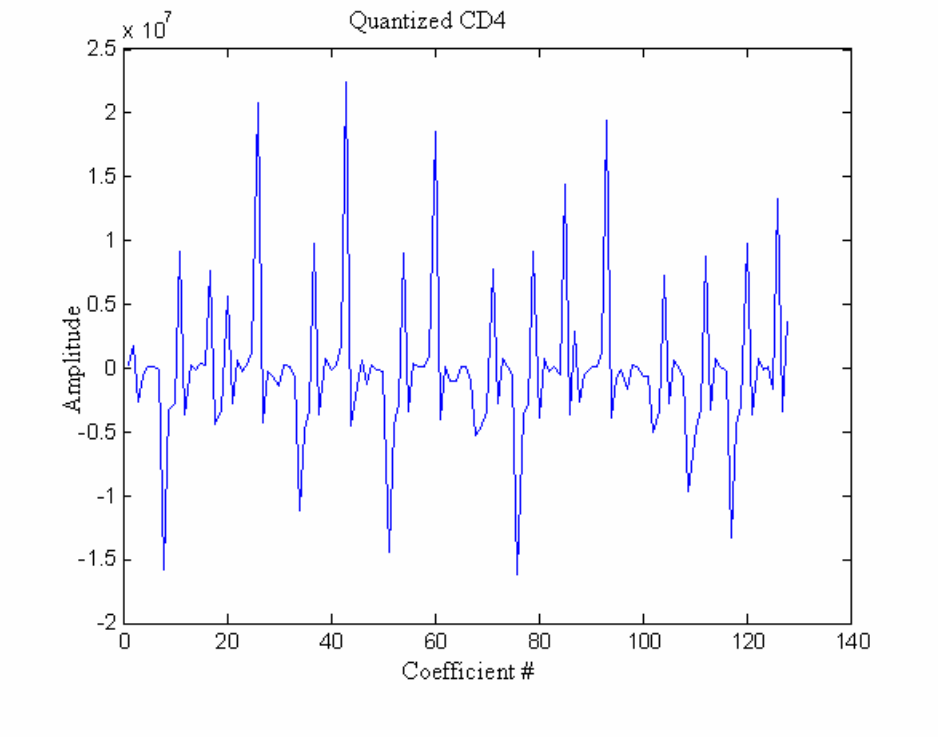

Figure 6.24 Quantized CD4 [0-128].

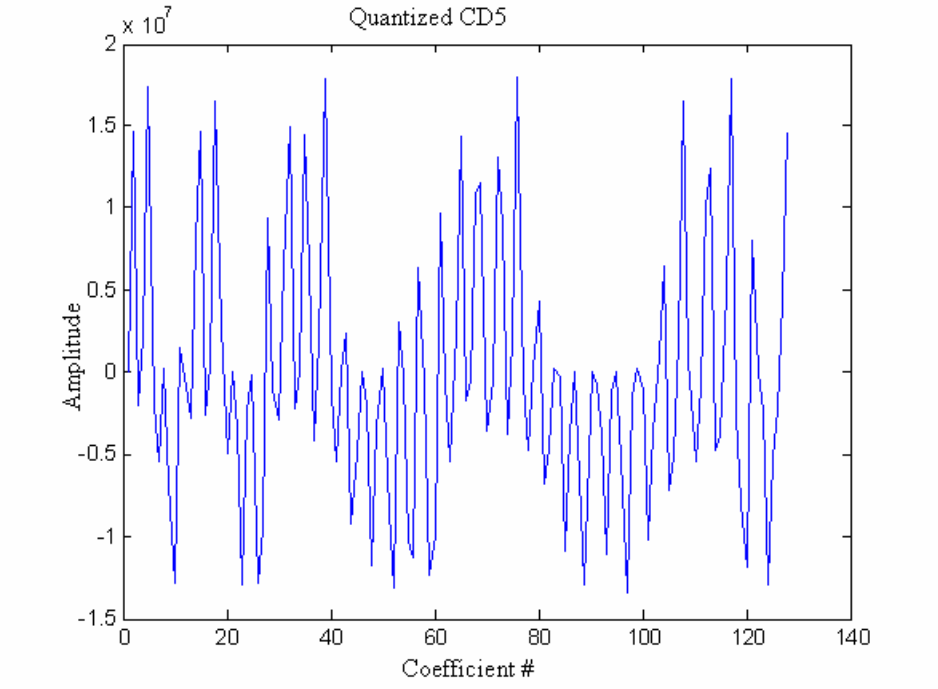

Figure 6.25 Quantized CD5 [0-128].

Table 6.1
Quantization step size and MSE for different DWT coefficients.

DWT coefficients	Quantization step size $\Delta[mV]$	Quantization MSE $[10^{-3}\,v^2]$
*CA*5	169,65	2,39
*CD*1	79,245	0,52
*CD*2	212,83	3,77
*CD*3	228,88	4,36
*CD*4	176,13	2,58
*CD*5	170,13	2,41

In the table above, quantization step size and the quantization mean square errors for each *DWT* coefficients are shown [7]. The quantization errors have values in the optimum range

6.3.5 LZW encoder

The input of the LZW block is the binary data sequence. The quantization levels created by the quantization of the approximation and the detail coefficients are converted into the binary data structure in order to use for the input of LZW encoding [16].

Prior of the LZW encoding, binary conversion is done.

$$CA5\_quantised \rightarrow CA5\_quan\_coded$$

$$i = 1:5$$

$$CDi\_quantised \rightarrow CDi\_quan\_coded$$

On Figure 6.26 LZW encoder block diagram is displayed.

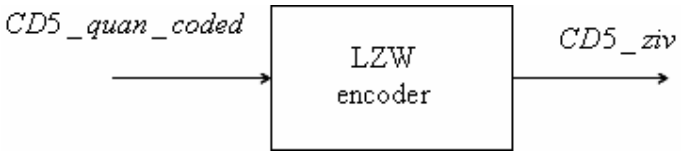

Figure 6.26 LZW encoder.

On Figure 6.27 LZW decoder block diagram is displayed.

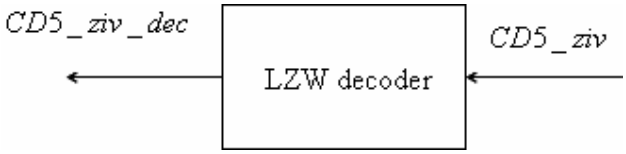

Figure 6.27 LZW decoder.

In the diagram shown above, $CD5$ is given for an example. In addition to that, quantized and binary coded data sequence of $CD4$, $CD3$, $CD2$, $CD1$, and $CA5$ are available at the input of the encoder and the decoder blocks.

The compression performance, namely the CR value is obtained as 12,91 by means of LZW coding algorithm [7]. This result is provided with the Equation of 6.8.

$CD5\_quan\_coded$ is the input of LZW encoder, and $CD5\_ziv\_dec$ is the output of the LZW decoder. The result that is implemented by MATLAB programming shows that, LZW method is a lossless compression algorithm. Both $CD5\_quan\_coded$ and $CD5\_ziv\_dec$ displayed on Figure 6.28 are same with one another.

```
K>> CD5_quan_coded

CD5_quan_coded =

  Columns 1 through 18

     0     0     1     1     0     1     0     1     0     0     1     1     0     1     0     1     1     0

  Columns 19 through 36

     0     0     0     1     1     0     1     0     0     1     0     1     0     0     0     0     1     0

  Columns 37 through 54

     1     0     0     0     0     0     0     0     0     0     1     1     0     1     1     1     1     1

  Columns 55 through 72

     1     1     0     0     0     0     1     0     0     0     1     1     0     0     1     0     0     1

  Columns 73 through 90

     1     0     0     1     1     1     1     1     0     0     1     1     0     0     0     0     1     0
```

```
K>> CD5_ziv_dec

CD5_ziv_dec =

  Columns 1 through 18

     0     0     1     1     0     1     0     1     0     0     1     1     0     1     0     1     1     0

  Columns 19 through 36

     0     0     0     1     1     0     1     0     0     1     0     1     0     0     0     0     1     0

  Columns 37 through 54

     1     0     0     0     0     0     0     0     0     0     1     1     0     1     1     1     1     1

  Columns 55 through 72

     1     1     0     0     0     0     1     0     0     0     1     1     0     0     1     0     0     1

  Columns 73 through 90

     1     0     0     1     1     1     1     1     0     0     1     1     0     0     0     0     1     0
```

Figure 6.28 LZW encoder input and LZW decoder output.

6.3.6 Wavelet reconstruction

When the recostruction process is realized that is mentioned in the previous sections, the reproduced signals for each level may be obtained shown in Figure 6.29.

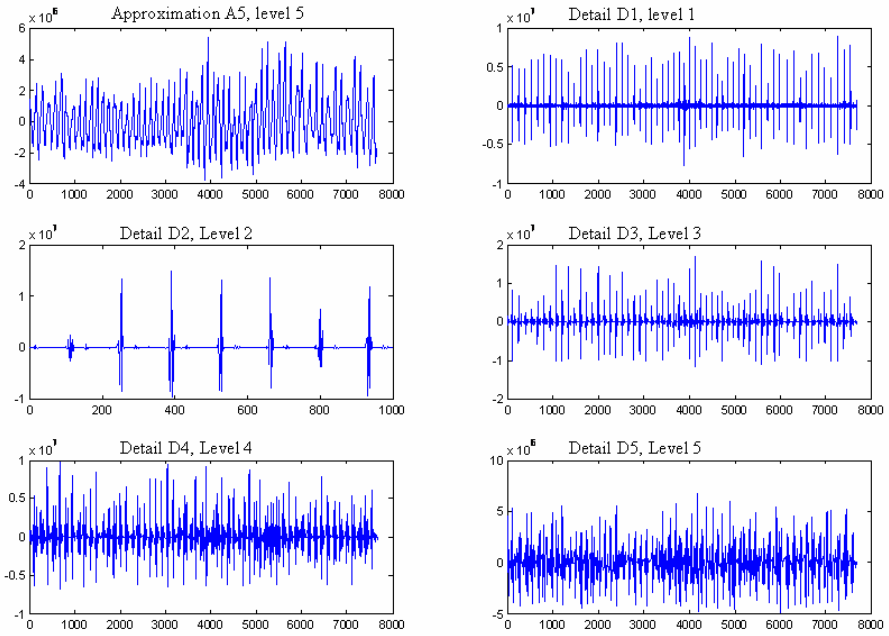

Figure 6.29 5 level wavelet synthesis.

In Figure 6.30, the same signal is analyzed for the limited coefficients, and the reconstructed waveform for 5 step decomposition is displayed as it is in the previous one.

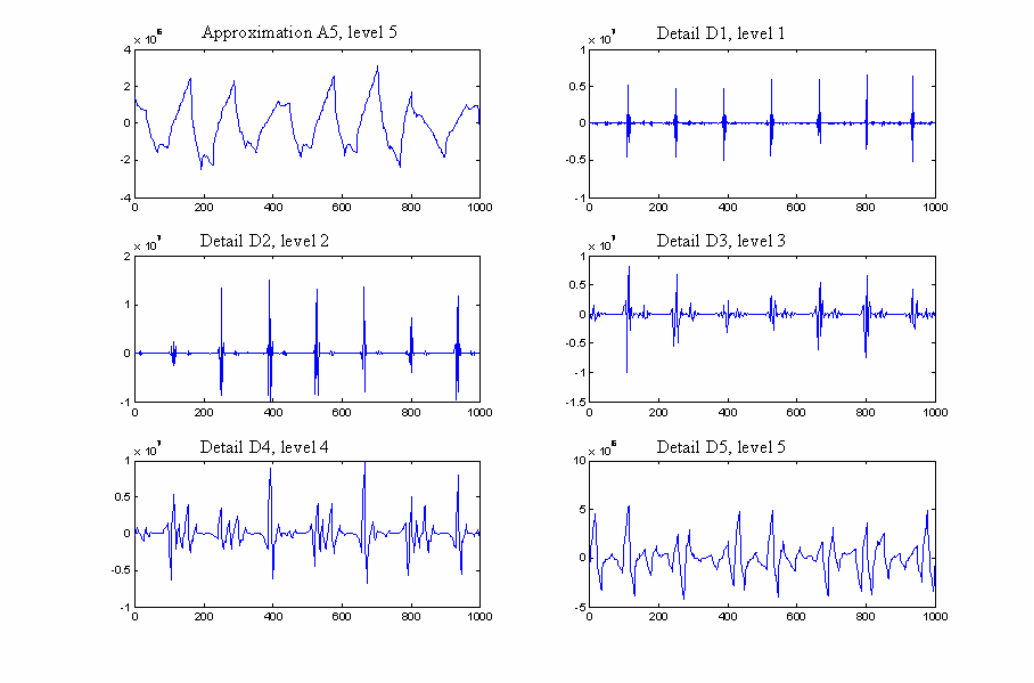

Figure 6.30 5 level wavelet synthesis for 0 to 1000.

The reconstructed signal provided after the synthesis process is shown in Figure 6.31.

The error trace diagram that is realized in the method of wavelet transform is displayed in Figure 6.32.

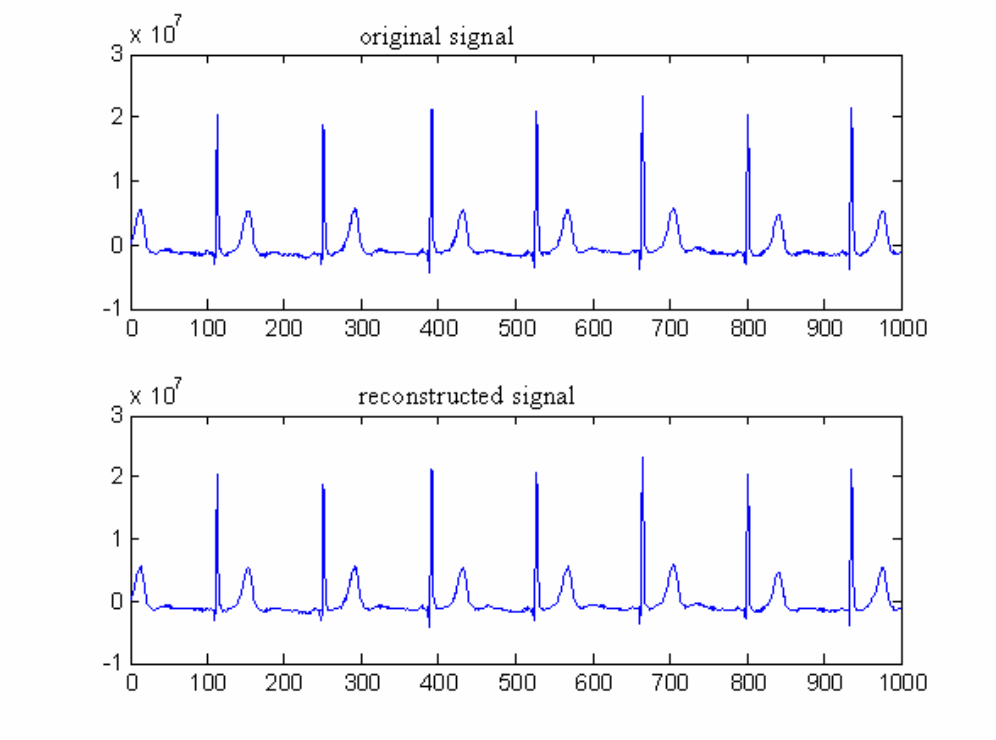

Figure 6.31 The Original signal and reconstructed signal.

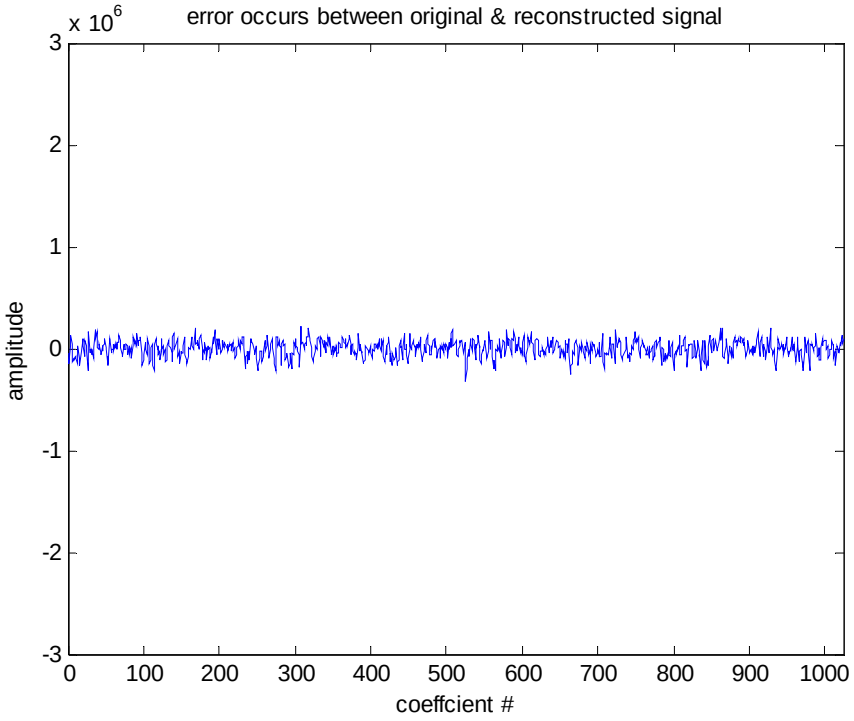

Figure 6.32 Error occurs between original and reconstructed signals in WT model.

6.3.7 Reconstruction mean square error

To make the results quantitatively comparable to other ECG compression methods, here it is used most widely-known numerical indexes of *PRD* (percent root mean square difference) and *CR* (compression ratio). In the following lines, the changes of these parameters are shown.

When the subsignals are quantized, for $1 \le j \le J$, $\{a_J, (d_j)\}$ the *RMSE* (Reconstruction Mean Square Error) between the original signal a_0 and the reconstructed a'_0 occurs.

RMSE between the original signal and its reproduced version can be exactly calculated from the quantization MSE's of the decomposed subsignals (a_J and d_j). So, for the first 7 segments that has 1024 samples, and the last segment that has 512 samples, *RMSE* is occurred [12], [13].

$$\gamma = \varepsilon_J + \sum_{j=1}^{J} \varepsilon_j^d$$

$$\gamma = \varepsilon_{CA5} + \varepsilon_{CD1} + \varepsilon_{CD2+}\varepsilon_{CD3} + \varepsilon_{CD4} + \varepsilon_{CD5} \tag{6.12}$$

Calculated as $\gamma = 16{,}03.10^{-3} v^2$

A widely used quantitative distortion measure for ECG coding is the *PRD*. *PRD* is calculated the result of 7,3%

6.4 Discrete Cosine Transform & Discrete Sine Transform

Orthogonal transforms provide alternate signal representations that can be useful for ECG data compression. The goal is to select as small a subset of the transform coefficients as possible which contain the most information about the signal, without introducing objectionable error after reconstruction.

Based on the research, more than 99% of the power in *DCT* and *DST* is contained within the first 20% of the coefficients. The coefficients after the first 20%, are approximated as zero [3].

A wide variety of techniques are available for ECG data compression [1]. With the emergence of fast DSP processors, and fast algorithms for the computation of many orthogonal transforms, transform compression can be effectively used in real-time applications [15].

Using orthogonal transform in data compression, a subset of the coefficients is selected in the transform of the input signal with which can be reconstructed the signal without introducing significant error. To obtain an optimal transform, an error criterion is necessary the mean square error is often used in ECG applications. The optimum orthogonal transform in the mean square criterion is the Karhunen-Loeve Transform (KLT).

Original ECG signal is divided into blocks (subsignals). Each block is quantized with the help of thresholding factor. Threshold factor is obtained empirically. By using the threshold, the coefficients which have values below the threshold level are discarded and only the remaining coefficients are taken into consideration. At the end, in order to evaluate the performance of the compression, realized, the same parameters namely, *PRD* and *CR* are used [7].

ECG signal compression via *DCT* & *DST* algorithms is displayed in the block diagram, namely Figure 6.33, below.

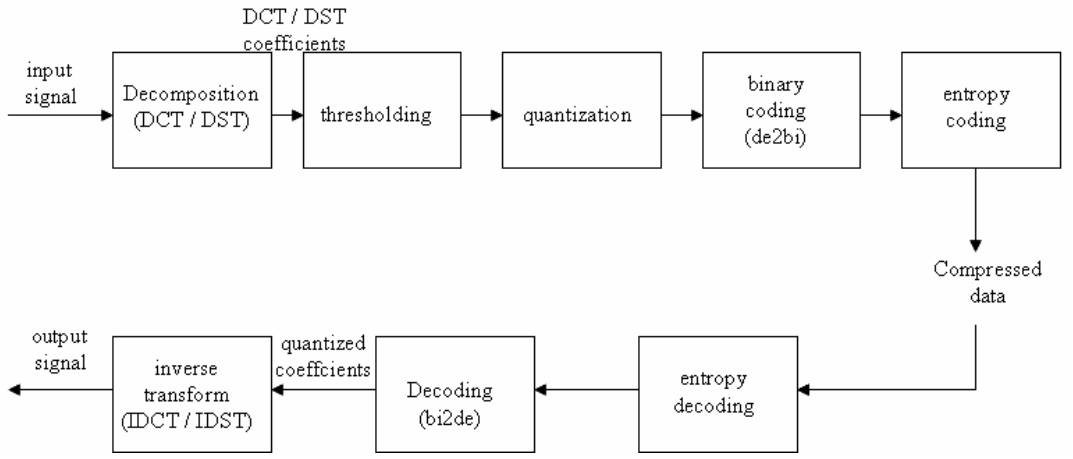

Figure 6.33 DCT & DST block diagram.

The first block includes the decomposition process in the diagram, comprise the transformation procedure of *DCT* or *DST* [10]. After the implementation of thresholding, the required coefficients are uniformly quantized. The output of the quantization will be the input of LZW coding. Now, the digital data is compressed at the end of entropy coding. This situation is somehow is the representation of the digital signal with decreased size. Thus, entropy coding is so important in signal compression. LZW coding method is used for the purpose of entropy encoding [16]. The remaining issue is the inverse of the forward diagram.

6.4.1 Decomposition with DST & DCT

ECG signal taken from MIT-BIH database is used for this purpose. *DST* or *DCT* transformation is the process of creating subsignals each has L input samples: In other words, this is the procedure of *DCT* & *DST* block generation.

$$7680 = (1024x7) + 512$$

$$7 segments[1...7] \rightarrow L = 1024$$

$$8.segment \rightarrow L = 512$$

Below the first and the last *DST* block is given as an example displayed on Figures 6.34 and 6.35.

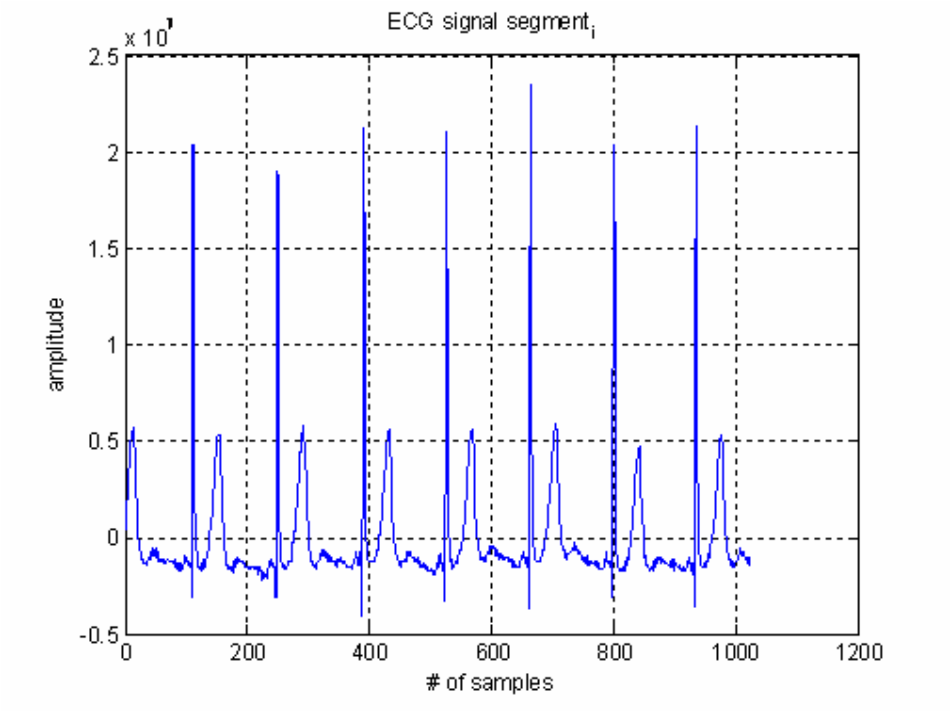

Figure 6.34 1st DST block, L=1024, segment1.

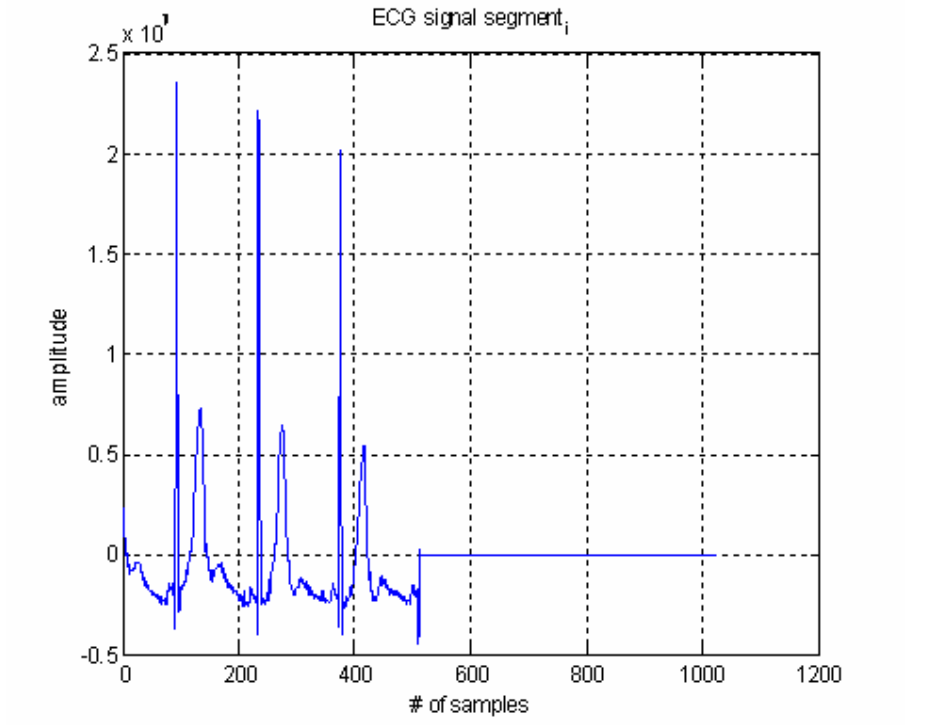

Figure 6.35 8th DST block, L=512, segment8.

As it is mentioned above, there are 7 *DST* or *DCT* block available, with 1024 samples, and only one *DST* or *DCT* block with 512 samples, each has different from one another.

W_i is the *DST* or *DCT* form of the input ECG signal segment ($segment_i$, $(i = 1,...,8)$). Each W_i has the same size with $segment_i$. That is to say, when, $(segment_i)_{1x1024}$, then $(W_i)_{1x1024}$. Blocking diagram is shown in Figure 6.36

Figure 6.36 Blocking.

6.4.2 Threshold factor

Thresholding process is used in *DCT* and *DST* method. Thresholding provides the increase of the number of quantized samples to zero, and let the LZW coding as efficient as possible. Same threshold value is applied for each segment [5].

2 different parameters are used in the thresholding. For $i = 1,...,8$, *counterbidct* is the number of indexes different from zero in W_i , before thresholding. On the other hand, *counteraidct* is the number of indexes different from zero in Y_i, after thresholding. This process is seen in the Figure 6.37, below.

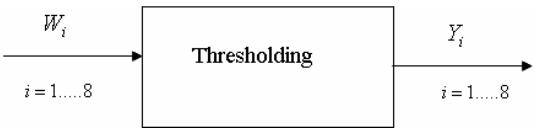

Figure 6.37 Thresholding.

In order to keep the value of *PRD* and *CR* in acceptable level, threshold factor is calculated as $0{,}2v$ in *DCT* and $15v$ in *DST* [5].

If threshold is set to 0, means that if threshold factor is not applied, it is observed that Compression Ratio (*CR*) decreases, *PRD* and *RMSE* increases, actual quantization *MSE* for each segment increases.

The effect of thresholding is displayed in Table 6.2.

Table 6.2
Thresholding effect.

i (segment #)	*counterbidct* (DCT/DST)	*counteraidct* (DCT/DST)	# of samples quantized to 0 (*counterbidct* - *counteraidct*) (DCT/DST)
1	1024 / 1024	697 / 471	327 / 533
2	1024 / 1024	700 / 468	324 / 556
3	1024 / 1024	727 / 483	297 / 541
4	1024 / 1024	827 / 530	197 / 494
5	1024 / 1024	748 / 509	276 / 515
6	1024 / 1024	761 / 517	263 / 507
7	1024 / 1024	729 / 511	295 / 513
8	512 / 512	384 / 230	128 / 282

6.4.3 Uniform quantization

Δ is the quantization step size, and each sample is represented with 8 bits $(n = 8)$. $\Delta = (2 * A_{\max})/(2^n)$ can be defined. $A_{\max}$ is different for each ECG segment. Thus quantization step size is different for every ECG segment

Also, the MSE values in each segment is different from one another

$$e = \frac{1}{N}\sum_{i=1}^{N}(x_i - y_i)^2$$

While x_i is defined for quantized $segment_i$, and y_i is the DCT / DST taken and threshold applied data sequence. In Table 6.3, quantization step size and real quantization mean square error for only DCT is displayed.

Table 6.3
Quantization step size and real MSE values for each segments.

Quantized signal	Quantization step size Δ[v]	Real MSE e[10^{-3} v^2]
$segment_1$	0,275	4,3054
$segment_2$	0,329	5,4926
$segment_3$	0,201	2,2382
$segment_4$	0,314	6,273
$segment_5$	0,335	6,7621
$segment_6$	0,331	6,5035
$segment_7$	0,242	3,2778
$segment_8$	0,169	1,7407

6.4.4 LZW encoding

The quantized and binary coded levels are also the inputs of LZW encoder. This conversion is shown in Figure 6.38. For every quantized and binary coded ECG segments, LZW coding is applied displayed in Figure 6.39.

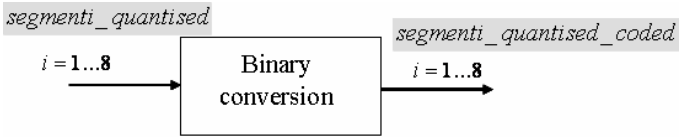

Figure 6.38 Binary conversion.

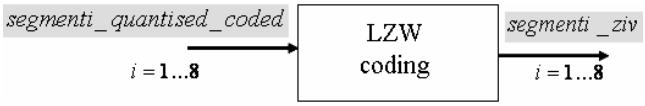

Figure 6.39 LZW encoder.

At the end of the LZW encoder, the compressed digital binary data sequence is available. By using *DCT* and *DST* algorithms, the *CR* values are 11,08 in *DCT* , and 11,708 in *DST* calculated

6.4.5 LZW decoding

$segmenti\_ziv-dec, i = 1...8$, is the decimal converted form of the binary data sequence, shown in Figure 6.40.

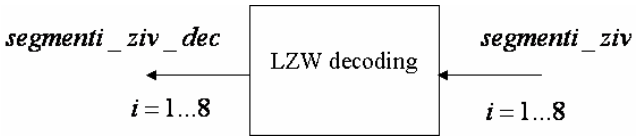

Figure 6.40 LZW decoder.

6.4.6 Inverse DST/DCT

It would be possible to reconstruct the ECG signal with the help of inverse discrete cosine/sine transform that has L input samples in each subsignal. In Figure 6.41, *IDST* block diagram is displayed.

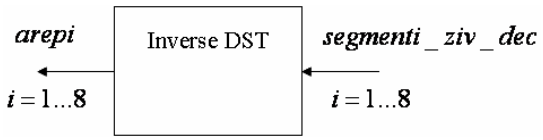

Figure 6.41 IDST block diagram.

$arepi, i = 1...8$, is the reconstructed ECG segments generated by *IDCT* algorithm. In Figure 6.42 and 6.43, it may be possible to see the reconstructed $arep_1$ that is belong to $segment_1$ and last reproduced segment $arep_8$, related with $segment_8$.

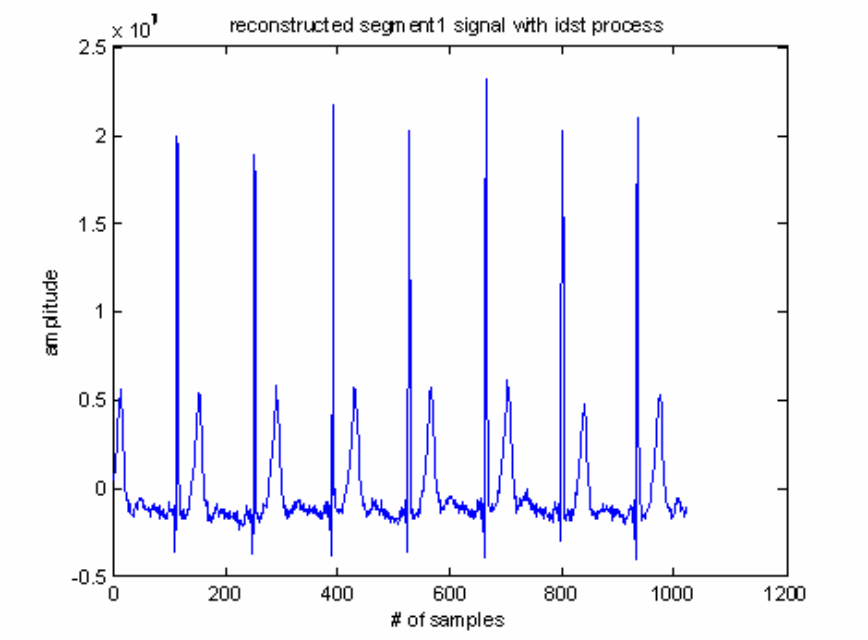

Figure 6.42 Reconstructed signal, arep1, L=1024.

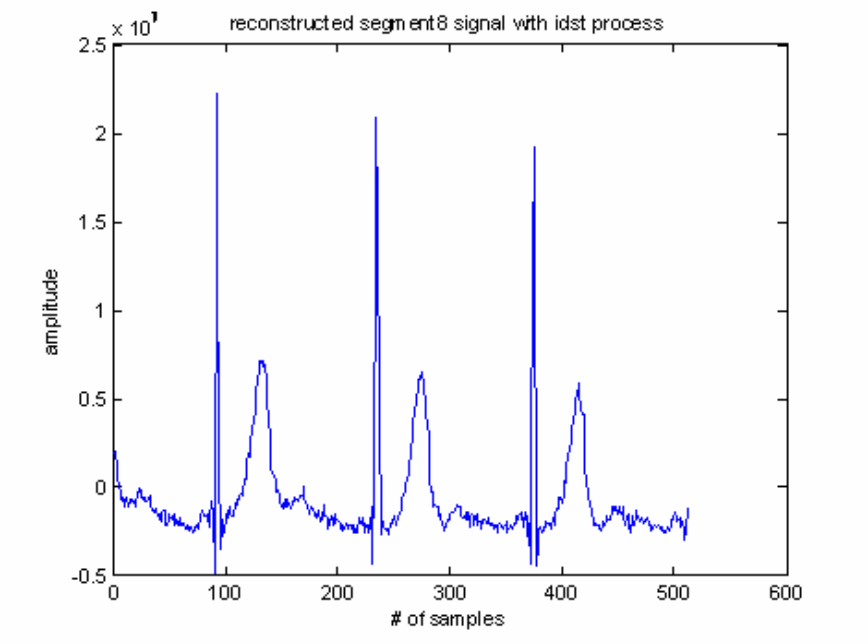

Figure 6.43 Reconstructed signal, arep8, L=512.

The reconstructed signal waveform is shown in Figure 6.44. In that case, reconstruction error in *DCT* is $e = 1{,}014.10^{-3} v^2$ and in *DST* $e = 1{,}54.10^{-6} v^2$ is calculated.

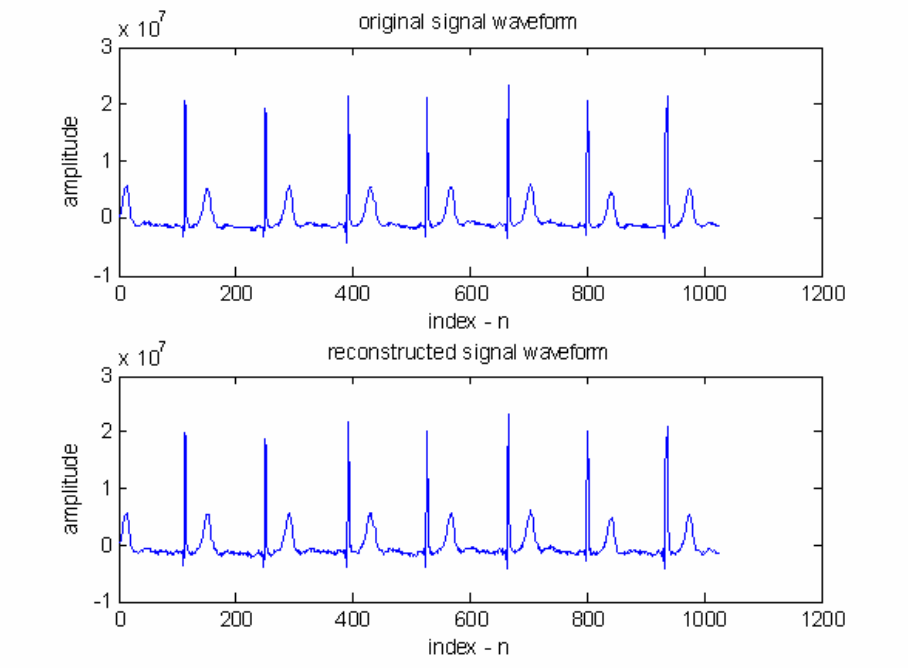

Figure 6.44 Original and reconstructed signal waveform.

The error trace diagrams for the discrete cosine & sine transform methods are displayed in Figures 6.45 and 6.46, respectively.

Distortion evaluation parameter PRD is calculated as $PRD = 2{,}2357\%$ in DCT and $PRD = 2{,}75\%$ in DST .

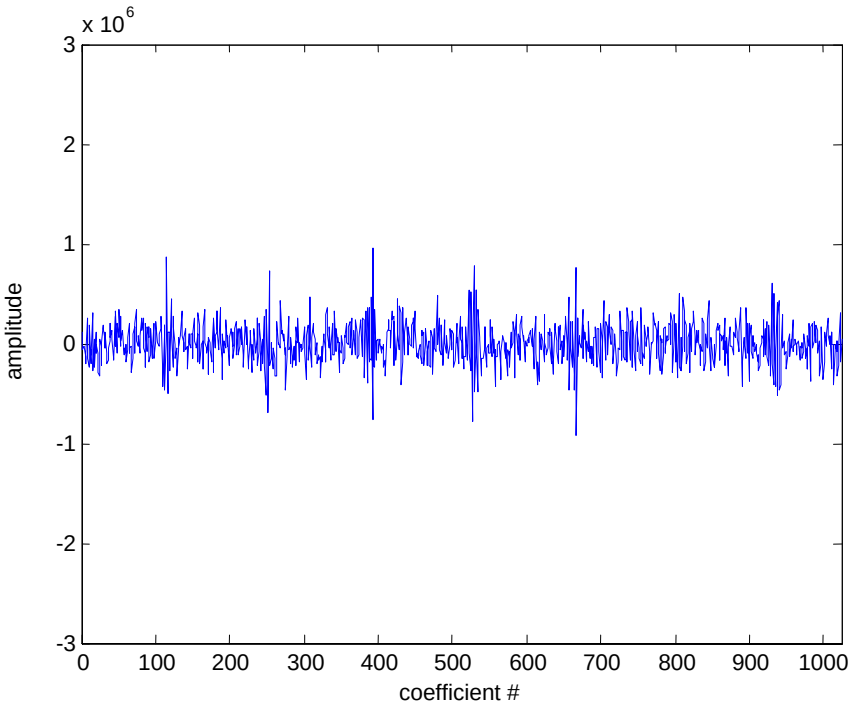

Figure 6.45 Error between original and reconstructed signal in DCT model.

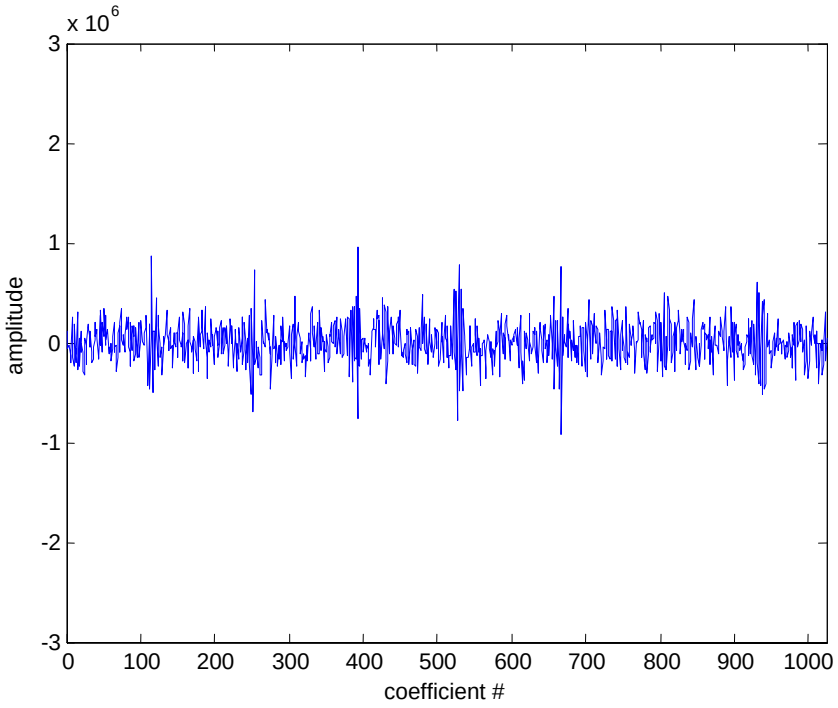

Figure 6.46 Error occurs between original and reconstructed signal in DST model.

6.5 Wavelet Packet Transform

Wavelet packet transform offers a richer range and a detailed investigation of the signal analysis. In wavelet packet analysis, the details as well as the approximations can be split [4], [9].

The # decomposition level that is used in wavelet transform is still be used in wavelet packet transform. $L = 5$ will be used for the implementation. For $W_{j,n}$, $j = 0,...,5$, $n = 0,...,31$, wavelet packet coefficients are generated. Then, with the help of the algorithms of uniform quantization and coding, the original signal is compressed.

LZW decoder and wavelet packet synthesis blocks, allows to reconstruct the original signal again.

In the wavelet packet transform method, the effect of different wavelet family in use is investigated on CR performance. Besides the changes, when the # of decomposition level is decreased, is analyzed and submitted as a report. For the

different wavelet family, the *CR* and the *PRD* values are evaluated for each transform methods.

The error trace diagram that is realized in the method of Wavelet Packet Transform is displayed in Figure 6.47.

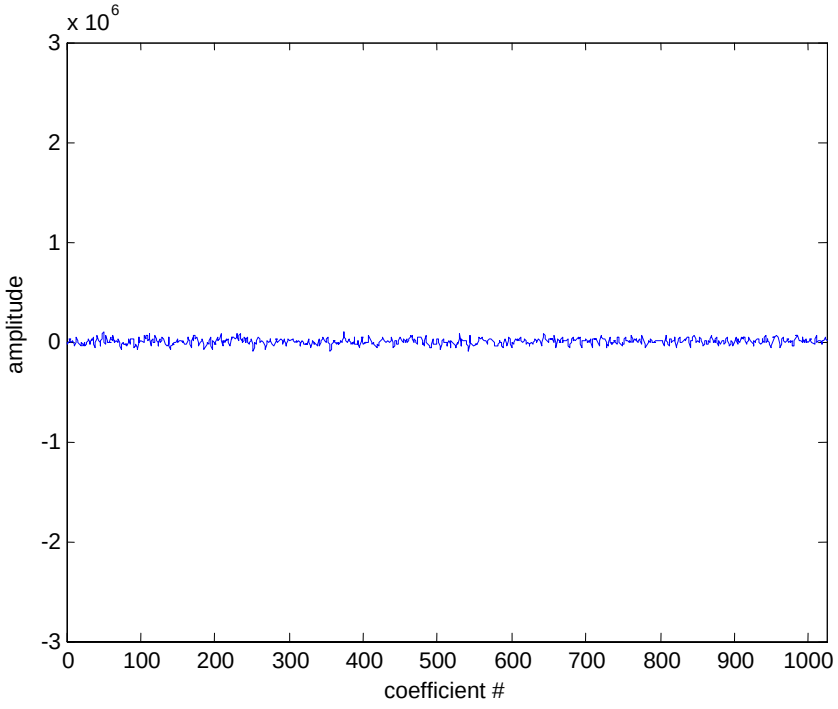

Figure 6.47 Error between original and reconstructed signal in WPT model.

6.6 Direct Compression Result

If the compression is done directly on the ECG samples, the compression ratio that is obtained is lower then the results achieved in transform methods, examples include wavelet transform, wavelet packet transform, discrete cosine transform, and discrete sine transform. The obtained *CR* value is 1,135. Decomposition, transformation, quantization and thresholding are not used. The original ECG samples are applied directly to entropy coding.

6.7 Analysis with Arrhythmia ECG signal

Digital signal with 4170 samples is used for arrhythmia case. Based on the applications, *CR* and *PRD* values are calculated as 16,28 and 34,269% successively. The error trace diagram for the arrhythmia ECG signal that is realized in the method of Wavelet Transform is displayed in Figure 6.48.

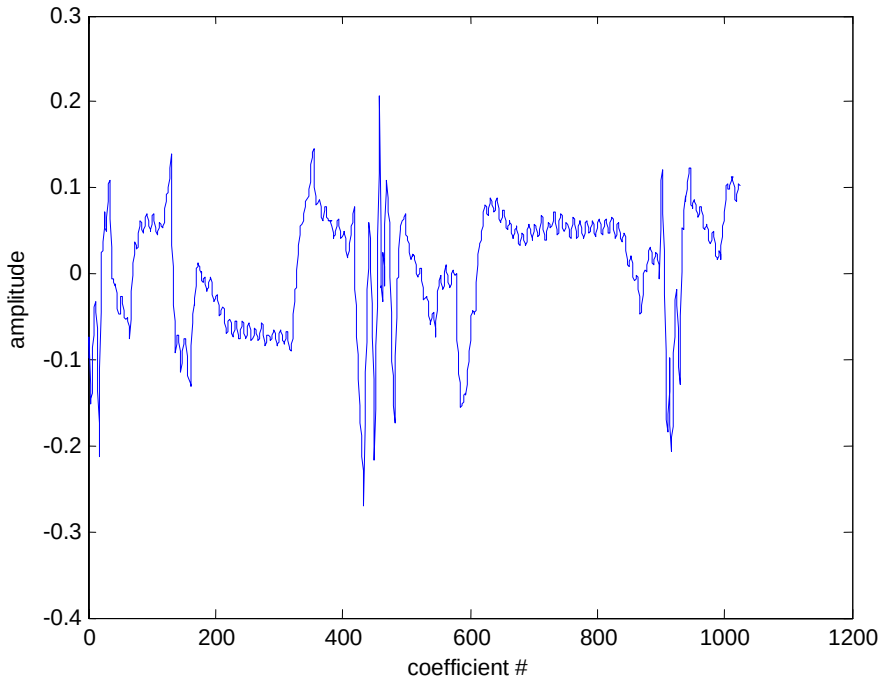

Figure 6.48 Error between original and reconstructed signal in WT model for arrhythmia.

The results of the evaluation show that the reproduced ECG waveform at specified *PRD* of 34,269% is defined as notably degenerated, some lost in diagnostic information, and clinically not acceptable. The original and reproduced forms for arrhythmia ECG signal are shown in the same plot in Figure 6.49.

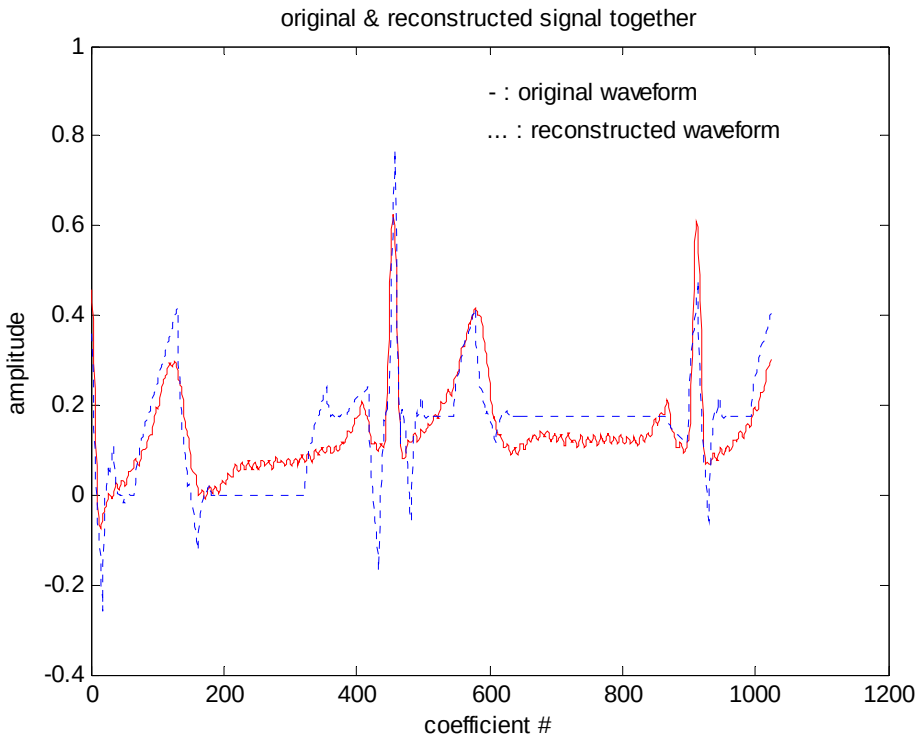

Figure 6.49 Original and reconstructed waveform for WT model of arrhythmia ECG signal.

The error trace analysis is also investigated in discrete cosine transform for the same arrhythmia ECG signal with 4170 samples. The distortion mentioned above is also occurred in *DCT* model with the *PRD* value of 18,95%. The *CR* value is 7,32. The error trace diagram for the arrhythmia ECG signal that is realized in the method of *DCT* is displayed in Figure 6.50.

The original and reproduced forms for arrhythmia ECG signal are shown in the same plot in Figure 6.51 for the *DCT* model.

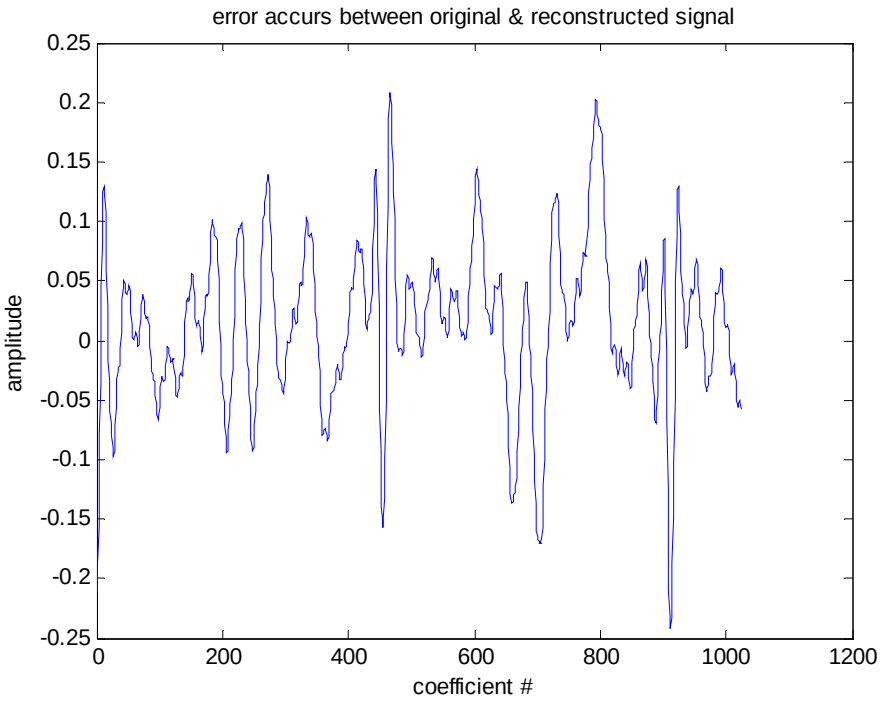

Figure 6.50 Error occurs between original and reconstructed signal in DCT model for arrhythmia.

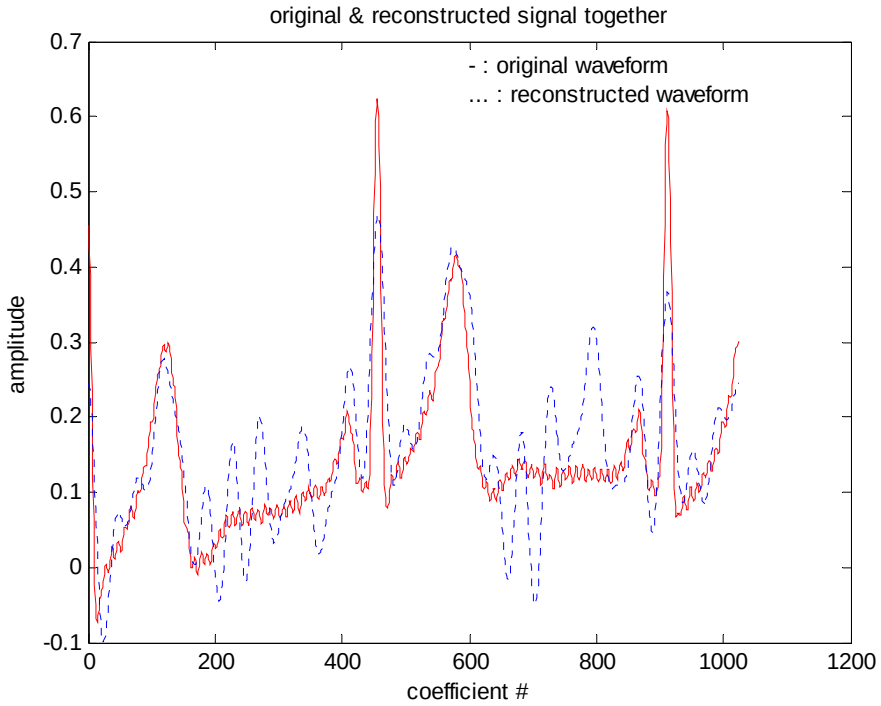

Figure 6.51 Original and reconstructed waveform for DCT model of arrhythmia ECG signal.

7. RESULTS

7.1 Application Details & Conclusion

Digital ECG signal compression is successfully realized with the four different methods of wavelet transform, wavelet packet transform, discrete cosine transform, and discrete sine transform. A Pentium 4, 2,4GHz CPU, 256 MB RAM PC is used to test all of the algorithms developed.

10 different wavelet families are applied to two different types of ECG signals (normal and arrhythmic). The efficiency of the methods are compared with each other using two quantitative parameters, namely the Compression Ratio (CR) and the Percent Root Mean Square Difference (PRD),

The CR values obtained by the WPT method is smaller then the CR values generated by the WT. It is clear that, the compressed data bits size (B) in WPT method is larger then (A) the WT method shown in Equation 7.1 and 7.2.

$$WT \rightarrow CR_{WT} = \frac{ODB}{A} \tag{7.1}$$

$$WPT \rightarrow CR_{WPT} = \frac{ODB}{B} \tag{7.2}$$

When, $B > A$

B is compressed data size in WPT, A is compressed data size in WP.

Then, $CR_{WT} > CR_{WPT}$ can be concluded.

On the other hand, CR values generated by the WT method is larger then the DCT and DST methods. Thus, the CR performance evaluation can be arranged as follows, only available for the same decomposition level

$$CR_{WT} > CR_{DST} > CR_{DCT} > CR_{WPT}$$

The second parameter that allows us evaluate the compression performance is the PRD. The distortion that results after a WT based compression is larger than those that results after WPT based compressions and some other transform methods, i.e.,

$$PRD_{WPT} < PRD_{WT}$$

The effect of decomposition level is analyzed only for the WPT method. If the value of L is increased, the CR decreases and in general the distortion in the reconstructed signal is also decreased. The effect of level is displayed in Table 7.5.

The threshold factor is also studied for the Discrete Sine Transform and Discrete Cosine Transform based methods and the effect of this factor on the CR and on the PRD values . If the threshold factor is not applied, the CR decreases, PRD increases, $RMSE$ increases, and actual quantization MSE for each segment increases. Threshold effect on actual quantization error both for DST and DCT are displayed in Tables 7.3 and 7.4.

To sum up, in all the techniques implemented, if the the CR increases the distortion, i.e., the PRD also increases. The expected and the optimal result is high compression ratio and low PRD value. This situation is directly related with the signal. For example, the most appropriate result for Table 7.1 is wavelet transform; on the other hand, the DCT method presents the best results in Table 7.2. In general, the highest compression ratio is realized with the wavelet transform based technique and the lowest PRD is obtained with the wavelet packet transform based method.

Table 7.1
CR and PRD values for the signal with 7680 coefficients.

Signal (7680 coefficients)	Transform method	L (Decomposition level)	Wavelet family	CR (Compression Ratio)	PRD (percent root mean square difference)
ECG	WT	5	db1	13,52	9,55
			db2	12,91	7,30
			db3	12,79	4,55
			bior2.2	14,10	5,18
			bior3.1	13,02	8,43
			bior4.4	12,99	0,51
			coif1	12,84	4,04
			coif2	13,14	3,65
			sym2	12,91	7,30
			sym5	13,19	2,46
	WPT	5	db1	7,98	0,17
			db2	7,76	0,94
			db3	7,69	3,70
			bior2.2	7,81	1,10
			bior3.1	7,68	0,54
			bior4.4	7,65	1,74
			coif1	7,76	2,3
			coif2	7,64	0,90
			sym2	7,76	0,93
			sym5	7,68	0,77
	DCT		thr=0	10,94	5,80
			thr=0,2	11,08	2,23
	DST		thr=0	9,53	5,76
			thr=15	11,708	2,75

Table 7.2
CR and PRD values for the signal with 5001 coefficients.

Signal (5001 coefficients)	Transform method	L (Decomposition level)	Wavelet family	CR (Compression Ratio)	PRD (Percent root mean square difference)
ECG	Wavelet transform	5	db1	12,6	5,58
			db2	13,44	3,04
			db3	13,89	4,41
			bior2.2	13,74	5,41
			bior3.1	14,49	5,42
			bior4.4	13,98	6,54
			coif1	13,66	6,21
			coif2	14,11	9,54
			sym2	13,44	3,04
			sym5	13,79	8,18
	WPT	5	db1	7,5	4,16
			db2	7,9	3,44
			db3	8,22	5,13
			bior2.2	8,05	0,75
			bior3.1	8,15	9,83
			bior4.4	8,73	3,19
			coif1	7,91	0,72
			coif2	9,4	1,92
			sym2	7,89	3,44
			sym5	8,53	3,95
	DCT		thr=0	13,66	0,45
			thr=0,2	13,68	0,44

Table 7.3
DST threshold effect on actual MSE.

	thr = 0	thr =15
segment #	Actual Quantization Error	Actual Quantization Error
segment1	2,07	0,93
segment2	2,22	1,04
segment3	2,08	0,98
segment4	4,07	2,05
segment5	3,67	1,85
segment6	3,97	2,01
segment7	3,4	1,75
segment8	0,98	0,46

Table 7.4
DCT threshold effect on actual MSE.

	thr = 0	thr =0,2
segment #	Actual Quantization Error exp(-3)	Actual Quantization Error (exp-3)
segment1	6,81	4,3
segment2	8,45	5,49
segment3	3,22	2,23
segment4	8,11	6,27
segment5	9,63	6,76
segment6	9,01	6,5
segment7	4,77	3,27
segment8	2,24	1,74

Table 7.5
Decompositon level effect on WPT.

Signal (7680 coefficients)	Transform method	L (Decomposition level)	Wavelet family	CR (Compression Ratio)	PRD (Percent root mean square difference)
ECG	WPT	L=5	db1	7,98	0,17
			db2	7,76	0,94
			db3	7,69	3,70
			bior2.2	7,81	1,10
			bior3.1	7,68	0,54
			bior4.4	7,65	1,74
			coif1	7,76	2,30
			coif2	7,64	0,90
			sym2	7,76	0,93
			sym5	7,68	0,77
		L=4	db1	9,31	2,45
			db2	9,18	2,36
			db3	8,91	3,01
			bior2.2	9,22	3,94
			bior3.1	9,26	2,67
			bior4.4	9,01	0,57
			coif1	9,22	0,26
			coif2	8,93	0,27
			sym2	9,18	2,36
			sym5	8,91	2,89
		L=3	db1	10,33	2,54
			db2	10,72	4,93
			db3	10,60	1,67
			bior2.2	10,94	3,82
			bior3.1	11,11	3,15
			bior4.4	10,84	2,82
			coif1	10,90	3,14
			coif2	10,90	2,69
			sym2	10,72	4,93
			sym5	10,61	3,24

7.2 Suggestions for Future Study

For further study, a new compression method may be studied and compared with the wavelet transform in terms of the compression ratio and the distortion measure (PRD). Another way of using these transform techniques may be provided by combining the strongest features to compress the digital ECG data as much as possible while maintaining clinically acceptable signal quality. The same threshold factor may be used for all of the segments and analyzed. This threshold factor is able to be determined based on the signal, and let the application to use the optimum threshold level after decomposition for every segment.

The most appropriate wavelet family for the analyzed signal can be studied. In this study, $Db2$ is used as a primary wavelet due to the similarity with the ECG signal. Such an intelligence may be provided to select the appropriate wavelet based on the signal, its amplitude and the number of coefficients, etc.

REFERENCES

1. Hilton M., "Wavelet and wavelet packet compression of electrocardiograms", *IEEE Trans. Biomed. Eng.,* vol. 44, pp. 394-402, May 1997.

2. Chen J., S. Itoh, "A wavelet transform-based ECG compression method guaranteeing desired signal quality", *IEEE Trans. Biomed. Eng.,* vol. 45, no. 12, pp. 1414-1419, December 1998.

3. Hammil S.C., J.H. O'Keefe, M. Freed, *The Complete Guide to ECG*, Physicians' Press, Minnesota, 2001.

4. Thakor N., Y. Sun, H. Rix, P. Caminal, "Multiwave: A wavelet-based ECG data compression algorithm", *IEICE Trans. Inform. Syst.*, vol. E76-D, no.12, pp. 1462-1469, 1993.

5. Ahmed N., P. J. Milne, S. G. Harris, "Electrocardiographic data compression via orthogonal transform", *IEEE Trans. Biomed. Eng.,* vol. 22, pp. 484-498, June 1975.

6. Ahmed N., T. Natarajan, K.R. Rao, "Discrete Cosine Transform", *IEEE Trans. Comput.,* vol.23, pp. 90-93, Jan. 1974.

7. Allen V.A., J. Belina, "ECG Data Compression using the Discrete Cosine Transform", *IEEE,* Cornell University, NY. 1992.

8. Jalaleddine S., C. Hutchens, R. Strattan, W. Cobberly, "ECG data compression tecniques-A unified approach", *IEEE Trans. Biomed. Eng.,* vol. 37, pp. 329-343, Apr. 1990.

9. Coifman R.R., M. V. Wickerhauser "Entropy-based algorithms for best basis selection", *IEEE Transactions on Information Theory,* vol.38, no.2, pp 713-718, March 1992.

10. Hosseini H. G., H. Nazeran, B. Moran, "ECG compression: evaluation of FFT, DCT, and WT performance", *Australas Phys Eng Sci Med.,* vol. 21, pp. 186-192., 1997.

11. Zou F., R. R. Gallagher, "ECG data compression with wavelet and discrete cosine transforms", *Biomed. Sci. Instrum.*, vol. 30, pp. 57-62, 1994.

12. Jayant N. S., P. Noll, *Digital Coding of Waveforms: Principles and Applications of Speech and Video,* Prentice-Hall, Englewood Cliffs, NJ: 1984.

13. Oppenheim A.V., R. W. Schafer, *Discrete-Time Signal Processing*, Prentice-Hall, Inc., Englewood Cliffs, New Jersey, 1989.

14. Proakis J.G., *Digital Communications,* McGraw-Hill, 2001.

15. Sayood K., *Introduction to Data Compression*, Morgan Kaufmann Publishers, Inc., SF, CA, 1996.

16. Strang G., *Discrete Cosine Transform*, Massachusetts Institute of Technology, http://www-math.mit.edu/~gs.

17. Strang G., T. Nguyen, *Wavelets and Filter Banks*, Wellesley-Cambridge Press, Wellesley, MA, 1996.

18. Vetterli M., J. Kovacevic, *Wavelets and Subband Coding*, Englewood Cliffs, NJ: Printice-Hall, 1995.

19. Ziv J., A. Lempel, "Compression of individual sequences via variable-rate coding", *IEEE Trans. Inform. Theory*, vol. 24, pp. 530-536, 1978.